JPRS-UMS-92-009
15 JUNE 1992

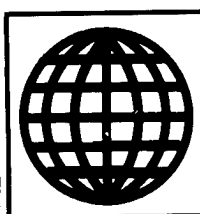

FOREIGN BROADCAST INFORMATION SERVICE

JPRS Report

Science & Technology

Central Eurasia: Materials Science

Science & Technology
Central Eurasia: Materials Science

JPRS-UMS-92-009

CONTENTS

15 JUNE 1992

Analysis, Testing

Coatings

Composite Materials

Ferrous Metals

Nonferrous Metals, Alloys, Brazes, Solders

Nonmetallic Materials

Preparations

Treatments

On Slab-Like Structure Development Mechanism in Al-Si Alloys

927D0127C Kiev METALLOFIZIKA in Russian Vol 13 No 12, Dec 91 pp 48-58

[Article by O.P. Fedorov, Ye.L. Zhivolub, Institute of Physics of Metals at the Ukrainian Academy of Sciences; UDC 548.5]

[Abstract] Transformations in the dendritic structure formed in Al-Si alloys during solidification, the conditions of tabular structure development, and its morphological characteristics as a function of the growth rate and component concentrations are examined within a broad composition range, and three stages characterized by different crystallization rates are identified: fast, with a 10^{-4} s local solidification time, and two slow stages with a solidification time measured in minutes and hours. It is demonstrated that during slow Al-Si alloy solidification, unstructured slabs consisting of virtually pure aluminum with "100" crystallographic planes form in the temperature gradient field, the slab position in the single crystal is determined by the mutual orientation of the growth direction, and the <100> direction. The slab forming process is due to the coagulation of the lateral dendrite branches leading to the development of solid slabs made of dendrite trunks and branches which coincide with the <100> crystallographic planes regardless of the external heat extraction direction. The dependence of the slab development process rate on the alloy concentration is examined; the structure formation rate does not depend on the concentration below the eutectic point. The slab development process intensity decreases with an increase in the slab forming plane deviation from the growth axis. Figures 6; references 9: 4 Russian, 5 Western.

Manifestation of Electron Transitions in Magnetic Susceptibility of Cu-Au Alloys Ordering on Cu_3Au Basis

927D0127D Kiev METALLOFIZIKA in Russian Vol 13 No 12, Dec 91 pp 59-65

[Article by Yu.P. Sereda, Kharkov State University; UDC 538.22]

[Abstract] The behavior of magnetic susceptibility in nontransition metals at the points of topological electron transitions and its utility for analyzing the electron spectrum of Cu_3Au structures near the Fermi level are discussed, and the magnetism of Cu-Au alloys which are ordering on the basis of the Cu_3Au stoichiometric composition is investigated experimentally; an attempt is made to establish the characteristics of the energy band structure related to the stability of the corresponding structural modification. To this end, the magnetic susceptibility of >300 single crystal $Cu_{1-x}Au_x$ alloys ($0.13<x<0.33$) is examined within a 4.2-300K temperature range by Faraday's method. The dependence of the Cu-Au alloy magnetic susceptibility on the component concentration and the dependence of the Cu-Au magnetic susceptibility on temperature at various component concentrations are plotted, and it is noted that the concentration dependence of χ has 37 sharp singularities (paramagnetic extrema) against the backdrop of a smooth diamagnetism sag with a minimum at x=0.205 at a 4.2K temperature at critical points in the *d*-band due to an overlapping of the *s*- and *d*-bands. The effect of heat treatment is discussed. The states near the edges and faces of Brillouin zone play a dominant role in stabilizing and destabilizing the crystal structure of the electron phases. It is shown that correct approach to solving the problem of phase stability in alloys and predicting the phase boundary positions calls for a detailed study of the corresponding fragments of the energy spectrum. The author is grateful to M.A. Obolenskiy for helping with the experiment and N.G. Sergiyenko for supporting the effort. Figures 4; references 16: 13 Russian, 3 Western.

Highly Anisotropic $Y(Co_{0.85}Al_{0.15})_2$ Weak Band Ferromagnetic With C14 Hexagonal Structure

927D0127E Kiev METALLOFIZIKA in Russian Vol 13 No 12, Dec 91 pp 109-112

[Article by I.A. Zorin, N.V. Baranov, G.V. Bondarkova, Institute of Physics of Metals at the Ukrainian Academy of Sciences, Kiev; UDC 538.652]

[Abstract] $Y(Co_{0.85}Al_{0.15})_2$ single crystals synthesized by Bridgeman's method at the Urals State University from polycrystalline samples made by alloying and annealing the initial components in a vacuum are investigated. Right hexagon-shaped 10-25 kg samples with the C14 structure are examined using a vibrational magnetometer in magnetic fields of up to 5 MA/m within a 4.2-30K temperature range in order to measure the magnetization of single crystal and polycrystalline samples; the temperature dependence of spontaneous magnetization of crystals with the cubic C15 and hexagonal C14 structure is plotted; the field dependence of the C14 single crystal magnetization is studied in magnetic fields perpendicular and parallel to the axis of easy magnetization (OLN). In addition, the dependence of the threshold field in the C14 single crystal perpendicular to the axis of easy magnetization on temperature and the dependence of the anisotropy constant of the C14 single crystal on temperature are plotted. An analysis of the curves shows that the single crystal has a metastable C14 structure and has a record high anisotropy among weak band ferromagnets; the anisotropy constant reaches $5 \cdot 10^4$ J/m^3 at liquid helium temperatures. Figures 4; references 3: 1 Russian, 2 Western.

Structural Changes in Molybdenum Upon Irradiation by Lithium and Beryllium Ions

927D0130A Moscow FIZIKA I KHIMIYA OBRABOTKI MATERIALOV in Russian No 5, Sep-Oct 91 (manuscript received 17 Oct 90) pp 5-8

[Article by G.V. Afanasyev, E.M. Diasamidze, A.N. Kalinin, and N.M. Kutsiya, Sukhumi; UDC 539.213:621.382]

[Abstract] The authors of the study reported herein examined the structural changes occurring in molybdenum when it is irradiated with lithium and beryllium ions. Polycrystalline molybdenum films 65 to 70 nm thick were bombarded with lithium and beryllium ions at room temperature in a dose of 3×10^{17} cm^{-2} at an energy of 15

keV (the number of displacements per atom amounted to four and six for the lithium and beryllium, respectively). An ER-100M electronograph with an initial electron energy of 100 keV was used to record the diffraction patterns. Bombarding polycrystalline molybdenum films with lithium ions at or below room temperature was found to result in complete breakdown of the diffraction pattern of the formation of a limited solid solution with significant impurity swelling of the film. Bombarding the molybdenum films with beryllium ions at room temperature resulted in the formation of $MoBe_2$ with a hexagonal structure. The study findings, coupled with an analysis based on the configuration model of transition metals bombarded with ions in threshold doses, led the authors to conclude that bombarding manganese, vanadium, and iron with lithium ions may lead to the formation of intermetallides, whereas bombarding yttrium, lanthanum, and actinium with beryllium ions may render them amorphous. Figure 1, table 1; references 10: 9 Russian, 1 Western.

A Method of Measuring Radiation Conductance When Modeling the Effect of Protons on Dielectrics in Outer Space

927D0130I Moscow FIZIKA I KHIMIYA OBRABOTKI MATERIALOV in Russian No 5, Sep-Oct 91 (manuscript received 11 Dec 89) pp 55-59

[Article by A.I. Akishin, N.M. Dunayev, and Yu.I. Tyutrin, Moscow; UDC 538.95-405;539.125.4: 537.312.5:537.79:001.8]

[Abstract] The authors have developed a method for express measurement of radiation conductance when modeling the effect of protons on dielectrics in outer space. The method is based on composition of the voltage of a capacitor bank as a function of the number of current pulses of the protons (electrons) irradiating the test dielectric, which is connected to the discharge circuit of the capacitor bank. The idea of the method is to reduce the charge stored in the capacitor bank discharged due to the radiation conductance of the dielectric being measured. Unlike the conventional measurement method, the new method does not entail any problems with respect to the specimen dimensions or determination of the radiation current. The new method may in fact be used to measure relatively thick specimens; its use is limited only by the length of the free path of the particles. The new method may be used to determine the radiation conductance of material regardless of that material's aggregate state or other physicochemical properties. Another advantage of the new method is that the measurement instruments required may be located at great distances from the specimen being measured. The method has been demonstrated to be effective in establishing the effect that cosmic radiation has on materials and in determining total radiation conductance. Comparisons of the new method and the convention method of measuring radiation conductance established that they result in values that coincide within the bounds of the precision of the source data. Figures 3, table 1; reference 1: Russian.

Magnetic Properties of Fine Fe-Ni Alloy Particles

927D0131A Sverdlovsk FIZIKA METALLOV I METALLOVEDENIYE in Russian No 9, Sep 91 pp 69-73

[Article by S.Ye. Langvagen, O.P. Lyubashevskiy, P.Ye. Chizhov, Branch of the Chemical Physics Institute at the USSR Academy of Sciences; UDC 669.15'24:669-492.2:537.622]

[Abstract] The factors responsible for a change in the coercive force of fine particles of Fe-Ni alloys with a change in concentration are examined in order to determine the magnetic properties of single-domain powder particles and help to develop new magnetic materials on the basis of fine metal and alloy particles. The Fe-Ni alloy particles with a mean size of 30 nm are produced by the method of gaseous phase metal vapor condensation which is based on metal evaporation from a metal drop in an inert gas flow while the drop is retained by a high-frequency magnetic field and is heated by eddy currents. Electron microscopy studies are carried out under a JEM-100CX and X-ray structural measurements are taken by a DRON 2-UM diffractometer in Fe*K* radiation; the magnetic properties are examined in a vibration magnetometer in up to 800 kA/m fields. The lattice constant of α- and γ-phases, the phase composition, the dependence of the specific magnetization on the magnetic field and the component concentration, the effective anisotropy constant of fine γ-phase particles, and the temperature dependence of the coercive force at various Ni concentrations are plotted. The particle size distribution is close to lognormal and the particle shape is close to spherical. Nickel and iron powders in the maximum field have a specific magnetization σ of 193 and 51 $A \cdot m^2/kg$ which amounts to 88 and 93 percent of the massive metal magnetization, respectively. A correlation between the coercive force and saturation magnetization during coherent magnetization reversal with a negligible crystalline anisotropy is found: $H_c \simeq 0.07 I_s$. Figures 5; references 9: 7 Russian, 2 Western.

Elastic Properties of $Ti_{70}Zr_{30}$ Alloy at up to 8.4 GPa Pressures

927D0131C Sverdlovsk FIZIKA METALLOV I METALLOVEDENIYE in Russian No 9, Sep 91 pp 81-86

[Article by V.A. Goncharova, G.G. Ilina, L.S. Smirnov, O.B. Tarasova, Metallurgy Institute imeni A.A. Baykov; UDC 669.295'296:539.32:53.092]

[Abstract] The characteristics of the elastic properties' behavior of the polycrystalline $Ti_{70}Zr_{30}$ alloy under the effect of hydrostatic pressure are investigated. To this end, the longitudinal and transverse elastic wave propagation time in alloy samples shaped as a truncated cone at room temperature under an 8.4 GPa pressure is measured by the ultrasonic (UZ) method at a three to five MHz frequency; the acoustic contact surfaces are lapped to a one to two μm accuracy and piezoelectric crystal wafers are used for measurements. The dependence of the longitudinal and transverse ultrasonic wave propagation velocity on the pressure in the alloy and the dependence of the bulk modulus on pressure, the dependence of the shear modulus

on pressure, and the dependence of the volume ratio on pressure in the alloy and in pure Ti and Zr are plotted. The findings demonstrate that the behavior of elastic constants and particularly the shear modulus of the alloy under hydrostatic pressure attest to the stability of the initial phase, i.e., there is no $\alpha \rightarrow \omega$ transformation, although the appearance of soft shear modes at pressures above 7 GPa is a precursor of phase transformations (FP). Figures 4; tables 1; references 14: 8 Russian, 6 Western.

Effect of Nonresonant Excitation on Echo Signal Shape in Magnetics

927D0131D Sverdlovsk FIZIKA METALLOV I METALLOVEDENIYE in Russian No 9, Sep 91 pp 87-93

[Article by I.G. Kiliptari, M.I. Kurkin, Tbilisi State University and Institute of Physics of Metals at the Urals Department of the USSR Academy of Sciences; UDC 539.143.43]

[Abstract] The use of nonresonant excitation methods in pulse nuclear magnetic resonance (YaMR) spectroscopy of weak magnetic materials, i.e., dia- and paramagnetics, due to the fact that nonresonant excitation is especially efficient under the signal saturation conditions, whereby the oscillator frequency detuning may lead not only to a decrease but also an increase in the signal strength and a change in the signal shape and spectral composition, is investigated. To this end, the effect of nonresonant excitation on the fine structure of the nuclear spin echo signals in magnetic materials, i.e., the usual Hahn's double-pulse echo, is examined and the echo signal strength is analyzed at various frequency deviations from resonance allowing for the gain nonuniformity and the nuclear magnetic resonance frequency nonuniformity. It is shown that as the detuning increases, the echo signal splitting, typical of resonant excitation by high-power pulses, disappears. This finding is consistent with the experimental results produced for an ordered Co_2MnSi alloy. It is recommended that these echo signal features be used for quickly finding the nuclear magnetic resonance center frequency in the case of narrow resonance lines. Figures 5; references 12: 7 Russian, 5 Western.

Magnetic Properties and Structure State of 50G13 and 50N20 Strained Metastable Austenitic Alloys

927D0131E Sverdlovsk FIZIKA METALLOV I METALLOVEDENIYE in Russian No 9, Sep 91 pp 94-99

[Article by S.V. Mamayev, V.I. Levit, M.V. Degtyarev, T.I. Chashchukhina, Institute of Physics of Metals at the Urals Department of the USSR Academy of Sciences; UDC 669.15-194.56:548.4:537.622]

[Abstract] The use of metastable austenitic alloys in structural members exposed to impact abrasive wear and the process of strain hardening due to a $\gamma \rightarrow \alpha$ martensite transformation are discussed and the magnetic properties of the 50G13 and 50N20 strained metastable Fe-Ni alloys whose characteristics of α-martensite formation are well known are examined; an attempt is made to confirm the conclusion that finely disperse strain α-martensite forms in the alloy with the help of a JEM 200CX electron microscope. The coercive force and specific magnetization behavior in a 0.8 MA/m magnetic field as a function of straining temperature and the behavior of the coercive force and specific magnetization in a 0.8 MA/m magnetic force as a function of straining degree at a 100°C temperature are plotted. The results of magnetic measurements show that the strain martensite forming in the alloys at elevated straining temperatures (>100°C) is finely disperse and has a 10-100 nm dimension. Electron microscopy confirms this conclusion. It is speculated that the high coercive force and rectangular hysteresis loops in strained carbon-containing Fe-Ni and Fe-Mn alloys attests to the formation of strain martensite in them. The authors are grateful to L.N. Romashev for discussing the findings. Figures 3; references 9: 6 Russian, 3 Western.

Nuclear Gamma Resonance in Beryllium Single Crystals

927D0131F Sverdlovsk FIZIKA METALLOV I METALLOVEDENIYE in Russian No 9, Sep 91 pp 200-202

[Article by V.S. Zotov, Yu.A. Kurinyy, V.D. Monkin, Chelaybinsk State Engineering University; UDC 669.725:539.172.3]

[Abstract] Moessbauer spectra of Be-Fe systems are discussed and the orientational dependence of nuclear gamma resonance (YaGR) in Be single crystals with a natural mixture of Fe isotopes (2.15 percent of ^{57}Fe) is investigated; in so doing, the sample thickness is selected so as to ensure that there is at least 0.3 mg of ^{57}Fe atoms per 1 cm^2 on the path of γ-radiation in order to obtain reliable absorption spectra. The experimental and analytical values of relative spectral line intensities and the additional doublet are summarized and absorption spectra on Be single crystals at a 10° and 90° *C*-axis orientation relative to the γ-quanta beam and the dependence of the doublet line intensity ratio on the angle between the *C*-axis direction in Be single crystals and the γ-radiation beam are plotted. The doublet of the solid solution of Fe in Be has the following parameters: an isomeric shift of -0.23+/-0.01 mm/s relative to Pt and a quadrupole splitting of 0.61+/-0.01 mm/s. It is also speculated that there is a second phase in the Be single crystal whose axis of symmetry is oriented perpendicular to the single crystal's *C*-axis and whose nuclear gamma resonance spectrum line parameters are close to those of the solid solution doublet. Figures 2; tables 1; references 16: 7 Russian, 9 Western.

Electron Microscopy and Radiographic Investigation of $YBa_2Cu_3O_{7-\delta}$ System Decay as Function of Cooling Rate From Sintering Temperature

927D0131G Sverdlovsk FIZIKA METALLOV I METALLOVEDENIYE in Russian No 9, Sep 91 pp 114-122

[Article by S.V. Sudareva, Ye.P. Romanov, T.P. Krinitsina, I.L. Deryagina, N.Ye. Khlebova, Yu.V. Ilyukhin, A.D. Nikulin, Institute of Physics of Metals at the Urals

Department of the USSR Academy of Sciences and VNIINM imeni Academician Bochvar, Moscow; UDC 669.3'794'893'787:621.785.78]

[Abstract] The effect of the cooling rate after sintering at 920°C on the fine structure of the $YBa_2Cu_3O_{7-\delta}$ phase where δ is not equal to zero is investigated. The samples are cooled outside the furnace thus ensuring that an orthorhombic phase modification is produced. An ambiguous dependence of the compound structure on the cooling rate after sintering is established; the "normal" orthorhombic phases forms when the samples are cooled in the air; when the cooling rate drops from 100 to 10°/h, the 1:2:3 system decays ($\delta<0.2$) and homologous phases and a tweed structure are formed. In samples cooled at a 10°/h rate, two phases are observed: one rich in oxygen and one poor. The ortho→tetra phase transition is determined by the *I*006, 020/*I*110 line intensity which tends to decrease with a decrease in the cooling rate. Figures 11; tables 1; references 13: 3 Russian, 10 Western.

Continuous Complex Ordering and Decay Reactions in Cu_3Au-Based Aging Alloys

927D0131H Sverdlovsk FIZIKA METALLOV I METALLOVEDENIYE in Russian No 9, Sep 91 pp 123-131

[Article by V.D. Sukhanov, T.S. Boyarshinova, Institute of Physics of Metals at the Urals Department of the USSR Academy of Sciences; UDC 669.3'21'24'292:(548,313,3+621.785.85)]

[Abstract] Transformations typical of binary systems which occur in the ternary solid solution when a binary ordering alloy is doped with a third constituent with a limited solubility in one or both base components and the possibility of a comprehensive development of the ordering and decay processes are discussed and the formation conditions and the mechanism of complex reaction whereby the precipitating phase nucleation is directly related to the nucleation and growth of the ordered matrix domains are considered. Aging alloys with a Cu_3Au-, Ni_2V- and CuPd-based ordered matrix are examined under JEM-150 and JEM-200CX electron microscopes and a DRON-3 diffraction analyzer in Cu*K* radiation. The existence of continuous and discontinuous complex ordering and decay reaction is established. A hypothetical phase diagram of ternary aging alloys with an ordered matrix and ordering *C*-curves of the supersaturated solid solution in alloys with a continuous phase transformation mechanism are plotted. An analysis of experimental data on continuous solid solution decay and ordering reaction indicates that the reaction is possible if atomic ordering is accompanied by the solid solution stratification along the excess constituent and if the alloy contains a constituent present in both the ordered and precipitating phase. The stratification degree on the domain boundaries of the ordered matrix determines the width of the two-phase ordering temperature range. Figures 4; tables 1; references 19: 13 Russian, 6 Western.

Structural and Electromagnetic Property Behavior of Carbonyl Iron

927D0132A Sverdlovsk FIZIKA METALLOV I METALLOVEDENIYE in Russian No 8, Aug 91 pp 97-101

[Article by O.V. Yermakov, O.I. Kolesova, A.V. Rayevskiy, Department of Chemical Physics Energy Problems Institute at the USSR Academy of Sciences; UDC (669.1+669-492.2):537.621.3:538.913]

[Abstract] The correlation between the stability of electromagnetic properties of carbonyl iron within a broad temperature range and the particle structure stability and chemical composition as well as the relationship between the impurity distribution and the behavior of carbonyl iron's complex dielectric permittivity μ^* during annealing and its dependence on structure are discussed. The kinetics of complex dielectric permittivity relaxation and its relation to the kinetics of the recrystallization, microstress behavior, and impurity transformation processes within a 250-350°C are investigated; in particular, the behavior of coherent scattering domains (OKR) and microwave (SVCh) magnetic permeability of carbonyl iron powders (KZh) during annealing is examined. The iron content is monitored colorimetrically using an Evans (UK) spectral absorption meter. Structural characteristics are examined with the help of a DRON-3M diffractometer and μ^* is measured by the resonance method. X-ray structural analysis and other measurements demonstrate that under the effect of temperature, ferrite materials change their magnetic properties due to the recrystallization and stress relaxation processes. The structure and magnetic permittivity kinetics can be used to predict the behavior of carbonyl iron-based ferrites under specific temperature conditions. It is shown that the particle structure behavior kinetics are largely determined by the amount and origin of the impurities distributed in them. The coherent scattering domain growth activation energy and the Fe_4N phase accumulation during the growth of α-Fe crystals and microstress relaxation are determined. Figures 3; tables 1; references 7.

Effect of Ordering Processes on Electric and Magnetic Properties of Pd_xCu_{1-x} ($0.40\leq-x\leq0.48$) Alloys

927D0132B Sverdlovsk FIZIKA METALLOV I METALLOVEDENIYE in Russian No 8, Aug 91 pp 106-111

[Article by A.A. Senchenko, I.I. Piratinskaya, L.P. Zelenin, Yu.A. Vereshchagin, Urals Polytechnic Institute imeni S.M. Kirov; UDC (669.3'234+548.313.3):537.621.4:537.311.31]

[Abstract] The inconsistency of data on the effect of composition and ordering degree on the magnetic properties of Pd-Cu alloys within a broad temperature range and the lack of information about the behavior of magnetic susceptibility χ during the phase transformation prompted a comprehensive study of the crystalline structure transformation and the behavior of electric resistivity and

magnetic susceptibility of Pd_xCu_{1-x} in the close-to-stoichiometric composition homogeneity region within a 300-1,200K temperature range. Single phase nonordered and ordered samples with x=0.40, 0.45, 0.46, and 0.48 are examined. The phase composition and lattice constants are studied by the Debye-Scherrer method in Cu*K* radiation and the high-temperature diffraction analysis is performed using a DRON-3 diffractometer. The ordering parameters and specific volume behavior of the crystal as a function of the Pd and Cu concentration are summarized and the diamagnetic susceptibility of the crystal lattice, electron state density at the Fermi level, and its behavior during the alloy ordering are measured. The study shows that the A1→B2 phase transition is accompanied by a crystal lattice compression and phase strain hardening; in the ordered state, there are no pure Cu or Pd sublattices yet there is predominant Cu of Pd atom distribution in the sublattices; the ordering process is accompanied by a sharp resistivity and magnetic susceptibility drop due to a decrease in the *d*-electron state density at the Fermi level resulting in a weakening of the *s-d* scattering. The authors are grateful to Yu.V. Serdyuk for help with data processing. Figures 3; tables 2; references 10: 8 Russian, 2 Western.

Characteristics of $TmFeO_3$ Magnetic Properties in Weak Magnetic Fields

927D0132C Sverdlovsk FIZIKA METALLOV I METALLOVEDENIYE in Russian No 8, Aug 91 pp 112-115

[Article by S.S. Karneyeva, N.P. Kolmakova, D.I. Sirota, Bryansk Institute of Automotive Engineering and Radiophysics and Electronics Institute at the Armenian Academy of Sciences, Ashtarak; UDC 669.1'867'787: 537.621]

[Abstract] The magnetic and phase properties of rare earth orthoferrites and their domain structure and magnetic hardness are discussed and the dependence of $TmFeO_3$ magnetization and magnetic susceptibility on temperature is investigated at various levels of magnetic field strength, from $6.4 \cdot 10^3$ A/m to $8 \cdot 10^4$ A/m or from ≈80 Oe to ≈1,000 Oe within an 80-120K temperature range. The crystal magnetization is measured by a vibrational magnetometer along the **a** and **c** crystallographic axes. A theoretical model which makes it possible numerically to explain the experimental curves, primarily within the temperature range above the orientational phase transition (OFP) from the angular phase to the Γ_4 phase, is developed. It is assumed that there is a plane parallel domain structure in the Γ_4 phase with magnetization along the anisotropy axis and that the magnetic field is oriented along the *c*-axis, so magnetization under the effect of the magnetic field occurs due to jumps of domain wall (DS) attached to defects. After the domain wall jump, the corresponding domain disappears. It is noted that the domain structure disappears in an 80 Oe field in the low-temperature phase. Figures 2; references 3: 2 Russian, 1 Western.

Thermal and Deformational Stability of τ-Phase in MnAl-C Hard Magnetic Alloys

927D0132D Sverdlovsk FIZIKA METALLOV I METALLOVEDENIYE in Russian No 8, Aug 91 pp 116-121

[Article by M.A. Uymin, Ye.I. Teytel, A.V. Shangurov, A.Ye. Yermakov, Institute of Physics of Metals at the Urals Department of the USSR Academy of Sciences; UDC 669.71'74'784'620.181]

[Abstract] The effect of the chemical composition on the thermal and deformational stability of the MnAl-C alloy's ferromagnetic τ-phase which is metastable and may breakup into the equilibrium nonmagnetic β-Mn and MnAl(r) phases during heat treatment and ausforming—the main processes used in making permanent magnets—is investigated. Specifically, the effect of the principal constituents and such alloying additions as Ni, Zr, and Hf on the hysteretic properties and stability of the alloy with a $L1_0$ structure is examined in order to determine the optimum alloy composition and its permissible variations. To produce the τ-phase, the ingots smelted in an induction furnace in an Ar atmosphere are subjected to diffusion annealing at 1,150°C for 2 h, oil quenching at 1,000°C, and another annealing at 700°C for 10 min. The alloy structure is examined using a DRON-1UM diffractometer and JEM-200CX electron microscope; the magnetic properties are measured by a vibrational magnetometer. The dependence of the maximum specific magnetization on the annealing duration at various manganese concentrations, the dependence of specific magnetization on the manganese and carbon concentration after annealing and after straining under various conditions, the dependence of the the specific magnetization and coercive force on the manganese concentration after annealing and straining, and the dependence of the specific magnetization after straining and annealing at various Mn and Ni concentrations are plotted. An analysis of experimental data on the ternary Mn-Al-C alloys' properties shows that the maximum of the deformational stability of the τ-phase falls at the following composition: 53.3 percent Mn, 44.6 percent Al, and 2.1 percent C. Given a 2.1 percent C concentration in an alloy doped with nickel, the optimum composition is 52.3 percent Mn, 45.2 percent Al, and 0.4 percent Ni. Nickel expands the range of permissible Mn concentration variations and increases the coercive force after straining and annealing. The authors are grateful to A.S. Gerasimov for preparing the alloys, A.G. Kuchin for measuring the magnetic properties in strong fields, and V.S. Gaviko for X-ray analyses. Figures 6; references 13: 4 Russian, 9 Western.

Characteristics of Microstructure and Superconducting Properties of Thick $Y_1Ba_2Cu_3O_{7-\delta}$ Alloy Films Synthesized on Ceramic Substrates

927D0132E Sverdlovsk FIZIKA METALLOV I METALLOVEDENIYE in Russian No 8, Aug 91 pp 122-126

[Article by V.G. Pushin, G.Ye. Vedernikov, V.G. Sagaradze, L.I. Yurchenko, S.Ya. Tubin, Ye.V. Kaplyuk, Institute of Physics of Metals at the Urals Department of the USSR Academy of Sciences; UDC (546.562+538.945): 539.216.2]

[Abstract] The characteristics of the microstructure and superconducting properties of thick high-T_c superconducting (VTSP) $Y_1Ba_2Cu_3O_{7-\delta}$ alloy films synthesized on ceramic substrates are investigated. To this end, the HTSC paste is "burned-in" at a 900-1,000°C temperature, then subjected to standard low-temperature oxygen annealing. The structure and phase and elemental composition of the samples are examined by transmission and scanning electron microscopy, electron diffraction analysis, and radiographic analysis. The critical temperature T_c and the superconducting transition gap width Δ_c are measured by the four-probe resistive method. The dependence of the critical temperature on the burn-in temperature is plotted for various paste particles sizes is plotted and the microstructure and diffraction patterns of the samples are cited. The critical temperature of samples annealed at 970°C with a mean HTSC particle size of three and five μm is below 77K while that of coarse grain paste with an eight μm particle annealed at 920°C is 89K. The T_c decreases sharply if the burn-in temperature is increased to 980°C; likewise, the critical current density j_c increases by more than tenfold in samples with the maximum T_c, reaching $(1.0\text{-}1.5)\cdot 10^3$ A/cm^2. Figures 3; references 3.

Effect of Spin Resonator on Nuclear Stimulated Echo Signals in Magnetics

927D0133A Sverdlovsk FIZIKA METALLOV I METALLOVEDENIYE in Russian No 10, Oct 91 pp 44-49

[Article by O.V. Nazarova, N.P. Fokina, K.O. Khutsishvili, Tbilissi State University imeni I. Dzhavakhishvili; UDC 539.143.43]

[Abstract] The shortcomings of accumulating small nuclear spin echo (SE) signals in order to record them and the need to amplify echo signals with the help of an additional RF (RCh) passive circuit (PK) which is connected to the echo spectrometer, is not coupled with the oscillator, and has the necessary parameters is noted. This RF passive circuit is tuned to the center frequency of nuclear magnetic resonance (YaMR). It is speculated that this spin echo amplification method makes it possible to shorten the signal accumulation time and get rid of the noise accumulation in the case of weak spin echo signals. The effect of the spin resonator on the stimulated echo signal is investigated on the basis of constraint equations for the nuclear magnetization components and magnetic field in the spin resonator with lumped parameters. It is shown that the effect of the passive circuit is determined by the parameters of the driving pulses and the circuit itself as well as the sample characteristics. The dependence of the first and stimulated echo gain on the magnetization rotation angle is plotted for lithium ferrite at 77K; numerical estimates for ^{57}Fe in lithium ferrite show that under certain conditions, the spin resonator may significantly affect the spin echo signal amplitude, e.g., amplify the signals. Figures 1; references 8.

Computation of Transport Heat Due to Thermal Lattice Expansion

927D0133B Sverdlovsk FIZIKA METALLOV I METALLOVEDENIYE in Russian No 10, Oct 91 pp 50-53

[Article by T.G. Vozmishcheva, I.A. Murtazin, Ye.I. Salamatov, Engineering Physics Institute at the Urals Department of the USSR Academy of Sciences, Izhevsk; UDC 539.219.3.001]

[Abstract] The difficulty of computing the transport heat Q^* in the theory of thermotransport prompted an attempt to express the heat of transport through known thermodynamic functions and evaluate the role of the temperature gradient in the process. It is speculated that the temperature gradient is responsible for the slope of the fiducial line of the diffusion energy barrier diagram and changes the probability of the diffusant jumps from a given site to the nearest equilibrium position. This probability is denoted with the help of Boltzmann's distribution and an expression is derived for the diffusion heat transfer which takes into account the effect of the temperature gradient more fully. Morse's potential is used in order to account more fully for the contribution of the lattice's nonuniform thermal expansion to the activation energy and transport heat. The temperature dependence of the activation energy and transport heat is plotted for self-diffusion in copper. An analysis shows that the transport heat is positive, exceeds the activation energy by 15-25 percent, and increases with temperature while the activation energy decreases with temperature. Within a temperature range of volume diffusion, transport heat variation fall within 5 percent and activation energy variations fall within 10 percent. Figures 1; references 8: 5 Russian, 3 Western.

Electromagnetic-Optical Transformation During Spin-Reorientation Transition in Iron

927D0133C Sverdlovsk FIZIKA METALLOV I METALLOVEDENIYE in Russian No 10, Oct 91 pp 54-60

[Article by V.A. Komarov, R.S. Ilyasov, V.V. Merzlyakov, Engineering Physics Institute at the Urals Department of the USSR Academy of Sciences, Izhevsk; UDC 669.018.5:534-8]

[Abstract] The ultrasonic vibration attenuation and propagation velocity in the vicinity of phase transitions and the behavior of macroscopic magnetic characteristics which also undergo significant transitions in such processes are discussed and the effect of the spin-reorientation transition on the manifestations of a double reciprocal transformation of electromagnetic and acoustic waves—the electromagnetic-acoustic-electromagnetic transformation (EMAP)—on the field dependence of the phenomenon, a change in velocity, and sound attenuation is investigated. To this end, single crystals of silicon iron (with 3.8 percent Si) cut from the same single crystal sheet whose long axes are oriented along the [100], [110], and [111] direction are examined. The field dependence of the double EMAP emf in three magnetization direction are plotted by the resonance and pulse method and the dependence of the resonant frequency in the [111] direction near the spin-reorientation transition is examined. The study shows that the resonant EMAP has a higher resolution than the pulse EMAP in observing the transition. It is shown that the EMAP efficiency in the transition area is largely determined by elastic stresses developing in the sample, making it possible to measure stresses induced by elastic vibrations. Figures 5; references 10.

Structural Study of Phase Transformation in TiNi

927D0133G Sverdlovsk FIZIKA METALLOV I METALLOVEDENIYE in Russian No 10, Oct 91 pp 134-140

[Article by I.L. Barmina, O.K. Belousov, S.P. Kulagin, Metallurgy Institute at the USSR Academy of Sciences; UDC 669.24'295:620.186.1]

[Abstract] The heterophase martensitic transformation process in titanium nickelide and the evolution of the TiNi structure with a transition through the critical point M_H are discussed and successive structural changes occurring during the martensitic transformation in four stoichiometric or close-to-stoichiometric TiNi alloys with different compositions and critical points are investigated. The alloys are produced by arc melting in an atmosphere of pure argon and rolled into 0.5-0.7 mm dia. rods from which samples are made after hardening at 1,213K for 1 h. X-ray structural analyses are carried out in a diffractometer, chemical analysis—in a JSM35CF microanalyzer, and electron microscopy study—under a JEM-200A transmission electron microscope. The study of the martensitic transformation (i.e., B2→B19) shows that at the initial stage, the B2 phase is stratified into Ti-rich and Ti-poor areas while the structure is undergoing simultaneous rhombohedral distortions B2→B2'+R. Martensite forms in the nonequilibrium B2' areas which are highly twinned; the R→M transformation occurs later; the shift processes occurring in the alloy approaching M_H are related to the atomic displacement which is responsible for the B2 phase stratification. Figures 4; tables 1; references 12: 2 Russian, 10 Western.

X-Ray Structural Study of Perfection Degree Variation in Single Crystal Turbine Blades in Operation

927D0133I Sverdlovsk FIZIKA METALLOV I METALLOVEDENIYE in Russian No 10, Oct 91 pp 154-159

[Article by M.B. Bronfin, E.D. Darchinov, N.A. Protasova, All-Union Institute of Aviation Materials, Moscow and Kazan Motor Manufacturing Production Association; UDC 669.245:669-172:548.4:539.26]

[Abstract] The fragmentation of single crystals during the growing of single crystal turbine blades from a high-temperature nickel alloy and the importance of understanding the substructure development patterns and orientation behavior of such single crystals under high-temperature plastic deformation during operation is stressed. The process of substructure formation during heating in a 1,000-1,250°C temperature range without a load application and under the simultaneous effect of temperature and static loading are investigated and the structural state of blades is analyzed after various lengths of service. Radiographic studies are carried out in a DRON-3.0 diffractometer in Cu*K* radiation. The samples for the study are cut from single crystal castings after standard heat treatment at 1,250°C for three hours and 1,050°C for 10 hours. The samples are then heated in a KS-600/25 furnace with a 30 min exposure. After various operating runs (from 150 to 4,000 h), samples are cut from the blade's root attachment and "hot" area. The findings and a comparison to model samples attest to the single crystal rotation during operation relative to the initial orientation whereby identically oriented areas are fractured into multiple microareas whose disorientation increases with time. A structure of coherent scattering blocks with a high dispersion degree forms inside the microareas. Such dislocation structure parameters as the dislocation density, coherent scattering areas, and the mosaic structure angles are determined and the critical dislocation density is calculated ($2.60 \cdot 10^9$ cm^{-2}). The resulting data characterize the service life margin of the material and can be used in manufacturing for determining the product life and the overhaul period. Figures 8; tables 1; references 4.

Effect of Ultraviolet Radiation on Hydrogen Penetration Through Armco Iron

927D0138F Kiev FIZIKO-KHIMICHESKAYA MEKHANIKA MATERIALOV in Russian Vol 27 No 3, May-Jun 91 pp 28-31

[Article by O.Kh. Kozyrev, I.L. Tazhibayeva, L.A. Zolotova, O.G. Romanenko, V.P. Shestakov, Kazakh State University imeni S.M. Kirov, Alma-Ata; UDC 533.15+539.219.3]

[Abstract] The possibility of activating the process of metal permeation with hydrogen by ultraviolet radiation in order to establish the character of the physical and chemical processes related to photodesorption which occur in the accumulation rings of high-energy accelerators and thermonuclear fusion reactors is investigated. To this end, a 0.8 mm thick Armco iron membrane with a 14 mm diameter is irradiated by a DRSh-250 mercury-arc ultraviolet (UV) source in a vacuum chamber through a quartz glass window, making it possible to measure radiation on a 160 nm wavelength at a 7.7 eV energy. The Arrhenius dependence of the effective hydrogen diffusivity in Armco iron with and without ultraviolet irradiation, Armco iron's hydrogen permeability isothermal curves, the Arrhenius dependence of the effective constants of Armco iron permeability to hydrogen, and the effective coefficient of hydrogen adhesion to Armco iron with and without irradiation are plotted. The experiments demonstrate that when the membrane's exit side is irradiated during the permeation process, its steady-state flow increases somewhat; a study of transient flows and the steady-state condition settling time shows that ultraviolet radiation substantially affects the penetration kinetics by shortening the settling time and thus increasing the apparent diffusivity or transmembrane transport coefficient. The effect of irradiation on unsteady permeability of α-Fe is attributed to an increase in the desorption rate of both hydrogen and carbon on the membrane's exit side and an increase in the rate of the hydrocarbon synthesis catalytic reaction. The need for further studies is stressed. Figures 3; references 4.

On Fracture of VNZh-7-3 and VNM-3-2 Alloys Under Shock Wave Loading

927D0138G Kiev FIZIKO-KHIMICHESKAYA MEKHANIKA MATERIALOV in Russian Vol 27 No 3, May-Jun 91 pp 72-74

[Article by V.Yu. Belov, V.K. Golubev, N.I. Kachalin, Yu.S. Sobolev, N.A. Yukina, All-Union Scientific Research Institute of Experimental Physics, Arzamas; UDC 539.4]

[Abstract] The dynamic strength of the VNZh and VNM tungsten alloys which are characterized by high density and strength as well as good ductility and are used in rotors, jet engine nozzles, and penetrating radiation screens is investigated; to this end, the spalling strength of the VNZh-7-3 (7 percent Ni and 3 percent Fe by mass) and VNM-3-2 (3 percent Ni and 2 percent Cu by mass) alloys is measured at normal and elevated temperatures. The test samples are made by the powder metallurgy methods with hydrostatic compaction at a 200 MPa pressure. The samples are loaded by an impact of an aluminum projectile slab accelerated to the necessary velocity by sliding detonation of a thin explosive layer. The effect of density and temperature on the spalling fracture conditions is plotted and the cleavage fracture nucleation and propagation is examined. An analysis of experimental data shows that heating to a 750°C temperature significantly increases the spalling strength; the tendency toward an increase in spalling strength with temperature is roughly the same for both alloys; thus, the presence of tungsten which passes from the brittle to ductile state during heating is the principal factor affecting the structure of these alloys. Under static uniaxial tensile tests, heating leads to a monotonic decrease in strength. The maximum ductility characterized by elongation at rupture is realized at 400°C for both alloys. Figures 4; references 4.

Deformation Properties of Titanium-Based Amorphous Alloys

927D0138H Kiev FIZIKO-KHIMICHESKAYA MEKHANIKA MATERIALOV in Russian Vol 27 No 3, May-Jun 91 pp 77-79

[Article by A.V. Mineyev, Moscow Automotive Engineering Institute; UDC 669.295:533.537]

[Abstract] The results of creep and tensile tests of samples from the $Ti_2Cu+Ti_2Ni+TiCu+Ti_5Si_3$ alloy produced by spinning at the Metallurgy Institute at the USSR Academy of Sciences are discussed. Three samples annealed at a 200-280°C temperature and three nonannealed samples are tested in tension at a 0.7 mm/min rate; then 20 samples annealed at 250°C are tested for creep. The sample strength as a function of the annealing temperature, the sample creep under load, and the elongation behavior after relieving the load are plotted. Negative residual deformation is discovered and the cluster relaxation under tension and sample contraction after the load relief are examined. The results are explained from the cluster theory viewpoint and the negative residual deformation is attributed to the fact that "frozen" clusters freed under tension take a more advantageous positions as a result of local displacements and rotation. Stepwise sample elongation under load are attributed to local cluster shifts and flops from one energy position to another. Figures 3; references 4.

Hydrogen Diffusion and Penetration Through Cobalt Foil

927D0138J Kiev FIZIKO-KHIMICHESKAYA MEKHANIKA MATERIALOV in Russian Vol 27 No 3, May-Jun 91 pp 124-125

[Article by I.Ye. Gabis, A.A. Kurdyumov, V.G. Sorokin, Leningrad State University; UDC 620.197.4]

[Abstract] The lack of research data on the hydrogen interaction with transition metals is noted and hydrogen diffusion and penetration through a cobalt foil within a 520-1,050K temperature range is investigated with the help of an automated hydrogen permeability testing unit at a 100-800 Pa hydrogen pressure. To this end, 0.1 mm thick Co foils containing less than 0.1 percent of impurities are cleaned and degreased, then degassed at a 660K temperature, i.e., somewhat below the $\varepsilon \rightarrow \alpha$ transition point. Then permeability and diffusion are measured. At temperatures below the transition point, the initial sections of the rate curve edge lag somewhat and the flow settling is delayed, probably due to a large number of defects which serve as hydrogen atom traps. The steady-state condition settling curves of the flow through the Co foil and the temperature dependence of diffusivity and penetrating flow are plotted. An analysis reveals that rate curves can be adequately described by a straight line. Microleaks are detected after the first crossing of the $\varepsilon \rightarrow \alpha$ transition point. The resulting diffusion and penetration activation values are higher than those reported earlier and are attributed to a difference in the experimental data processing methods. Figures 2; references 3.

Phenomenological Patterns of Structural Superplasticity

927D0139A Moscow IZVESTIYA VYSSHIKH UCHEBNYKH ZAVEDENIY: CHERNAYA METALLURGIYA in Russian No 11, Nov 91 pp 47-49

[Article by M.A. Tsepin, A.N. Yershov, Moscow Steel and Alloy Institute; UDC 621.7.043:539.374]

[Abstract] The principal task of the phenomenological theory of structural superplasticity is quantitatively and reliably to describe the patterns of superplastic deformation (SPD) of materials with ultrafine grains within a broad temperature and straining rate range and formulate on this basis assumptions and underlying premises for applied mathematical models which describe the superplastic metal working processes and make it possible to select sound process parameters. The dependence of the flow stress, rate sensitivity index, and maximum elongation of the VT6 alloy with various structures at a 900°C temperature, the dependence of the flow stress, rate sensitivity index, and maximum elongation of the VT14 alloy with various structures on the homologous temperature at a 10^{-3} s^{-1} straining rate, and the dependence of the flow stress on the mean grain size and the corresponding size distribution of the VT6 alloys at 900°C are plotted. The

mathematical correlations underlying the phenomenological model reflect the principal patterns of superplastic deformation and make it possible to make sufficiently accurate estimates of the main process parameters (i.e., the temperature, straining or stress rate, and structure). In order to use the model in practical engineering applications, it is necessary to obtain reliable experimental estimates of the phenomenological equation parameters on the basis of high-temperature mechanical test data on alloys with various structures. Figures 3; references 1.

Loss Analysis of Binary Alloy Components During Vaporization by Olette's Equation Allowing for Internal Mass Transfer

927D0139F Moscow IZVESTIYA VYSSHIKH UCHEBNYKH ZAVEDENIY: CHERNAYA METALLURGIYA in Russian No 11, Nov 91 pp 94-95

[Article by L.N. Belyanchikov, N.L. Belyanchikov, Moscow Steel and Alloy Institute; UDC 669.187.4]

[Abstract] Olette's equation is used to calculate the loss of the binary alloy's base metal and alloying addition during vacuum refining; Olette's assumption made in deriving the coefficient α that vaporization of both components is limited to the evaporation event is refuted and it is asserted that both internal and external mass transfer must be taken into account. An expression for the generalized evaporation coefficient "ash" (of which α is a particular case) is derived allowing for internal mass transfer. If the external mass transfer is taken into account, "ash"→1 and the chemical composition of the alloy does not change. The new coefficient can be used in the case where the component vaporization process is limited to the evaporation event and to internal mass transfer. References 1.

Study of Phase Equilibria in Mn-P-La System at 1,873K

927D0139G Moscow IZVESTIYA VYSSHIKH UCHEBNYKH ZAVEDENIY: CHERNAYA METALLURGIYA in Russian No 11, Nov 91 p 94

[Article by A.V. Pavlov, Yu.V. Kazakov, Yu.I. Utochkin, Moscow Steel and Alloy Institute; UDC 669.74.017.3]

[Abstract] Phase equilibria in an Mn-P-La system are examined by the hardening method using a resistance furnace with a graphite heater in an atmosphere of argon at a 1,873K temperature in order to develop and improve the methods of manganese-containing alloy dephosphorization; an isothermal cross section of the Mn-P-La constitution diagram is plotted and compared to that of the Fe-P-R (R=rare earth element) system obtained from published sources; one can see that phosphorus has a much higher affinity for manganese than for iron. Consequently, the process of reduction dephosphorization of Mn-containing alloys requires greater thermodynamic outlays than iron-based melts. Figures 1; references 1.

Effect of Yttrium on Aluminum Viscosity and Resistivity

927D0142D Sverdlovsk RASPLAVY in Russian No 6, Nov-Dec 91 pp 100-102

[Article by S.V. Golubev, V.I. Kononenko, Chemistry Institute at the Urals Department of the USSR Academy of Sciences; UDC 546+62-143+546.64-143]

[Abstract] The lack of data on the physical and chemical properties of liquid Al-Y system alloys—promising light refractory materials—and the need for such information in order to predict the properties of these alloys in the solid state prompted a study of the viscosity of Al-Y alloys by the method of torsional vibration damping in a crucible with a melt while the resistivity is measured by the electrodeless method in the rotating magnetic field. The melting point, density at the melting point, temperature coefficient of density, exponential factor, viscous flow activation energy, electric resistivity, and the temperature coefficient of resistance of Al-Y alloys at various Y concentrations are summarized and the isothermal kinematic viscosity curve of the Al-Y melt at a 1,373K temperature is plotted. Hysteresis is discovered virtually at all alloy compositions. The results shown that electric resistance of the alloys increases significantly with additions of yttrium and that the temperature dependence of resistance is virtually linear within the measurement error for all alloy compositions. When an yttrium atom is added to the melt, electrons are additionally scattered by the impurity atom thus increasing resistivity. Moreover, chelation in the melt also requires a certain number of electrons, thus further increasing the electric resistivity. An increase in the yttrium concentration increases the kinematic viscosity; viscosity also increases with an increase in the degree of ordering while additions of yttrium to the melt lead to an increase in the volume fraction of ordered phases. Figures 1; tables 1; references 6: 5 Russian, 1 Western.

Type 4007 Diagnostic Center For Studying and Checking Polymer-Based Composite Product Properties

927D0143A Sverdlovsk DEFEKTOSKOPIYA in Russian No 8, Aug 91 pp 12-15

[Article by A.V. Sandalov, R.V. Veys, Polymer Mechanics Institute at the Latvian Academy of Sciences; UDC 620.179]

[Abstract] The shortcomings of existing diagnostic methods and devices based on the results of indirect measurements which call for accumulating large files of experimental data on a range of material properties and making complex calculations and evaluations prompted the development of a new type 4007 diagnostic center (DTs) intended for solving these problems for organic-, carbon-, and glass-based plastics and other composites. The diagnostic center designed by the Polymer Mechanics Institute at the Latvian Academy of Sciences and its

special instrument-making design office is a microcomputer-based data measurement system capable of collecting and processing data on the parameters measured in composite materials by various nondestructive testing methods, e.g., acoustic emission, thermal, dielectric, ultrasonic, strain-gauge, etc.. A block diagram of system integration for various types of tests and estimates carried out for predicting the properties of composite products is cited. The principal software package (PPP) used by the center is Diagnostic Station-1989 developed for IBM PC/XT microcomputers with an MS-DOS operating system; the diagnostic center's hardware requirements are listed. Figures 1; references 3.

Magnetic Field of Surface Defect in Ferromagnetic Slab

927D0143B Sverdlovsk DEFEKTOSKOPIYA in Russian No 8, Aug 91 pp 33-39

[Article by R.V. Zagidulin, V.Ye. Shcherbinin, Institute of Physics of Metals at the Urals Department of the USSR Academy of Sciences; UDC 620.179.14]

[Abstract] Formulas derived earlier by the authors for calculating the magnetic field of a crack-like surface defect in a ferromagnetic half-space (*Defektoskopiya* Nos. 3 and 10, 1988) are extended to the case of a plane parallel slab. In so doing, the field pattern developing in the slab is represented as a field of defects symmetrically positioned relative to the slab boundaries inside a linear infinite ferromagnetic medium; the surface charges on the defect boundaries are distributed at a constant density. The magnetic field inside the ferromagnetic slab with a surface defect is denoted in a complex form. The effect of the ferromagnetic slab boundaries on the field is taken into account graphically and the magnetic fields of the crack calculated by different method are compared. The variation in the extremal values of the defect's magnetic field components along the x- and y-axes with the slab depth are plotted and the results of various theoretical calculations and experimental data are compared. The surface charge values on the crack sides vary within 4,675-7,448.3 A/cm. The effect of the ferromagnetic slab's boundary surfaces on the defect's magnetic field is taken into account mathematically by the mirror mapping method, making it possible to derive analytical formulas and calculating the density of surface charges on the defect sides and their field in the air rather accurately. The effect of the slab's second boundary surface on the defect's magnetic field is insignificant for defects extending less than 20 percent into the slab. Figures 4; tables 3; references 4: 3 Russian, 1 Western.

Automating Product Thickness Monitoring

927D0143C Sverdlovsk DEFEKTOSKOPIYA in Russian No 8, Aug 91 pp 64-70

[Article by L.V. Myakinkova, A.Ya. Teterko, Ye.D. Mikhaylova, S.B. Bosik, A.L. Khlyunev, L.V. Truba, M.S. Morunyak, A.G. Aleshchenko, Central Scientific Research Institute of Building Materials, Khotkovo, Physics-Mathematics Institute at the Ukrainian Academy of Sciences, Lvov, and Forestry Engineering Institute, Lvov; UDC 620.179.18]

[Abstract] A report to the third interbranch scientific and engineering conference on "Methods of Nondestructive Testing of Polymer Material Products" held in Tuapse in 1990. The development of computer-aided measurement data systems (AIIS) for monitoring the thickness of thick-walled rubber-like coats of varying standard sizes on metal attachments is reported and the conditions imposed on the transducers for measuring the thickness of elastic materials are described. A block diagram of the computer-aided measurement data system is cited and its operating principle is explained. The principal component of the system is a DVK-3M interactive (DVK) microcomputer used as an intelligent terminal; it also contains an operator panel (PO), an interface unit (BS), vertical and horizontal coordinate control units (BUDG, BUDV), a calibrating mechanism control unit (KUKM), a transducer unit (BIP), an operator panel interface unit (BPPO), a service data generating unit (BFSSI), and a scanning device (SKU) with a transducer (ID) and calibrating mechanism (MK). The system has a Q-bus architecture. The software flow chart for controlling the accuracy of the positional scanner at various trajectories and the gauge mechanism control flow chart are presented. Tests of the system demonstrate that its calibration accuracy does not exceed 0.1 mm and the thickness gauging error within a 1-30 mm range does not exceed 0.03 mm. Figures 4; references 13.

Using SF_6 Gas as Probe Substance for Seal Testing

927D0143D Sverdlovsk DEFEKTOSKOPIYA in Russian No 8, Aug 91 pp 79-85

[Article by M.I. Seliverstov, Scientific Research Institute of Machine Building Methods at the Tekhnomash Scientific Production Association; UDC 620.165.29]

[Abstract] The shortcomings of existing leak detectors, both foreign and domestic, e.g., "SF_6" by Analytical Instruments, Bantom 2310 and 2320, or 13TE-9-001, prompted the development of a new TP-2 plasma leak detector for recording the effluent of electronegative gases. The new device's operating principle is based on measuring the quench frequency of an RF (VCh) oscillator as a function of the electronegative gas concentration in the gaseous mixture present in the discharge gap. A block diagram of the TP-2 plasma leak detector and its general view are shown. The TP-2 is a portable instrument consisting of a test prod and a secondary unit; the test prod contains a measurement chamber with a leak, an RF oscillator, and an amplifier. The instrument's detection threshold for an insulating gas flow (SF_6) is $1 \cdot 10^{-10}$ W and its detection threshold for the insulating gas concentration in the air of nitrogen is $1 \cdot 10^{-6}$ percent by volume. Moreover, its response is linear. Pilot operation at a taxi garage demonstrates that all defects can be detected reliably. The possibility of increasing the leak testing sensitivity by concentrating the SF_6 gas in cryogenic traps is considered. Figures 4; references 9.

Multiparameter System for Nondestructive Testing of Materials and Products

927D0144A Yekaterinburg DEFEKTOSKOPIYA in Russian No 12, Dec 91 pp 3-9

[Article by M.M. Mikhovskiy, A.P. Popov, G.D. Dinev, Mechanics and Biomechanics Institute at the Bulgarian Academy of Sciences, Sofia; UDC 620.179.1]

[Abstract] The use of multiparameter nondestructive quality control methods whereby the acoustic, magnetic, electric, thermoelectric, and other characteristics convey information about the condition of materials and items is discussed and two types of problems solved by multiparameter nondestructive testing of materials (MNKM)—estimating the condition of a given material and then classifying different materials—are outlined. Several such methods are considered as a function of *a priori* data on the entities under study. A nondestructive testing system developed on the basis of an 8-bit KLK-8 computer containing a primary data unit, an analog-to-digital converter (ATsP), and single-board processor, and software is described. A flow chart of the MNKM nondestructive testing system software architecture is shown and the results of two- and three-parameter testing of powder metallurgy materials after sintering and hardening are presented. The tolerance domains for grading steels 45 and 35 and the results of grading with the help of the MNKM system are plotted. Figures 7; references 9.

Ultrasonic Testing of Mechanical Properties of Thermal Power Plant Superheater Pipes

927D0144B Yekaterinburg DEFEKTOSKOPIYA in Russian No 12, Dec 91 pp 10-17

[Article by A.V. Sharko, V.V. Muravyev, Ye.V. Karkeshko, Novosibirsk Railroad Engineers Institute; UDC 620.179.16]

[Abstract] Experience in commercial uses of the acoustic nondestructive testing method for identifying areas with an insufficient mechanical strength and determining the numerical values of the metal strength properties of power generating equipment in order to predict its residual life is outlined. The method makes it possible to pinpoint areas of local structural and mechanical changes in the metal of extended products, such as steam superheater pipes at thermal power plants made from steel 12Kh1MF and 12Kh2MFSR, by measuring and recording the speed of surface and subsurface acoustic waves. Calibration curves of the dependence of the autocirculation frequency on the HB hardness, ultimate strength, and yield strength for steel 12Kh1MF and 12Kh2MFSR are plotted and the results of ultimate strength and yield strength measurements taken by the acoustic method and directly using samples cut from the pipes are summarized. The hardness, yield strength, and ultimate strength distributions in the tube cross section are plotted. The tests make it possible to develop recommendations for use in superheater pipes at the Kuzbassenergo Production Association; it is noted that acoustic nondestructive testing methods should be used as an independent technological procedure in replacing pipelines in order to eliminate the possibility of pipe damage due to an incorrect position of the firing and rear sides. Figures 4; tables 6; references 6.

Using ΔE Effect To Control Slanted Waveguide Ultrasonic Beam

927D0144C Yekaterinburg DEFEKTOSKOPIYA in Russian No 12, Dec 91 pp 27-33

[Article by V.M. Klyachin, V.D. Boltachev, Institute of Physics of Metals at the Urals Department of the USSR Academy of Sciences; UDC 620.179.16]

[Abstract] Several methods of controlling the ultrasonic (u.z.) beam by manipulating the speed of sound in the waveguide and their shortcomings are discussed and a method which employs the dependence of the Young modulus on the magnetic field in magnetostrictive materials (MS)—the ΔE effect—is considered. A block diagram of the experimental unit which utilizes the method is cited and its operating principle is described. The unit consists of a magnetostrictive waveguide with a winding generating a static magnetic field, a piezoelectric vibrator generating ultrasonic vibrations, a half-disc, an ultrasonic pulse detector, a magnetic field control unit (BRMP), and an acoustic control unit. The dependence of the Young modulus variation on the magnetic field in the 50KF alloy, the beam pattern of the slanted waveguide, the dependence of the angle of refraction on the angle of incidence interface of the duralumin half-disc and the 50KF alloy, and the dependence of the scanning sector variation of the refracted beam on the angle of incidence are plotted. Theoretical data are compared to the experimental results and the discrepancy is attributed to an ultrasound speed measurement error. An analysis of the findings shows that the variation in the scanning sector increases when the angle of incidence approaches the critical angle for total reflection and the refraction angle deflection due to the magnetic field increases when the angle of refraction approaches the angle of polarization. The authors are grateful to S.P. Perevalov for help. Figures 5; references 7.

Logic Analysis of Fissure Modulation Characteristics in Composites

927D0144D Yekaterinburg DEFEKTOSKOPIYA in Russian No 12, Dec 91 pp 48-57

[Article by V.S. Khandetskiy, Dnepropetrovsk State University, imeni the three hundredth anniversary of the reunification of Ukraine and Russia; UDC 620.179.14]

[Abstract] The characteristics of the cracking process in composites and the methods of separating the effect of changes in the clearance and skewing on the results of eddy current nondestructive testing are discussed and it is stressed that the tuning-out methods based on changing the direction of the fissure's impact relative to the eddy current transducer (VTP) and electric potential fixing of the clearance needs further improvements. To this end, the scanning trajectory is divided into N equidistant samples and the sample sequence of the induced signals is transformed into sets of two-valued quantities characterizing the sign and magnitude of the signal variation in each discrete scanning trajectory step. Tables of the Boolean

truth function which describe the nondestructive testing process are compiled and the Boolen function spectra are plotted. An algorithm based on the autocorrelation function of the binary set is developed, making it possible to expand the number of adjacent scanning points α_i being analyzed while maintaining the necessary speed. This makes it possible to analyze longer scanning trajectory sections and improve the reliability of identifying oblique fissures in the fibrous composite whose modulation characteristic widens asymmetrically with a decrease in the angle between the symmetry plane of the fissure and the material surface. Figures 6; tables 4; references 8.

Structural Characteristics of Diamond and Boron Interaction at High Temperatures and Pressures

927D0145A Kiev SVERKHTVERDYYE MATERIALY in Russian No 1 (76), Jan-Feb 92 pp 10-14

[Article by N.P. Semenenko, G.S. Oleynik, V.F. Britun, V.M. Volkogon, N.V. Danilenko, I.I. Timofeyeva, Institute of Materials Science Problems at the Ukrainian Academy of Sciences, Kiev; UDC 621.921:621.385]

[Abstract] The effect of boron additions on the properties of adamantine composite materials and the processes of solid phase interaction in diamond- and boron carbide-based composite materials are discussed, and the mechanism of structural transformations occurring in diamond + boron (both amorphous and crystalline), diamond + B_4C, and amorphous boron + graphite composites is investigated. Samples for the study are produced at a 7.7 GPa pressure within a 900-2,300°C temperature range. In order to trace the structural transformation evolution in these systems, sintering was performed under intermittent conditions by raising the temperature in 100 or 200° increments. X-ray phase and radiographic microanalyses and transmission electron microscopy demonstrate that the reordering in the system is due to the combined development of such elementary processes and melting and crystallization of amorphous boron; boron interaction with the graphite present on the diamond grain surface accompanied by the formation of a highly disperse boron carbide layer; recrystallization boron carbide grain growth and microtwinning in the grains; boron carbide interaction with diamond accompanied by the development of secondary carbon-enriched boron carbide; and crack- and pore-formation on the interface during the secondary boron carbide development on the diamond grains leading to a loss of the diamond-boron carbide boundary. Recommendations are formulated for developing diamond + B_4C-based composites. Figures 4; references 8: 5 Russian, 3 Western.

Polarographic Analysis of Carbon's Adamantine Phase

927D0145B Kiev SVERKHTVERDYYE MATERIALY in Russian No 1 (76), Jan-Feb 92 pp 14-16

[Article by A.L. Vereshchagin, L.A. Petrova, P.M. Brylyakov, Altay Scientific Production Association, Biysk, Altay kray; UDC 666.233]

[Abstract] The importance of understanding the composition of the groups present on the surface of ultradisperse diamond for solving the problems of adhesion, chemical compatibility, and hardening of adamantine composites is emphasized, and the shortcomings of existing methods are noted. Thus, the adamantine carbon phase produced by detonation of explosives is investigated by polarographic analysis in a PU-1 polarograph with a dropping Hg electrode and a mercury reference electrode. The volt-ampere characteristic of samples of primary explosive detonation product (UDAG) without iron impurities containing 30-50 percent adamantine carbon is plotted. An analysis of the findings indicates that quinone, lactone, and carboxyl groups characterized by reduction waves are present on the surface. The composition of surface groups in UDAG samples and the composition of surface groups of the adamantine carbon phase are summarized. The results demonstrates the possibility of using polarography for examining the composition of surface adamantine carbon phase produced by detonation synthesis. Figures 1; tables 2; references 5: 3 Russian, 2 Western.

X-Ray Emission Spectra of Carbon Films

927D0145C Kiev SVERKHTVERDYYE MATERIALY in Russian No 1 (76), Jan-Feb 92 pp 17-21

[Article by V.Ye. Strelnitskiy, Ya.V. Zaulichnyy, Ye.A. Zhurakovskiy, Kharkov Engineering Physics Institute at the Ukrainian Academy of Sciences and Institute of Materials Science Problems at the Ukrainian Academy of Sciences, Kiev; UDC 546.26-162.02]

[Abstract] The issue of producing wear resistant carbon film-based coats is addressed and published data on the structure of carbon films are reviewed. Emission spectra of diamond-like films (AP) are examined with the help of an RSM-500 ultralong wave spectrometer in *CK* radiation using an echelette diffraction grating with a 6,000 mm radius of curvature; the instrument's energy resolution is $\leq$0.3 eV. Adamantine film samples with less than 1 percent hydrogen (atomic) and hydrogenated carbon films with 20 and 25 percent hydrogen on polished copper substrates are examined and the sample thickness, density, microhardness, resistivity, energy gap, and carbon concentration are summarized. The study demonstrates that the emission band of the adamantine film with a 3.3 g/cm^3 density virtually merges with the band of ultradisperse diamond powders with a body centered crystal lattice (OKR) size of 3 nm, pointing toward the predominantly tetrahedral short-range order type of the carbon matrix in the condensate. Valence bands of hydrogenated films are similar to graphite's *CK* bands while the fine structure of the hydrogenated films' *CK* bands makes it possible to conclude that hydrogen *s*-electrons interact with P_z orbital electrons and broken *sp*-hybrid orbitals of graphite-like clusters. In adamantine films, an increase in the proportion of tetrahedrally coordinated atoms always leads to an increase in density and subsequent localization of π-electrons with a corresponding increase in resistivity and energy gap. Figures 2; tables 1; references 15: 10 Russian, 5 Western.

Endurance Limit of Ceramic Materials at Elevated Temperatures

927D0146G Kiev POROSHKOVAYA METALLURGIYA in Russian No 2 (350), Feb 92 pp 42-47

[Article by V.N. Yakovkin, V.A. Kuzmenko, A.G. Maslovskiy, Institute of Materials Science Problems at the Ukrainian Academy of Sciences; UDC 539.3/.5:666]

[Abstract] The issues of improving the reproducibility and narrowing the spread of ceramic material test data and of the endurance strength of ceramic materials at high loading frequencies and elevated temperatures are addressed and the results of endurance tests of polycrystalline aluminum oxide samples conducted at room and elevated temperatures (up to 900°C) and at a loading rate of close to 10 kHz are discussed. Silicon nitride-based ceramics are studied for reference in order to check the generality of the resulting data. The results of bending tests and the ultimate strength and limit of endurance of ceramic materials at various temperatures are summarized. The findings indicate that the endurance limit of the best samples of the MK-3 nitride ceramics heated to 800°C increases from 320+/-10 to 360+/-10 MPa while that of the A995 corundum ceramics—from 170+/-10 to 190 MPa. A study of the notch sensitivity index (KIN) threshold in both types of ceramics reveals that the breaking stress range narrows when the loading rate increases to 10 kHz. A "training" phenomenon is discovered after exposure to cyclical loading. It is recommended that dynamic tests results be used for estimating the limit of endurance since static test may result in a >50 percent error. Figures 1; tables 2; references 9: 8 Russian, 1 Western.

Experimental Data Analysis During Nondestructive Testing of Sintered Carbon Steel Products

927D0146I Kiev POROSHKOVAYA METALLURGIYA in Russian No 2 (350), Feb 92 pp 52-55

[Article by A.I. Ulyanov, R.P. Petrov, S.G. Novikov, R.G. Fayzullin, Engineering Physics Institute at the Urals Branch of the USSR Academy of Sciences; UDC 621.762]

[Abstract] The effect of the residual pore volume on the stability of strength properties and the effect of the graphite distribution uniformity in the initial mixture of powders and the gaseous medium during sintering with subsequent heat treatment on the carbon concentration in carbon steel are discussed; the process of nondestructive testing of the structural state of products from structural powder steels with an on-line statistical analysis of large experimental data files is investigated and the need for algorithms and procedures necessary for this purpose is stressed. A criterion and technique for selecting the informative physical parameters are proposed and algorithms and a software package are developed, making it possible considerably to shorten the analysis duration and increase the confidence level. The package is used to examine the possibility of monitoring the quenching quality of sintered carbon steels alloyed with Ni and Mo by manipulating the carbon content within 0.3-0.7 percent and density—within 6.4-7.4 g/cm^3 as well as calibrate the MPK-1 multiparametric analyzer. An Elektronika MS 0507.02 microcomputer is used. The method is also applicable to materials with a nonlinear relationship between physical and monitored parameters in which case the problem is solved step by step, using piecewise linearization. Figures 1; tables 1; references 5.

Deposited Chromium Structure Under Magnetron Spraying

927D0146J Kiev POROSHKOVAYA METALLURGIYA in Russian No 2 (350), Feb 92 pp 56-63

[Article by Ye.V. Turtsevich, A.N. Rakitskiy, T.G. Rogul, N.I. Zakharenko, V.Ye. Marushko, V.F. Gorban, V.A. Sagaydak, Institute of Materials Science Problems at the Ukrainian Academy of Sciences; UDC 620.192.4:669.268]

[Abstract] The need for thin coats and films with specified properties and known advantages of magnetron spraying prompted an investigation of the structure and phase composition of chromium coats deposited by the magnetron method. To this end, low-alloyed chromium is deposited with the help of a magnetron system equipped with a UKR-77P-1 vacuum spraying unit onto 5 mm thick quartz slices and 10 μm thick copper foil. The structure and phase composition of the deposited chromium layer are examined by transmission electron microscopy under JEM-100 CX and JEM-1000 microscopes, local X-ray microanalysis, and X-ray structural analysis. The effect of the precipitated layer thickness on the grain size, crystal lattice microdistortions, and electric resistivity is plotted. The effect of the base temperature on the coat structure and phase composition is examined and the structure and phase composition behavior during heat treatment is analyzed. A correlation between the precipitated chromium's structural transformations, microstresses, and microhardness is established. The *Ky* coefficient characterizing the difficulty of transmitting slip through the grain boundary decreases when grain boundaries are torn off from the disperse inclusions attaching them, then increases with heating due to the disperse oxide dissolution and oxygen precipitation. This is consistent with the results of structural analyses. Figures 7; references 14.

Tungsten Solubility and Solubility Kinetics in Liquid Nickel at 1,525°C

927D0146K Kiev POROSHKOVAYA METALLURGIYA in Russian No 2 (350), Feb 92 pp 73-77

[Article by Ya.V. Natanzon, V.P. Titov, R.V. Antonchenko, Institute of Materials Science Problems at the Ukrainian Academy of Sciences; UDC 621.762:669.24:669.27:669-154:532.73:541.8]

[Abstract] The discrepancy between experimental and theoretical data on the tungsten solubility in liquid nickel at a 1,525°C temperature prompted a study of the tungsten solubility in liquid nickel under the conditions where the solubility kinetics is the measured parameter, i.e., while stirring the melt in a given hydrodynamic condition. Brand N-1 electrolytic nickel of a 99.98 percent base element purity, 0.5 mm thick sheets of tungsten of a 99.95

percent purity, and a rod of single crystal tungsten of a 99.998 percent purity are used in the experiment. The temperature dependence of tungsten solubility in liquid nickel, the dependence of the tungsten concentration in liquid nickel on the dissolution duration, the dependence of the dissolution constant on the sample angular rotation speed, and the dependence of dynamic viscosity on the W concentration at various temperatures are plotted. An analysis of the results obtained by the spinning disc method shows that the W solubility in liquid Ni is 50 +/- 1.4 percent by mass rather than 45-46 percent according to other sources and its diffusivity is $(1.41 +/- 0.07) \cdot 10^{-8}$ m^2/s. Tungsten dissolution rate constants are calculated. Figures 4; tables 1; references 14: 11 Russian, 3 Western.

Extractive-Fluorimetric Gold Detection by Unsubstituted Rhodamine

927D0147A Moscow ZAVODSKAYA LABORATORIYA in Russian Vol 57 No 9, Sep 91 pp 1-2

[Article by S.V. Kachkin, L.P. Poddubnykh, V.K. Runov, Krasnoyarsk State University and Moscow State University imeni M.V. Lomonosov; UDC 546.59:543.426]

[Abstract] The extractive-fluorimetric gold detection method which is characterized by high selectivity and sensitivity is discussed and it is noted that among many metals, gold alone forms an ionic associate with unsubstituted rhodamine which fluoresces intensively and is extracted well by benzene and toluene. An experiment aimed at detecting Au in artificial mixtures containing Ga, Sb, Tl, Hg, and platinic metals by the extractive-fluorimetric method is described and the results are summarized at a 95 percent confidence level. The method makes it possible to produce reliable results, has a good convergence, and is recommended for analyzing natural and artificial auriferous specimens. It is capable of detecting less than 0.01 μg/ml for rhodanide ions and 0.2 μg/ml for bromide ions. Tables 1; references 5.

Extractive-Atomic Absorption Platinum and Palladium Detection in Sulfate Solutions

927D0147B Moscow ZAVODSKAYA LABORATORIYA in Russian Vol 57 No 9, Sep 91 pp 2-4

[Article by V.V. Belova, A.A. Vasilyeva; UDC 546.91:542.61: 543.42]

[Abstract] The need to concentrate the platinic metals in sulfate solutions due to nonselective interference appearing at high concentrations of base metals is stressed and a new extractive method of concentrating Pt and Pd and then determining these metals' concentration in the extracts by the atomic absorption spectrophotometry method is investigated. A Perkin-Elmer model 506 spectrophotometer with air-acetylene flame atomization source and an HGA-74 graphite atomizer is used and the Pt and Pd detection conditions are summarized. The effect of the palladium wavelength and concentration on its recovery from sulfate solutions is confirmed. The procedure of detecting Pd in sulfate solutions is outlined and the effect of the AAHCl concentrate and hydrocarbon sulfides on the Pt and Pd recovery from sulfate-chloride solutions is summarized. The procedure is tested in technological sulfate solutions with a low concentration of these metals; the relative standard deviation for both Pt and Pd is within 0.05-01. These findings make it possible to develop different versions of the extractive-atomic absorption method which are simple to carry out and are more proximate: they take two to three hours vs. one to two shifts for the chemical-spectral detection methods. The new methods are also characterized by a low detection threshold of 0.04 and 0.01 mg/l for Pt and Pd, respectively at a 95 percent confidence level and a good reproducibility. Tables 4; references 6.

Silver Detection in Copper Amalgams by Photometric Method

927D0147C Moscow ZAVODSKAYA LABORATORIYA in Russian Vol 57 No 9, Sep 91 pp 4-5

[Article by O.P. Yaroshenko, V.N. Gavrilova, N.P. Sumskaya, Kharkov State University; UDC 543.42.062: 669.791.5]

[Abstract] The high cost of instrumental detection techniques and the length of multistage detection methods which involve target metal separation from the interfering elements prompted the development of a photometric method of detecting silver in copper amalgams without filtering off the interfering background. The method is based on a photometric analysis of silver's ternary complex with *o*-phenanthroline and bromopyrogallol red (BPK) and masking the interfering effect of mercury and copper by trilon B; the standard method is modified somewhat in preparing the sample and performing the analysis. The analytical procedure and sample preparation are described and the results of Ag concentration measurement by the proposed method are summarized and compared to the results obtained by the atomic absorption method (AAS). Measurement data processing shows that the systematic error is eliminated by using the proposed technique, making it possible to recommend it for Ag detection in copper amalgams at a 0.1 percent concentration. The method does not call for separating the impurities beforehand and is rather simple to use and sufficiently accurate. Tables 1; references 9: 6 Russian, 3 Western.

Iridium and Copper Detection by 2,2'-dipyridyl in Standard Platinum Concentrate Composition Samples

927D0147D Moscow ZAVODSKAYA LABORATORIYA in Russian Vol 57 No 9, Sep 91 pp 6-8

[Article by V.N. Losev, V.K. Runov, Moscow State University imeni M.V. Lomonosov; UDC [546.93+546.56]: 543.426]

[Abstract] The task of developing highly selective and sensitive methods of detecting platinic and nonferrous metals, particularly iridium and copper, formulated by the State System of Standard Composition Samples necessitated a search for methods based on measuring the intensity of luminescence with charge transport of these elements' complexes with amines. Consequently, the use of 2,2'-dipyridyl (Dipy) as a highly sensitive and selective luminescing iridium and copper reagent is investigated. The

detection procedure is outlined and the optimum luminescent detection conditions are determined by the mathematical experimental design method. The iridium detection threshold is $5 \cdot 10^{-3}$ μg/ml and the lower concentration bound is 0.02 μg/ml. The relative standard deviation does not exceed 0.03. In using commercial FL and Kvant-5 fluorimeters and Dipy, the Ir detection threshold is $1 \cdot 10^{-2}$ and $8 \cdot 10^{-2}$ μg/ml, respectively. The maximum quantities of elements which do not hinder detection of 1 μg of Ir are determined and the results of Ir detection by Dipy in the presence of platinic metals and the results of copper and iridium detection in standard composition samples are summarized. The new luminescent method of Ir and Cu detection with the help of 2,2'-dipyridyl is recommended for analyzing commercial and natural platinum-containing formations. Tables 4; references 7.

Improving and Standardizing Auriferous Material Blending Process in Assaying

927D0147E Moscow ZAVODSKAYA LABORATORIYA in Russian Vol 57 No 9, Sep 91 pp 13-16

[Article by V.A. Shvetsov, V.V. Pakhomova, Kamchatgeologiya Production Association, Petropavlovsk-Kamchatskiy; UDC 669.9:543.05]

[Abstract] The poor state of research in the field of assay blending, despite the discovery of new gold ore deposits, is noted and the need for standardizing the blending process as a means of improving the quality of assaying and concentrating is emphasized. The problem of limiting the range of reagents used and developing simple methods of calculating their quantities is identified as the necessary and sufficient condition for standardizing the blending process. Consequently, the feasibility of reagent selection for the blending process is investigated. Various reagent compositions are tested and their assay results for gold and silver are summarized, showing a standard deviation of -0.7 to -6.1 percent; the dependence of the noble metal recovery during an assay smelting with litharge as a flux on temperature is measured and the effect of the blend composition on the Au and Ag behavior during the assay smelting process is examined. An analysis of the findings indicates that litharge and soda should be used as a basic flux, borax as an acid flux, sodium nitrate as an oxidant, and starch as a reducer; if sodium nitrate is not available, potassium nitrate can be used instead. The selection of starch as a reducer is due to its availability and practicality. Tables 3; references 9.

Procedure for Testing Pressure Vessel Models With Through Cracks

927D0147F Moscow ZAVODSKAYA LABORATORIYA in Russian Vol 57 No 9, Sep 91 pp 65-66

[Article by A.M. Abmetko, M.I. Burak, V.M. Tishkevich, Belarussian Branch of the Central Scientific Research Institute of Metal Structure Design imeni Melnikov, Minsk; UDC 620.162.4]

[Abstract] The need for data on the load carrying capacity of structural members with through cracks in order to analyze the limiting depressurization and failure states of containment structures in the framework of the "leak precedes fracture" concept is emphasized. The characteristics of pressure vessels are examined using large-scale models since the loading type and level greatly affects the material's crack resistance characteristics and because of the general difficulty of full-scale tests. Model 20 mm thick samples with a 680 mm inside diameter are made from steel VSt3Gps and consist of a cylindrical shell and an end element with flat bottoms. A schematic diagram of the pressure vessel model is shown and the test procedure is outlined. The tests are aimed at finding the optimum methods of heat insulation and sealing of the pressure vessel walls. Notches are incised on the outer side of the model and a multilayer heat insulating lining is fastened by a polyvinyl acetate (PVA) glue to the inside surface. Then holes are drilled in the incisions, displacement transducers are inserted, and the model is strained. The crack growth is monitored. Test data demonstrate that within a 0-60°C temperature range, a combined cloth and cardboard layer is the best heat insulator ensuring a temperature gradient of no more than 0.2°C/mm in the wall. Crack sealing tests show that after 100 loading cycles, P_{max}/P_{min}=87/3 kgf/cm^2. Figures 2.

Electric Signal Generation in Shielded Wire Under Transverse Shock

927D0148C Kishinev ELEKTRONNAYA OBRABOTKA MATERIALOV in Russian No 5 (161), Sep-Oct 91 pp 46-47

[Article by V.I. Tambovtsev, N.A. Petrichenko, V.K. Usachev, Chelyabinsk State University]

[Abstract] The effect of the shielded wire exposure to mechanical factors on the electrical interference excitation in the wire is investigated and it is noted that under an impact load, charge is transferred between two substances with different free carrier concentrations, so the substance with a higher conductivity yields electrons to the one with a lower conductivity. Oscillograms recorded during the interference signal measurement in a single shielded wire and a multiconductor shielded wire are shown, and the dependence of the minimum electromotive force (EDS) on the shock energy in a single-conductor two mm diameter shielded wire is plotted. The shock interference excitation mechanism is inertial, and the maximum electric signal strength is determined by the forbidden gap width. Figures 2; references 2.

Electrohydrodynamic Phenomena During Corona Pulse Discharge in Strong Aqueous Electrolytes

927D0148D Kishinev ELEKTRONNAYA OBRABOTKA MATERIALOV in Russian No 5 (161), Sep-Oct 91 pp 51-54

[Article by L.Z. Boguslavskiy, Ye.V. Krivitskiy, V.N. Petrichenko, Pulse Processes and Technologies Institute at the Ukrainian Academy of Sciences, Nikolayev]

[Abstract] The role of gas generation in pulse electric breakdown in a liquid and the factors affecting the phase homogeneity of liquid dielectrics before the onset of electric breakdown are discussed, and the discharge ignition

stage in a highly heterogeneous field in a strong aqueous electrolyte with a conductivity of over 0.1 Ω^{-1} m^{-1} is investigated. The highly inhomogeneous field is created by a needle-plate electrode system with a high-voltage capacitive integrator pulse applied to the discharge gap. The electrical characteristics are recorded using an S9-8 double-beam oscilloscope. The discharge ignition stage is recorded by an abrupt increase in the oscillogram current and the appearance of glow in the near-electrode area. An analysis of the oscillograms indicates that at a relatively low conductivity, there is no visible gas generation near or at the electrode surface from the start of voltage application until the start of the leader branch growth; the character of the process changes considerably with an increase in conductivity; the discharge is ignited in the presence of bubbles on the electrode surface and may ignite on bubbles located at a distance from the electrode; breakdown of the ignition centers occurs one to three μs before ignition on the electrode surface. The conclusion is drawn that as the conductivity increases, it is possible to ensure an energy release rate which leads to explicit gas generation near the electrode yet the discharge is ignited not on individual bubbles but directly on the electrode surface. Ignition on individual bubbles occurs when they are sufficiently large. Thus, the bubble model is consistent with the experimental data for a high electrolyte conductivity ($\sigma > \Omega^{-1}$ m^{-1}). Figures 3; references 11: 10 Russian, 1 Western.

Approximate Method of Thermoelastic Displacement Analysis in Solving Thermal Contact Problems for Plain Bearings With Thin Coats

927D0149A Minsk TRENIE I IZNOS in Russian
Vol 13 No 2, Mar-Apr 92 pp 237-250

[Article by V.A. Morozov, A.Z. Yermolayeva, Institute of Northern Engineering Physics Problems, Yakutsk; UDC 624.073:539.538]

[Abstract] The difficulty of solving thermal contact problems for the taut strained state (NDS) of contacting bodies, and the need to use approximate models and numerical methods are outlined and such approximate methods for determining the thermoelastic displacements in an annular thin layer in radial plain bearings are considered. Since the antifriction materials in these thin layers have much higher pliability and thermal expansion coefficient than metals, it is assumed that the metal parts are absolutely rigid bodies and their thermal expansion is ignored, thus significantly simplifying the problem. A precise solution of the antifriction insert problem is found and compared to the results of the approximate solution. The comparison shows that the method of approximate thermoelastic displacement analysis ensures the necessary accuracy for solving thermal contact problems and establish an explicit correlation between the layer surface displacements and the random contact pressures and temperature pattern. It is shown that the expressions may be extended to the case of a layer with a variable thickness. The authors are grateful to O.V. Bogatin and I.G. Goryacheva for constructive remarks. Figures 2; tables 2; references 14.

Analytical-Experimental Method of Solving Contact Problems

927D0149B Minsk TRENIE I IZNOS in Russian
Vol 13 No 2, Mar-Apr 92 pp 257-264

[Article by A.G. Kuzmenko, G.A. Kuzmenko, R.V. Sorokatyy, A.V. Dykha, Khmelnitskiy Technological Institute; UDC 539.3]

[Abstract] The difficulty of solving physically nonlinear problems in a traditional formulation prompted an effort to use the experimental dependence of the contact area dimensions on the total load as the initial condition in the problem formulation; in a general case, such problems are reduced to the decision functional and in particular cases—to a system of equilibrium and energy equations. The correlation between the contact area dimensions and the load characterizes the mechanical properties of the material and reduces the number of possible problems. The concept underlying the realization of the analytical-experimental (RE) method amount to constructing and minimizing the functional which, in essence, is the square deviation from the equilibrium condition over the entire loading process. A generalized problem of a sphere being indented into a half-space is considered and the case of a circular contact area is examined for simplicity's sake. The nondimensional contact pressure distribution is plotted and the contact problem solution obtained by the analytical-experimental method is compared to that produced by the finite elements method (MKE). It is demonstrated that the analytical-experimental method is invariant to the properties of the medium or the character of the structure inhomogeneity and is quite efficient and sufficiently precise for solving indentation problems. Figures 4; references 2: 1 Russian, 1 Western.

Effect of Sliding Velocity on Copper Contact Zone Structure and Composition in Copper-Steel 45 Friction Pair

927D0149C Minsk TRENIE I IZNOS in Russian
Vol 13 No 2, Mar-Apr 92 pp 295-299

[Article by A.V. Vereshchak, A.N. Gripachevskiy, V.V. Gorskiy, Institute of Physics of Metals at the Ukrainian Academy of Sciences, Kiev; UDC 669.017:531.43]

[Abstract] The development of protective layers from high-strength oxygen-doped alloys (LKS) with an amorphous-crystalline structure on the working surfaces as a result of friction and the conditions necessary for their formation are discussed. The effect of the sliding velocity on the structural and phase changes in the contact zone of the copper-steel 45 friction pair is investigated. To this end, a copper block-steel 45 roller system is examined in a standard 2070 SMT-1 friction tester at a 100 N normal load in the air; in so doing, the friction surfaces are water-cooled; the tests are carried out at a 0.2, 0.4, 0.7, 1.0, 1.5, 2.5, and 4.0 m/s sliding velocity. Metallographic, probing electron beam, and X-ray structural analyses show that within a 0.2-0.7 m/s range, the copper surface in contact with steel is well screened by the thin layer forming on its surface as a result of friction; within a 1.5-4 m/s range, the microvolumes pass to a principally new structurally unstable state whereby the

character of plastic flow changes and abnormal mass transfer of elements and oxygen occurs. In this case hardening results in the development of oxygen-doped Cu-Fe-O alloys which forms protective layers on the friction surfaces. Below the critical velocity, the reciprocal mechanical transport, mixing, and oxidation as well as plastic deformation and its localization in the surface layers develop by traditional mechanisms and do not lead to the protective LKS layer formation. The authors are grateful to Yu.F. Shvadskiy for help with X-ray structural analyses. Figures 2; references 3.

Study of Lubricating Properties of Oils With Cu-Containing Compound Additives

927D0149D Minsk TRENIE I IZNOS in Russian Vol 13 No 2, Mar-Apr 92 pp 324-327

[Article by T.I. Nazarenko, N.N. Loznetsova, G.G. Shchegolev, Yu.P. Toporov, Physical Chemistry Institute at the USSR Academy of Sciences, Moscow; UDC 621.891]

[Abstract] The use of various additives for improving the lubricating properties of oils, particularly the so-called metal-cladding additives, such as metal powders, salts, and oxides, which form a micrometer-thin metal layer on the friction surface is discussed. The effect of copper-containing additives and copper oleate and oleic acid separately on the friction parameters of oils is investigated and an attempt is made to compare the effect of uni- and bivalent copper compounds used as motor oil additives. The M-8 base motor oil without additives, HOl oleic acid, CuOl copper oleate, and $CuSt_2$ copper stearate are used for estimating the friction and wear parameters in a MAST-1 four-ball friction tester using steel ShKh15 balls with a 7.94 mm diameter at a 211 kg/mm^2 contact pressure at a $0.24 \cdot 10^{-3}$ m/s sliding velocity. An analysis of the findings shows that for most systems, the temperature dependence of the friction coefficient and the friction wear spot diameter is complex and extremal due to the breakup of the fatty acid soap film, surfactant adsorption and desorption, and changes in the reactions in the friction zone. The positive effect of the mixture of oleic acid and copper oleate is synergetic and is not merely a sum of positive effects of each component separately, attesting to a sharp change in the intensity of mechanochemical reactions. The higher efficiency of univalent copper compounds is attributed to the more intensive character of these reactions in the presence of univalent copper salts. Figures 4; tables 1; references 7: 6 Russian, 1 Western.

Quasistationary Roughness Under Pulse Laser Steel Treatment

927D0149H Minsk TRENIE I IZNOS in Russian Vol 13 No 2, Mar-Apr 92 pp 356-362

[Article by S.A. Fedosov, Samara Polytechnic Institute imeni V.V. Kuybyshev; UDC621.9.048.7:621.9.015]

[Abstract] The effect of laser treatment on the surface layer structure of steel and the effect of surface structure and roughness on the wear resistance and friction coefficient are discussed, and the effect of roughness in the extremum area on the tribological characteristics of steel ShKh15, 12Kh1, and R18 after pulse laser treatment is investigated. To examine the effect of the oxide film forming on the irradiated surface in the air, some samples are treated in an atmosphere of nitrogen. The roughness parameters are measured with the help of the TALYSERF 4 instrument and the roughness profile is recorded using the W 3Bcd Pert-o-meter and CW Pert-o-graph. Surface microphotographs are taken under a REM-200 electron microscope. The dependence of the surface roughness after laser treatment on the number of pulses per spot is plotted. The oxide film is found to have little effect on roughness and no effect on quasistationary surfaces. The development of quasistationary surface roughness after a few leaser treatment pulses is discussed and the stability of quasistationary roughness parameters to the laser irradiation conditions is noted. In general, the surface roughness tends to quasistationary roughness after a few pulses; the surface roughness can be lowered to R_a=0.2 μm by pulse laser treatment whereby the optimum condition is three pulses per spot. The quasistationary surface is gradually transformed into stationary after five to 30 pulses. The complex roughness parameter of the laser-hardened surface is usually higher than that of the machined surface which is undesirables from the viewpoint of the friction coefficient and contact pressures. Figures 4; references 8.

Silicon, Iron Silicide, and Metallurgical Ferrosilicon Density

927D0150I Moscow IZVESTIYA AKADEMII NAUK SSSR: SERIYA NEORGANICHESKIYE MATERIALY in Russian Vol 28 No 1, Jan 92 pp 78-80

[Article by R.V. Chernov, Institute of Materials Science Problems at the Ukrainian Academy of Sciences; UDC 546.28]

[Abstract] Phase transitions and structural transformations in silicon and iron silicides are discussed and the density of silicon-containing crystalline phase is investigated by the pycnometric method which ensures a measurement accuracy of up to 0.01 percent and is the most precise of known methods. To this end, polythermal density curves of the FS-75 and FS-65 ferrosilicon, iron silicides, and magnesium within a 20-50°C temperature range and polythermal curves of crystalline and semiconductor Si within a 10-50°C temperature range are plotted. All ferrosilicon, iron silicide, and magnesium samples display an abnormal density behavior within a 30.0-35.0°C range while in semiconductor and crystalline silicon, abnormal areas at 37.0 and 30.0°C coincide almost completely with those of Fe-Si phases; all abnormal changes are reversible. It is speculated that the anomalies are due to the structural transformations in Si which are also manifested in intermetallic phases; the jump-like transition is one of the main (yet not sole) signs of the first-kind phase transition and is a sufficient condition for identifying the type of phase transition although an analysis of polythermal heat capacity curves is necessary for making the final judgment. Figures 2; references 12: 7 Russian, 5 Western.

Calculating the Unevenness of the Thickness and Elemental Composition of Films Produced by Ion Sputtering of Several Targets

927D0130D Moscow FIZIKA I KHIMIYA OBRABOTKI MATERIALOV in Russian No 5, Sep-Oct 91 (manuscript received 3 Apr 90) pp 24-28

[Article by L.V. Kozlovskiy, Daugavpils; UDC 539.23]

[Abstract] The author of this article worked to develop a method of using a computer to calculate the unevenness of the thickness and elemental composition of films applied to a plane substrate by the method of ion sputtering of several randomly oriented plane targets. The method proposed is intended for use when the distance from the sputtered target to the substrate is greater than the length of the free path of the sputtered particles. The proposed method is also based on the assumption that the angular distribution of the particles is known. An example is presented to illustrate that the proposed calculation method may be used to determine the optimal location of targets relative to a substrate when the unevenness of the films' thickness (or elemental composition) is minimal and when the arithmetic mean of ($dN/d\sigma$), which is proportional to the film deposition rate, is relatively large. The optimal sputtering geometry may then be found by means of a computer experiment based on the proposed calculation method. The method is of great value from a practical standpoint because it may be used to calculate film deposition rate. Figures 2; references 11: 8 Russian, 3 Western.

Pulsed Heterogeneous Plasma Treatment of Titanium Alloy Coupled With Aluminum and Nickel Doping of the Surface Layer

927D0130J Moscow FIZIKA I KHIMIYA OBRABOTKI MATERIALOV in Russian No 5, Sep-Oct 91 (manuscript received 24 Oct 90) pp 60-66

[Article by V.P. Simakov, Ye.A. Budovskikh, P.S. Nosarev, and G.V. Bobrov, Novokuznetsk and Moscow; UDC 669.295.69:621.793]

[Abstract] The authors of the study reported herein examined the effect of treating a titanium alloy with heterogeneous plasma beams formed from the products of the electric explosion of aluminum and nickel foils. Specimens of the titanium alloy VT20 measuring 20 x 20 x 2.5 mm^3 were cut from a sheet as shipped from the factory. The specimens were subjected to treatment in a laboratory unit based on the principle of accumulation of a charge by a pulsed capacitor bank and subsequent discharge through foil that eventually melts and undergoes explosive vaporization. The exploded foil was placed 55 mm from the test specimens, which were oriented along the normal to the beam. The total capacitance of the capacitor bank amounted to 5,040 μF, and the discharge circuit had a fluctuation period of 100 μs. Metallographic, scanning electron microscopy, and x-ray studies were used to study the effect of various process parameters on the thickness of the test specimens' surface layers, their degree of alloying, their phase composition, and their structure and strength properties. The treatment regimen described was shown to result in the formation of doped surface layers with a thickness on the order of several tens of micrometers. The doping was accomplished by fusion of the surface layer of the base as it interacted with the vapor-plasma front of the beam and as finely dispersed drops subsequently entered the melt. The degree of alloying was found to depend on the treatment regimen and reached several tens of percentage points. The modified layers were found to have a fine-crystalline heterogeneous structure with a uniform phase composition throughout their depth. The modified layers had an improved (by a factor of two to three) microhardness and wear resistance (by a factor of two to four). These gains in strength were attributed to the formation of intermetallide phases. Figures 3, table 1; references 15: Russian.

The Heat Stability of Coatings Made of Thermodynamically Insoluble Elements

927D0130K Moscow FIZIKA I KHIMIYA OBRABOTKI MATERIALOV in Russian No 5, Sep-Oct 91 (manuscript received 15 Sep 90) pp 77-78

[Article by V.O. Valdner, V.T. Zabolotnyy, Ye.Ye. Starostin, Moscow; UDC 621.039.553]

[Abstract] The authors of the study reported herein examined the thermal stability of coatings made of elements that are thermodynamically insoluble with the substrate. For the studies, the researchers selected the pairs copper on tungsten and gold on tungsten as the clearest examples of systems lacking equilibrium solubility in both the solid and liquid states. The coatings were applied by the method of vacuum deposition coupled with simultaneous bombardment with argon ions so that the cascade commingling in the growing layer would dominate over the radiation-intensified diffusion and so that continuous series of metastable solid solutions 5 nm thick in the case of the copper-tungsten system and 4 nm thick in the case of the gold-tungsten system would form at the coating-substrate interface. The thickness of the coatings applied was on the order of 1 μm. Tungsten foil 100 μm thick served as the substrate. Annealing temperatures of 550, 650, 720, and 750 K were used for the system copper-tungsten, and annealing temperatures of 570, 620, 670, 770, and 820 K were used for the system copper-tungsten. The scribing method was used to measure adhesion of the coatings before and after annealing. The experiments established that scribing does not cause any microscopically visible stratification of the coatings either before or after annealing provided the annealing was performed at temperatures below 720 K in the case of the system copper-tungsten and below 770 K in the case of the system gold-tungsten. Figure 1; references 2: Russian.

The Effect of Ion Bombardment Heating on Properties of Low-Alloy Tool Steels With Coating Condensation

927D0130O Moscow FIZIKA I KHIMIYA OBRABOTKI MATERIALOV in Russian No 5, Sep-Oct 91 (manuscript received 18 Apr 89) pp 151-153

[Article by L.L. Ilichev and V.I. Rudakov, Orenburg; UDC 539.4:669.254+539.198]

[Abstract] The authors of this concise report examined the effect that the temperature to which CrWMn-type low-alloy steels is heated has on the condensation of titanium nitride ion-plasma coatings. Specifically, they studied the structural changes occurring in the said tool steels after they were heated by ion bombardment on an NNV-6.6-01 unit to temperatures of 573 to 773 K. The said temperature conditions were modeled on a VUP-4 unit that included an attachment that made it possible to maintain the temperature within +/- 1 at a pressure of 5.32 to 6.65 x 10^{-3} Pa. The hardness and microhardness of the specimens were measured, and metallographic analysis and X-ray diffraction studies were performed. The studies performed confirmed that ion bombardment may be recommended as a method of hardening tool steels with titanium nitride coatings. Heating CrWMn-type steels to temperatures of 573 to 623 K did not result in any decreases in their hardness or significant changes in their structural state. Condensation of titanium nitride coatings on the study steels was found to significantly increase the durability of the die tools and molds made from the steels. The hardness (HRC) of steel specimens tempered at temperatures of 373 to 473 K ranged from 54 to 56, whereas specimens tempered at temperatures of 673 to 773 K had a hardness of 44 to 46. The specimens' microstructure ranged from sorbite-austenite with a microhardness of 250-270 x 10^4 MPa and 360-370 x 10^4 MPa in the case low-temperature tempering to a mixture of granular and thin-plate perlite in the temperature range from 673 to 773 K with a microhardness of 170-240 x 10^4 MPa. The said structural changes were also confirmed by X-ray structural and metallographic analysis. Figures 2, table 1; references 3: Russian.

Time Instability of Magnetic Properties of Dy-Co Amorphous Films

927D0131B Sverdlovsk FIZIKA METALLOV I METALLOVEDENIYE in Russian No 9, Sep 91 pp 74-80

[Article by V.S. Zhigalov, A.V. Zhuravlev, G.I. Frolov, Physics Institute imeni L.V. Kirenskiy at the Siberian Department of the USSR Academy of Sciences; UDC 669.25'864:(539.213+539.216.2):537.622]

[Abstract] The instability of the magnetic parameters of rare earth metal-transition metal (RZM-PM) amorphous film alloys in the time domain—the principal shortcoming of magnetic data media—are discussed and the aging of Dy-Co amorphous films produced under the superdeep vacuum conditions with *in situ* monitoring of their magnetic and magnetooptical properties is investigated. To this end, the effect of aging on the coercive force and magnetooptical properties of films with a 33-60 percent Dy concentration by weight produced by thermal evaporation of Co and Dy simultaneously from two crucibles is examined. The dependence of the coercive force and Faraday effect on the storage duration, the dependence of the stability parameter on the production conditions, the chemical composition behavior during pickling in a vacuum measured by Auger spectral analysis, the behavior of the coercive force and Faraday effect under vacuum annealing, the dependence of the Faraday effect on storage duration, and the dependence of the coercive force and Faraday effect on the storage duration in films with 40 percent Dy are plotted. The results show that amorphous Dy-Co film precipitation in a vacuum improves the stability of their parameters in time while the behavior of the magnetic and magnetooptical properties of films is affected primarily by oxidation. Structural relaxation effects are observed at $T>300$°C. It is shown that protection of films by thin Dy layers on both sides prolongs the parameter stabilization time by more than three orders of magnitude. The authors are grateful to V.G. Myagkov for help with measurements and L.I. Vershinin for help with electron microscopy studies. Figures 6; references 7: 2 Russian, 5 Western.

Rotational Hysteresis Losses in Co-Ni-W Films

927D0133D Sverdlovsk FIZIKA METALLOV I METALLOVEDENIYE in Russian No 10, Oct 91 pp 96-99

[Article by V.M. Fedosyuk, M.U. Sheleg, N.N. Kozich, L.N. Makutina, Solid State Physics and Semiconductors Institute at the Belarussian Academy of Sciences; UDC 669.24'25'27':539.216.2:621.317.47]

[Abstract] The use of films from cobalt-based alloys with additions of nickel and tungsten as data media in devices with vertical and quasivertical recording principles due to their broad range of magnetic characteristics is discussed and torque in hard magnetic Co-Ni-W alloy films with perpendicular magnetic anisotropy is investigated. The torque curves in 0.7 μm thick Co-Ni-W films at various magnetic field strengths and the dependence of the rotational hysteresis losses on the magnetic field strength in Co-Ni-W films of various thickness are plotted. An analysis of the curves shows that in the case where torque does not depend on the angle between the magnetization angle and the external magnetic field, the sample is isotropic at all points or the dispersion of the axis of easy magnetization (OLN) at all points adds up to 360°. The conclusion is drawn that the magnetization reversal in the film occurs by means of a nonuniform curling of the magnetization vector. It is noted that correct analysis of the magnetization reversal process in films consisting of alternating areas with a different crystallographic texture and, consequently, areas with a different magnetization vector orientation, calls for numerically estimating the rotational hysteresis losses and the rotational hysteresis integral. Figures 2; references 12: 6 Russian, 6 Western.

Numerical Analysis of Magnetization Reversal Process and Magnetic Heterogeneities of Co-Ni-W Hard Magnetic Alloy Films

927D0133E Sverdlovsk FIZIKA METALLOV I METALLOVEDENIYE in Russian No 10, Oct 91 pp 100-104

[Article by M.U. Sheleg, V.M. Fedosyuk, Solid State Physics and Semiconductors Institute at the Belarussian Academy of Sciences; UDC 537.622:539.216.2]

[Abstract] The use of films from cobalt-based alloys with additions of nickel and tungsten as data recording and storage media in devices with vertical and quasivertical

recording principles due to their broad range of magnetic characteristics is discussed, and a model of the magnetic structure and magnetization reversal in this films is proposed; within a certain range of magnetic and geometrical parameters, the model makes it possible to ensure consistency of computational and experimental data. Hysteresis loops, the behavior of coercive force in the direction perpendicular to the film surface as a function of the magnetization direction, and the rotational hysteresis losses calculated under various assumptions are plotted. An analysis demonstrates the inhomogeneity of the magnetic parameters of Co-Ni-W hard magnetic alloy films; this inhomogeneity is numerically estimated and the probabilistic character of the estimate is emphasized; Student's *F*-criterion with a 10 percent significance level is used. Figures 1; references 6: 5 Russian, 1 Western.

Magnetic Properties of Y-Fe-B Films

927D0133F Sverdlovsk FIZIKA METALLOV I METALLOVEDENIYE in Russian No 10, Oct 91 pp 200-202

[Article by A.S. Solovyev, N.A. Manakov, Ye.V. Krasnikova, Irkutsk Teachers College and Voronezh Polytechnic Institute; UDC 669.15'893'794:539.216.2:537.622]

[Abstract] The properties and applications of magnets from hard magnetic $R_2Fe_{14}B$ alloys where R is a rare earth element (RZE) are discussed and the need to examine their properties in various structural states in order to realize their potential more fully is stressed. Magnetic properties of $T_{12}Fe_{82}B_6$ 10 μm thick films produced by ion plasma sputtering onto aluminum and silicon substrates cooled with liquid nitrogen in an argon atmosphere in an orienting magnetic field parallel to the film plane are studied in the amorphous and crystalline states. The field dependence of the alloy's magnetostriction in the amorphous and crystalline state, minor hysteresis loops of the crystalline alloy, and magnetization curves after thermal demagnetization, reverse field degaussing, and alternating field degaussing as well as the magnetization reversal curve and return curve of the crystalline alloy are plotted. The magnetic ordering temperature, saturation magnetization, coercive force, and magnetostriction of the alloy in the crystalline and amorphous state are summarized. An analysis shows that the magnetization curves are similar in shape for various degaussing methods but differ sharply in the critical field of irreversible magnetization change; the films are characterized by a high relative remanent magnetization in any direction parallel to their plane. Thus, the Y-Fe-B alloys may have both an extremely low (20 A/m) and very high ($2 \cdot 10^5$ A/m) coercive force and are useful for studies of the hysteretic properties in amorphous-crystalline materials. Figures 3; tables 1; references 11: 5 Russian, 6 Western.

Endurance Analysis Procedure for Multilayer Coats With External Ceramic Layer

927D0138A Kiev FIZIKO-KHIMICHESKAYA MEKHANIKA MATERIALOV in Russian Vol 27 No 3, May-Jun 91 pp 7-12

[Article by L.B. Getsov, A.I. Rybnikov, P.G. Krukovskiy, A.A. Rabinovich, Proletarskiy Zavod Leningrad Branch; UDC 539.219:405.08]

[Abstract] A procedure for analyzing the endurance of multilayer coats with an external silicon layer on gas turbine engine (GTD) parts is studied. To this end, the factors determining the coat's service life, such as external operating conditions, i.e., temperatures, stresses, salt exposure, composition and intensity of the corrosive mixture flow in gas, and intensity of the solid particles causing surface erosion as well as such internal factors as the coat composition, the base metal composition, and the characteristics of the coat deposition method are examined. The extent of corrosion damage to multilayer coats with the silicon layer, and after the layer has eroded, is measured and the behavior of the ceramic layer under prolonged operation is analyzed. The effect of the exposure temperature on the Al_2O_3 film thickness on the SDP8 sublayer, the effect of the exposure duration on the Al_2O_3 film thickness on the SDP8 sublayer, and the nickel distribution in the SDP8 coat after deposition and after a 10,000 h exposure to 800°C are plotted and the following stages are formulated for analyzing the corrosion endurance: the Al_2O_3 film growth stage on the ceramic layer's boundary with the metal coat accompanied by a Ni redistribution; and corrosion of metallic coat layers following the peeling of the ceramic layer accompanied by a change in the coat composition. The corrosion endurance is then assessed by computing the service life of the ceramic layer and solving the problems of corrosion and nickel redistribution between the layers and the base metal. Figures 4; references 3.

On Issue of Protecting EP202 Nickel Alloy With Pd-Si Palladium Coats

927D0138C Kiev FIZIKO-KHIMICHESKAYA MEKHANIKA MATERIALOV in Russian Vol 27 No 3, May-Jun 91 pp 18-21

[Article by Ye.A. Antonova, L.P. Petrova, L.P. Yefimenko, Silicate Chemistry Institute at the USSR Academy of Sciences, Leningrad; UDC 621.793]

[Abstract] The urgency of protecting the EO202 nickel-based alloy from high-temperature corrosion in aggressive media with palladium-based coats and the difficulty of producing coats with a Pd concentration exceeding 80 percent by mass for this purpose are discussed, production of coats with a palladium concentration reaching 95.0-99.0 percent by mass on a nickel base with the help of powder roasting technology whereby the nickel concentration does not exceed 2.5 percent by mass is reported, and the possibility of protecting the EP202 nickel alloy with Pd-Si coats containing 1.0-3.5 percent Si by mass formed by the powder roasting method is investigated. To this end, the coat formation conditions, the coat structure, and the role of the intermediate nickel layer are studied. The ChPD-2 palladium and KR-1 crystalline silicon are used for preparing the powder composition and steel samples are used as the base. The coats are roasted in a vacuum furnace at a $133.3 \cdot 10^{-9}$ MPa residual pressure for 10 minutes. The phase composition of a coat containing 98 percent Pd and 2 percent Si, by mass is examined and the element distribution in the coat on the EP202 alloy with an intermediate nickel after roasting at 1,000°C for 10 minutes and heat

treatment 750°C for 15 hours is plotted. The microhardness of the same coat on various bases after the same roasting and heat treatment conditions with and without the intermediate layer is measured and compared to published data. The results demonstrate that a high-quality Pd-Si coat with a 96.0-99.0 percent Pd content by mass may be produced on the EP202 alloy without the intermediate layer. Figures 1; tables 2; references 7: 6 Russian, 1 Western.

Effect of Plasma-Sprayed Coats on Fatigue Strength of Aluminum Alloys

927D0138D Kiev FIZIKO-KHIMICHESKAYA MEKHANIKA MATERIALOV in Russian Vol 27 No 3, May-Jun 91 pp 21-24

[Article by N.S. Surov, S.V. Babin, Moscow Aviation Engineering Institute imeni K.E. Tsiolkovskiy; UDC 621.793.73]

[Abstract] The use of gas-thermal deposition, particularly plasma-jet spraying, for improving wear resistance and the effect of plasma jet sprayed coats on the endurance strength of aluminum alloys are discussed; the effect of plasma-sprayed PN70Yu30 coats on the endurance strength of samples from the D1ch and D16A-T is investigated. Fatigue tests of the samples are conducted in the resonance mode on a VDES-200 vibroelectrodynamic tester. The sample base temperature after a different number of loading cycles to failure, the coat and base stress, porosity, and deposition conditions are summarized and sample fractograms are cited. The number of loading cycles to failure is lower for plasma-jet sprayed samples than for uncoated samples. An analysis of the experimental findings indicates that plasma-jet sprayed coats decrease the endurance strength of samples from the D16A-T alloys by 30 percent and those of the D1ch alloy—by 85 percent; the fatigue strength of the D1ch alloy samples plasma-jet sprayed with the PN70Yu30 powder after hardening and artificial aging increases by an average of 100 percent and that of the D16A-T alloy samples after hardening and natural aging increases by more than 50 percent. Figures 4; tables 3; references 7.

On Effect of Gas Saturated Layer Removal Depth on Repeated Static Endurance and Ductility of OT4 and VT6ch Titanium Alloys

927D0138E Kiev FIZIKO-KHIMICHESKAYA MEKHANIKA MATERIALOV in Russian Vol 27 No 3, May-Jun 91 pp 25-28

[Article by A.B. Kolomenskiy, B.A. Kolchayev, A.V. Degtyarev, A.N. Roshchupkin, Voronezh Aviation Production Association; UDC 621.785.3:669.295]

[Abstract] The effect of the degree of the gas saturated layer (formed in the course of annealing) removal by pickling on the repeated static endurance is discussed, and the effect of incomplete gas saturated layer removal on the ductility of high-strength alloys and their behavior after straining under cyclical loading conditions is investigated. To this end, 0.8-3.0 mm thick VT6ch and OT4 sheet alloy samples are tested; some of the VT6ch cyclical test samples are made from the base metal and some—with a weld made by argon arc welding with through penetration. The samples are annealed before repeated static tensile tests and Erichsen tests in an MTL-10G-1 unit. The interstitial impurity distribution in the surface layers is measured by a Camebax X-ray spectral analyzer and the X-ray structural analysis is carried out in a DRON-3m unit. An analysis of the test results shows that all samples are characterized by the same pattern: incomplete removal of the gas saturated layer by pickling vs. complete removal leads to a certain increase in the repeated static endurance (by a factor of 1.1-1.25) while the optimal increase in microhardness amounts to 7-12 percent. Thus, the optimum removal depth ensuring the maximum cyclical endurance exceeds the pickling depth necessary for restoring ductility. Consequently, regulated incomplete removal of the gas saturated layer may have a positive effect on the resistance of titanium alloy sheets to repeated static loads without sacrificing ductility; it is expedient to use this feature only for low- and medium-strength alloys. Figures 3; references 4.

Increasing Steel 12Kh18N10T Endurance by Palladium Coat Under High-Temperature Thermal Cycling in Ammonia Decomposition Product Medium

927D0138I Kiev FIZIKO-KHIMICHESKAYA MEKHANIKA MATERIALOV in Russian Vol 27 No 3, May-Jun 91 pp 111-113

[Article by V.V. Zyryanov, Yu.D. Nikiforov, Physicomechanical Institute imeni G.V. Karpenko at the Ukrainian Academy of Sciences, Lvov; UDC 620.193.5:620.197.6]

[Abstract] Methods of developing a highly efficient protective coat for increasing the service life of parts from steel 12Kh18N10T operating in contact with a nitrogen- and hydrogen-containing gaseous mixture under the rigid conditions of high-temperature thermal cycling within a 20-1,000°C temperature range are investigated. Palladium is selected is the protective coat material due to its ductility and inertness to nitrogen at temperature of up to 1,400°C. Tubular samples are tested in the vacuum chamber of the IMASh-20-75 tester in the medium of ammonia decomposition products. Tests show that high-temperature nitriding is the principal cause of corrosion in steel. The nucleation of cracks which facilitate access to the inner metal areas is due to a significant difference in the thermal expansion coefficients and ductility of the base metal and the resulting nitrogen-containing phases. Palladium coats can effectively protect steel for high-temperature nitriding under isothermal and cyclical exposures. The resistance of Pd-coated steel 12Kh18N10T is much greater than that of the NMR-15-10 alloy while the protective properties are maintained at any Pd concentration within a 65-100 percent range. Palladium may be thus recommended for use with steel 12Kh18N10T and the NMR15-10 nickel alloy. Figures 4; references 6.

Using Plasma-Assisted Chemical Vapor Deposition Method To Produce Oxycarbonitride Coats on Hard Alloys

927D0146C Kiev POROSHKOVAYA METALLURGIYA in Russian No 2 (350), Feb 92 pp 18-23

[Article by L.A. Ivashchenko, G.V. Rusakov, Institute of Materials Sciences Problems at the Ukrainian Academy of Sciences; UDC 621.793:620.197:669.018.45:621.9.02]

[Abstract] The plasma-assisted chemical vapor deposition (PACVD) method and its advantages are discussed, and the possibility of depositing mono- and bilayer coating onto the T15K6, VK8, and KTS-2M alloys by the plasma-assisted chemical vapor deposition method at temperature above 550°C is evaluated. Square samples degreased in ethyl alcohol and pretreated by bombarding them with atomic hydrogen for 10 min are used in the experiments; titanium tetrachloride produced by vacuum distillation, methane, and hydrogen are used as raw materials for producing Ti and TiCNO. The films of titanium compounds are examined by visual inspection; the microhardness is measured at a 10-50 g load. The development conditions of mono- and bilayer coats are summarized. An analysis of the test results demonstrates that the best Ti-containing CVD coat is deposited on the VK8 alloy while the most porous near-surface zone forms on the KTS-2M alloy. Furthermore, an intermediate barrier layer which does not contain Ti and prevents the decarburization and loosening of the base metal—such as silicon carbide or aluminum oxide—is necessary for producing high-quality CVD coats on hard alloys containing titanium carbide. Figures 3; tables 5; references 6: 4 Russian, 2 Western.

Structural Changes in Gas Thermal Coat's Surface Layer Under Ultrasonic Steel Ball Machining

927D0146D Kiev POROSHKOVAYA METALLURGIYA in Russian No 2(350), Feb 92 pp 23-28

[Article by Yu.S. Borisov, A.G. Ilyenko, A.L. Gaydarenko, A.A. Gordonnaya, V.N. Sladkova, Electric Welding Institute at the Ukrainian Academy of Sciences; UDC 621.793]

[Abstract] The structural changes in the coat's surface layer resulting from flame spraying, e.g., the development of microcracks and internal residual tensile stress, a decrease in the bearing surface area of the newly formed microrelief, etc., which considerably degrade the coat's protective properties under normal operating conditions are considered, and methods of improving the surface quality by machining are discussed. Attention is focused on using ultrasonic machining with steel balls for improving the structure and properties of the deposited coats. In particular, the effect of ultrasonic surface treatment distinguished by the effect of "soft" impact due to the relatively low impact energy with multiple repetitions is investigated. Coats of $1 \cdot 10^{-4}$ m and $4 \cdot 10^{-4}$ m thick PG-10N-01 powder are deposited on steel 3 with the help of the Kiyev-7 unit, and the ultrasonic surface machining is performed with ShKh-15 steel balls with a $2 \cdot 10^{-3}$-$5 \cdot 10^{-3}$ m diameter using a unit consisting of the 2-4M ultrasonic generator (UZG) and a PMS-15A-18 magnetostrictive converter. The surface roughness is measured by a model 252 surface roughness recorder and surface roughness gauge. An analysis shows that ultrasonic machining of flame sprayed surfaces with a microhardness of 5,630-7,890 MPa reduces the surface roughness by 1.5-2 times whereby the process duration depends on the residual compressive stresses and properties of the base metal. The steel ball impact affects the surface mosaic block dimensions, dislocation density, and microstresses in the coat surface layer. Under fretting conditions, the ultrasonic-machined surface wear resistance increases by fourfold. Figures 4; references 16: 15 Russian, 1 Western.

Physicochemical Aspects of Detonation Coats' Adhesive Bond Formation. II. Coat-Base Composite Failure Characteristics

927D0146E Kiev POROSHKOVAYA METALLURGIYA in Russian No 2 (350), Feb 92 pp 28-32

[Article by S.N. Buravova, A.A. Goncharov, Yu.N. Kiselev, E.A. Mironov, Yu.P. Fedko, Structural Macrokinetics Institute at the USSR Academy of Sciences, Energy Science Research Institute, and Scientific Research Institute of Automotive Industry; UDC 621.793.7]

[Abstract] The ability of dissimilar materials to resist separation, i.e., their adhesion, is examined from two viewpoints: the formation of the adhesive contact and the failure of the adhesive seam. In particular, the physicochemical aspects of the adhesion bond formation of detonation coats and the failure characteristics of the coat-base composite are investigated. To this end, the adhesive seam is examined on M40 aluminum oxide coats deposited onto a base from steel 3 after four pretreatment procedures: regular sand blasting with No. 125 grain synthetic corundum; joint (regular and detonation) sand blasting; detonation sand blasting with No. 50 grain synthetic corundum; and no treatment. The failure mechanism of the transition zone during normal coat tear and the dependence of the adhesive bond strength and the metallic phase content on the tearing surface on the surface roughness are plotted. An analysis of experimental data indicates that a strong adhesion bond under detonation spraying is due to the plastic deformation of the materials on the contact surface with a high compressive stress level; it is speculated that this bond cannot be classified as mechanical since its energy exceeds the Van der Waals energy, nor can it be regarded as chemical. The strong bond forms at the initial deposition phase, and the taut strained state of the base and coat material makes the principal contribution to the bond strength while the recrystallization and nonchemical plastic welding are the most likely bond formation mechanism. The origin of the forces holding the coat on the base needs further systematic studies. Figures 4; references 9.

Kinetics of Chromium Carbide Alloy Coat Deposition by Electrospark Alloying Method

927D0146F Kiev POROSHKOVAYA METALLURGIYA in Russian No 2(350), Feb 92 pp 32-37

[Article by V.N. Klimenko, V.K. Gayuk, A.D. Verkhoturov, V.A. Maslyuk, Institute of Materials Science Problems at the Ukrainian Academy of Sciences; UDC 621.762:621.793:661.665:669.26:621.9.048.4]

[Abstract] The shortcomings of the standard TK and VK hard alloy electrodes used for electrospark alloying (EIL) and the increasing scarcity and cost of tungsten prompted an investigation of chromium carbide-based compositions (KKhN25, KKhNF15, chromium carbide with Ni and NiP binders, and Cr_3C_2 chromium carbide) as materials for electrospark alloying electrodes; it is assumed that steels 60 and 65G and stainless steel 12Kh18N9T are used as the base, i.e., cathode. A formula for determining the electrospark alloying efficiency is derived; an analysis of the kinetics of the elecrtospark alloying shows that that the best coat development conditions are attained by alloying with the KKhNF15 electrodes. It is recommended that intermediate Ni and ferrochrome layer be applied in order to improve the coat formation conditions; successive alloying of the surface with the KKhNF15 alloy, nickel, and ferrochrome makes it possible to produce solid and uniform corrosion resistant coats. The secondary structures forming on the electrode surface do not degrade the coat development conditions. A chemical analysis of the electrospark alloy deposited by the KKhNF15 electrode on steels 60, 65G, and 12Kh18N9T reveals that it contains α-Fe, γ-Fe,, a Fe-Ni solid solution, and chromium carbide. Figures 5; tables 1; references 2.

Low-Temperature Shaping of Thick-Walled Composite Rings

927D0129A Riga MEKHANIKA KOMPOZITNYKH MATERIALOV in Russian No 4, Jul-Aug 91 pp 721-724

[Article by Ye.I. Stepanychev, V.V. Musatov, V.S. Pichugin, A.P. Ryazanov, Moscow Aviation Engineering Institute imeni K.E. Tsiolkovskiy and Central Scientific Research Institute of Specialized Machine Building, Moscow oblast; UDC 678.027.94(088.8)]

[Abstract] The shortcomings of dry and wet winding—a simple method of making composite material (KM) products—and the limitations of programmed winding necessitated the development of a new method of making thick-walled composite items: the fibrous filler impregnated with a liquid binder is wound while the layers already placed on the mandrel are cooled to a temperature at which the binder viscosity increases sharply. Consequently, the radial pliability of the semifinished product being shaped decreases, and the binder filtering through the sheets ceases; as a result, products with an identical tension of the reinforcing material and a uniform binder concentration are manufactured. The effect of the winding method on the composite material density is investigated and such physical and mechanical characteristics of thick-walled composite rings as density, tangential strength, specific tangential strength, radial strength, specific radial strength, interlaminar shear strength, and specific interlaminar shear strength are summarized. An analysis of the results shows that the use of low-temperature shaping makes it possible to increase the radial tensile strength by 13 percent and the interlaminar tangential shear strength by 11 percent. Figures 1; tables 1; references 7.

Effect of Static and Cyclical Loads on Elasticity Moduli of Al-B Composite

927D0129B Riga MEKHANIKA KOMPOZITNYKH MATERIALOV in Russian No 4, Jul-Aug 91 pp 737-739

[Article by N.L. Kuzmin, V.I. Sidorov, V.A. Chelnokov, Leningrad State Engineering University; UDC 539.37:678.067]

[Abstract] The effect of component properties and macrostructure and its defects on the properties of fibrous composite materials (VKM) and the problem of identifying microstructural defects—ruptured fibers and loss of bonding between the matrix and the fiber—are addressed, and an Al-B fibrous composite produced by hot rolling is investigated. To this end, moduli of elasticity are measured by the vibrational and pulse methods after thermal cycling and flexural cyclical loading; in addition, the modulus is measured directly under a static load. The curves of the dependence of elasticity modulus variation measured by both methods on the number of bending cycles, thermal cycles, and the load value, the dependence of elasticity modulus variation on the external load in the initial state and after cycling, and the dependence of the moduli of elasticity on the exposure to 777K and flexural cycling are plotted. An increase in the elasticity modulus under loading is noted. The difference in the vibrational and pulse elasticity moduli makes it possible to differentiate the interface fracture from the fiber rupture defects. Figures 3; references 4.

Technique for Cyclical Bending Tests of Thin Elastic Specimens

927D0129C Riga MEKHANIKA KOMPOZITNYKH MATERIALOV in Russian No 4, Jul-Aug 91 pp 740-743

[Article by V.M. Parfeyev, Yu.Yu. Silis, A.Kh. Dukats, Polymer Mechanics Institute at the Latvian Academy of Sciences, Riga; UDC 620.17:678]

[Abstract] The limitations of existing cyclical bending tests which are intended primarily for rigid polymer materials and thick elastomer specimens are discussed, and a new procedure for cyclical bending tests of this elastic items is proposed. Samples with an extended damaged zone used in structural or biomedical research are made by rolling the specimen through cylindrical rolls; in a UPK-2 tester, an elastic sample is passed through a reciprocating carriage with five rolls as a result of which the sample undergoes alternating bending. Schematic diagrams of the device and the sample zone subjected to cyclical bending are cited, and strain cycles at various wrap angles are plotted. The results of cyclical bending tests of polystyrene, polyethylene oxide, organosilicon rubber reinforced with knitted fabric, polyurethane, and other materials at various wrap angles are summarized. Figures 5; tables 1; references 6: 5 Russian; 1 Western.

Investigation of Adhesive Properties of Organosilicon Compounds for Optical Fiber Joining

927D0129D Riga MEKHANIKA KOMPOZITNYKH MATERIALOV in Russian No 4, Jul-Aug 91 pp 743-747

[Article by R.Ye. Tolchinskaya, Ye.I. Alekseyeva, S.P. Nanushyan, I.Yu. Ruskol, V.A. Pechenin, State Scientific Research Institute of Heteroorganic Compound Chemistry and Technology, Moscow; UDC 539.612:532.6]

[Abstract] The use of optical fibers with double cladding necessitated the use of the JOINT organosilicon compounds produced by an addition+curing reaction for joining them. The adhesion of the JOINT compound to the surface of osch fused quartz fibers with a 200-300 μm diameter, to steel fibers with a 150 μm diameter, to optical fibers coated with the SIEL compound during the drawing with a 410 μm diameter, and to optical fibers coated with the SABS compound during the drawing with a 450 μm diameter is investigated experimentally; the SIEL organosilicon elastomers are used as reflecting and buffer coats and the SABS siloxanarylate block copolymers are used as the reinforcing coats. The JOINT compound is cured in the presence of platinum catalysts at a 180°C temperature as well as by a beam of accelerated electrons at an up to 1,200 kgR dose. The quality of adhesion is determined by tearing the fiber from the assembly while the assembly destruction tests are performed using an adhesion meter. The dependence of the adhesion strength on the contact area, the effect of the curing duration on the adhesion strength, and the effect of the curing temperature on the

adhesion strength are plotted. In addition, the dependence of the adhesion strength of the JOINT-steel fiber joint on the irradiation dose is summarized. At a 1,200 kgR doze, there is no curing of the JOINT-metal fiber joint, probably due to the presence of phenyl radicals with a high absorptance in the compound. The results demonstrate that the adhesion strength of the JOINT organosilicon composites with optical fiber elements does not significantly depend on the compound composition and the type of the substrate but depends more on the contact area and curing conditions. The highest adhesion strength corresponds to polymer-steel fiber joints with $l/d<3$. Figures 3; tables 1; references 5.

Computational-Experimental Analysis of Nonisothermic Composite Curing on Mandrel

927D0129E Riga MEKHANIKA KOMPOZITNYKH MATERIALOV in Russian No 4, Jul-Aug 91 pp 747-750

[Article by S.V. Bochkareva, A.I. Tsaplin, Perm Polytechnic Institute; UDC 678.2.001:678.067:539.373]

[Abstract] The effect of the curing conditions on the quality of polymer composite materials (PKM) and the final physical-mechanical characteristics of the material and the problem selecting optimum curing parameters are discussed, and it is shown that the problem can be successively solved by developing a mathematical model. A system of conjugate thermal energy transfer equations, which fails to account for the heat accumulation by the mandrel affecting the composite's temperature field, proposed earlier is inadequate; consequently, the process of nonaxisymmetric curing in an annular composite with specified inside and outside composite shell radii placed onto a cylindrical mandrel with a given radius rotating at a constant angular velocity is considered, and the curing the process is described by a system of conjugate thermal energy transport equations and curing kinetics expressed in a nondimensional form. The computational experiment is performed by the finite difference method, and the computation algorithm is realized in Fortran for two types of mandrels: aluminum and sand-polymer composite (PKK). The model's adequacy is checked by experiments with a model organic plastic shell being cured on a massive sand-polymer composite in a furnace; experimental data are consistent with the theoretical results. Figures 4; references 4: 3 Russian, 1 Western.

An Investigation of the Compatibility of a Titanium Alloy Matrix With Ceramic Fibers

927D0130M Moscow FIZIKA I KHIMIYA OBRABOTKI MATERIALOV in Russian No 5, Sep-Oct 91 (manuscript received 1 Jun 90) pp

[Article by V.I. Bakarinova, V.N. Meshcheryakov, T.T. Nartova, and O.B. Tarasova, Moscow; UDC 669.018.9:669.295]

[Abstract] The authors of the study reported herein compared the compatibility of the matrix of a titanium alloy with one of three possible matrices (boron fibers, boron coated with silicon carbide [borsic], and silicon carbide). The model titanium alloy studied was doped with a constant (3 percent by weight) amount of Al, Zr, and W. The matrix alloy was used in the form of foil up to 100 μm thick, and the diameter of the reinforcing fibers ranged from 100 to 150 μm. The study composites were manufactured by the technique of vacuum diffusion welding of built-up blanks. The process used to produce the fiber composites resulted in a fiber-matrix interface that was free of metallographically visible interaction. The degree of interaction resulting from adding each of the aforesaid reinforcing fibers to the matrices was determined from metallographic studies and from microscopy studies with a Neofot microscope at magnifications of 500 to 1,000x. Microscopy was also used to estimate the thickness of the diffusion zones formed after vacuum heat treatment at temperatures of 800 to 1,000°C for one to 100 hours. A JSM-U3 scanning electron microscope was used for fractographic and microanalysis of the fiber composites. The studies performed revealed that in the case of the fiber composite reinforced with silicon carbide fibers, a diffusion zone formed and grew along the perimeter of the fiber at the fiber-matrix interface in the form of a ring of even thickness. When boron reinforcing fibers were used, the diffusion zone only remained uniform in the initial stage; temperature increases caused the zone to become nonuniform. In the case of borsic, the interaction initially followed the same course as that involving silicon carbide; after the coating's integrity broke down or after it dissolved, a reaction resulting in the formation of titanium borides occurred. In the titanium-silicon carbide systems studied, TiC, Ti_5Si_3, and $TiSi_2$ phases were found at the interface; in the titanium-boron systems, titanium di- and monoboride were found to form. At a temperature of 800°C, all of the reinforcing fibers tested had similar interaction zone thicknesses. At temperatures of 900 and 100°, however, interaction at the titanium fiber-composite interface was found to increase in the following sequence: boron - borsic - silicon carbide. Figures 4, table 1; references 4 (Russian).

Effect of Titanium Nitride Coat Application Conditions on Its Wear Under Fretting Corrosion

927D0149G Minsk TRENIE I IZNOS in Russian Vol 13 No 2, Mar-Apr 92 pp 350-355

[Article by A.G. Molyar, A.I. Vasilyev, Kiev Civil Aviations Engineers Institute; UDC 621.91:669.295]

[Abstract] The use of wear resistant coats applied by various methods, such as ionic plasma-jet deposition in the cathode material erosion product vapors, i.e., condensation with ionic bombardment (KIB), and its principal shortcoming—the excessive dependence of the operating properties of the resulting coats on the application process parameters—are discussed. The wear resistance of friction surfaces during the fretting corrosion of a TiN coat applied under various conditions in a friction pair with steel 30KhGSA is investigated. An experiment conducted for determining the effect of the nitrogen pressure on the coat properties is described; the nitrogen pressure is the sole manipulated variable; the remaining parameters are maintained constant. The microhardness variation throughout the layer cross section on steel 11Kh11N2V2MV is

plotted, demonstrating the increasing effect of the substrate near the interface with the coat. Fretting corrosion tests are conducted in an MFK-1 tester and coats are applied in an NNV-6.6-I1 to polished surfaces of cylindrical samples from the VT22 titanium alloy. The effect of the nitrogen pressure during the sputtering on the sample wear and the surface microhardness under fretting corrosion is plotted and the surface topology is examined under a JSM-35C scanning electron microscope. The results show that the wear of the TiN coat and the friction pair counterpart depends on the nitrogen pressure and, therefore, on the coat composition and structural state. The latter two factors affect the character of coat fracture under friction. Surface defects which serve as crack nuclei under both brittle and steady-state fracture mechanisms influence the coat cracking during fretting corrosion tests. Figures 3; references 3.

Tribological Characteristics of Polymer Composite Materials and Carbon-Carbon Composites on Their Basis

927D0149I Minsk TRENIE I IZNOS in Russian Vol 13 No 2, Mar-Apr 92 pp 373-377

[Article by Z.Zh. Ovcharova, M.I. Lyubcheva, I.M. Todorov, L.A. Lyubchev, Burgas, Bulgaria; UDC 620.178.162.4]

[Abstract] The advantages of friction and antifriction materials made from composites with various matrices and fiber and disperse fillers, e.g., carbon fibers, are discussed, and the need to modify the carbon fibers in order to change their physicochemical surface properties as well as the physical and mechanical properties of composites on their basis is emphasized. Carbon plastics (UP) and carbon-carbon composites on their basis are investigated, and their physical, mechanical, and tribological characteristics are analyzed. A novolac soluble phenol formaldehyde resin oligomer is used as the polymer matrix, and two types of carbon plastics are uses as the reinforcing filler. The friction coefficient and wear rate are measured using a pin-disk friction gauge with steel 45 as the counterbody. The density, modulus of elasticity, bending strength, friction coefficient, and wear rate of various carbon-carbon composites, the density, bending strength, and friction coefficient of carbon plastics on the basis of a nonwoven textile carbon material (UNTM) and novolac oligomer, and the dependence of the friction coefficient on the testing speed and load for a carbon plastic with 5 percent of talc are summarized. All the materials tested have a good temperature resistance and chemical inertness; their friction coefficient can be manipulated by using various disperse fillers within a 0.20-0.27 range for carbon fiber materials and 0.33-0.47 for carbon-carbon composites. Tables 4; references 5: 4 Russian, 1 Western.

On Radiation Strength of Carbon-Carbon Composites

927D0150H Moscow IZVESTIYA AKADEMII NAUK SSSR: SERIYA NEORGANICHESKIYE MATERIALY in Russian Vol 28 No 1, Jan 92 pp 66-71

[Article by Y.S. Virgilyev, I.P. Kalyagina, K.P. Vlasov, V.P. Ilin; UDC 621.039.532.21]

[Abstract] The use of fiber- and fabric-based carbon-carbon composites (UUKM) as diverters and shields in thermonuclear reactors and their behavior under irradiation are discussed; the radiation strength of KUP-VM, termar-TD, and carboxylar carbon-carbon composites is investigated. The density, thermal coefficient of linear expansion, electric resistivity, thermal conductivity, dynamic modulus of elasticity, bending and compressive strength, and the lattice constant are summarized. Devices used for extended temperature tests and in-pile measurements of ten round or square rod samples are described. The dependence of the change in the KUP-VM sample size under irradiation on the neutron fluence at various temperatures parallel and perpendicular to the reinforcing fibers measured by the passive and active methods, the dependence of the change in electric resistivity of the KUP-VM material on the neutron fluence at various temperatures, the dependence of the change in the termar-TD sample size on the neutron fluence at various temperatures perpendicular and parallel to the reinforcing fibers, and the dependence of the change in the carboxylar sample size on the electron fluence at various temperatures with and without a 5.9 MPa compressive load are plotted. The results of active (in-pile) and passive (after irradiation) tests of samples cut perpendicular and parallel to the reinforcing fibers show that the changes in the sample size and electric resistivity measured by both methods are almost identical, attesting to the absence of dynamic phenomena. The relationship between the sample size and the irradiation temperature, neutron fluence, and material structure is very complicated. Under the experimental conditions within a 320-1,700K temperature range and up to $2.8 \cdot 10^{21}$ neutron/cm^2 fluence at ≥ 0.18 MeV, all samples maintained their integrity. Figures 4; tables 1; references 8.

Mechanism of Compact Graphite Inclusion Formation in Pig Iron

927D0140A Moscow LITEYNOYE PROIZVODSTVO, No 1, Jan 92 pp 3-5

[Article by A.K. Biletskiy, V.S. Shumikhin, A.M. Verkhovlyuk; UDC 621.746.62:669.13]

[Abstract] The problem of compact graphite inclusion formation in the pig iron melt necessitated an investigation of the interface properties and characteristics of pig iron in the liquid state. The characteristic shapes of graphite crystals in carbon-saturated Fe-C melts on a pyrographite base under isothermal conditions produced by ionic etching are examined. The interface tension is analyzed by the sessile drop method under the condition identical to those of the crystal growth; a correlation between the difference in the wetting angles and adhesion energy on pyrographite's base and prismatic faces, a correlation of the minimum solidification rate which ensures production of spheroidal graphite, and the heat of carbon mixture with the solvent metal are plotted. The study demonstrates that the development of compact graphite inclusions in the pig iron melt is due to the suppression of the effect of the growing graphite crystal's crystallographic orientations at the optimum residual amount of spheroidizing elements in the melt and to the melt cooling within a certain rate range. By controlling the cooling rate, it is possible to fix the necessary liquid state until the moment of eutectic solidification and maintain a quasidiffusive inclusion growth condition as well as prevent chilling. Figures 3; references 11: 10 Russian, 1 Western.

Environmentally Sound Technology of Ladle Pig Iron Inoculation

927D0140B Moscow LITEYNOYE PROIZVODSTVO in Russian No 1, Jan 92 pp 8-9

[Article by V.M. Korolev, S.P. Korolev, N.I. Bestuzhev, V.M. Mikhaylovskiy, A.S. Dubrovin, Belarussian Polytechnic Institute and Chelyabinsk Scientific Research Institute of Metallurgy; UDC 621.74:669.131]

[Abstract] In order to improve the method of ladle inoculation—the most environmentally sound procedure—the possibility of using low-magnesium (2.5 to 3.5 percent Mg) inoculants whose poor spheroidizing ability is compensated for by increasing the concentration of rare earth metals (RZM) in them is examined. In so doing, the inoculant content is selected allowing for the thermodynamic characteristics of the interaction among magnesium, the rare earth metals, oxygen, and sulfur simultaneously added to the melt. These characteristics are analyzed by the Gibbs energy minimization technique. An environmental series and rate characteristics of magnesium-containing inoculants for ladle pig iron refining are plotted, and the cost of treatment is measured. Graphite modification transitions (from flake to interdendritic to vermicular to globular) with an increase in the magnesium concentration is examined. An analysis demonstrates that by substituting the FSMg7 inoculant with the Vermikulyar-2 inoculant developed in Chelyabinsk for ladle refining, one can significantly lessen the environmental impact of the process and reduce the amount of discharges and smoke release; by substituting the ChShG inoculant with the ChVG brand, it is possible to decrease the number of 8DVT engine block rejects due to shrinkage defects. Figures 1; references 1.

Using Production Waste for Pig Iron Alloying

927D0140E Moscow LITEYNOYE PROIZVODSTVO, No 1, Jan 92 pp 11-12

[Article by I.Ye. Illarionov, A.A. Agrayev, V.S. Moiseyev, Chuvash State University and Tsentrolit Foundry, Ulyanovsk; UDC 621.74:669.131.622]

[Abstract] The advantages of pig iron alloying with nickel are outlined. The high cost and scarcity of granulated nickel, ferronickel, and Cr-Ni cast iron prompted a search for a new process of alloying pig iron with the waste and byproducts of cobalt production, i.e., highly moistened nickel carbonates and hydrocarbonates with a 70-75 percent water content. An alloying composition for this purpose is prepared by heat treating, dehydrating, and enriching the mass, resulting in a loose granulated material with a high porosity containing 39-40 percent Ni. The nickel concentration and calcination losses (PPP) are measured and the phase composition is determined by an X-ray structural analysis. The Ni concentration and calcination loss behavior of Ni-containing cobalt production waste with temperature is plotted, and the Ni reduction and dissolution in cast iron in the ladle and in the mold are investigated. The results indicate that cobalt production waste is a suitable and potentially efficient alloying composition after heat treatment at 400-500°C; it makes it possible to produce Ni-containing cast iron in all types of cupolas. Figures 1.

Technologically Stable Processes of Making Pig Iron Castings With Increased Strength and Ductility

927D0140F Moscow LITEYNOYE PROIZVODSTVO in Russian No 1, Jan 92 pp 12-13

[Article by A.A. Zhukov, A.B. Yanchenko, S.V. Davydov, Vinnitsa Polytechnic Institute and Bryansk Automotive Engineering Institute; UDC 621.74:669.13.04]

[Abstract] Production of cast iron with vermicular graphite (ChVG)—the most technologically stable foundry process—is discussed and it is shown that cast iron with vermicular graphite occupies an intermediate position between grey cast iron with flaky graphite (ChPG) and high-strength cast iron with globular graphite (ChShG) with respect to its properties. The advantages of using cast iron with vermicular graphite—often referred to as cast iron with compact graphite (ChKG)—which forms at a high S:Mn concentration ratio as a result of alloying with sulfur or a decrease in the manganese concentration include chilling and rapid graphitization in the solid state. Method of improving the mechanical properties of compact graphite cast iron by inoculating it with Bi, Te, and Bi_2Te_3 additions and heat treatment are described and the

optimum conditions of graphitizing annealing are suggested. The mechanical properties of cast iron as a function of chemical composition and annealing duration at 1,223-1,253K are summarized. The new stable graduated process can be implemented even in old foundries with cupola heat smelting; each process step makes it possible to equalize and even eliminate the results of the previous step's instability. Figures 1; tables 2; references 2.

Wear Resistance and Mechanical Properties of Copper- and Boron-Alloyed Cylinder Cast Iron

927D0140G Moscow LITEYNOYE PROIZVODSTVO in Russian No 1, Jan 92 pp 14-15

[Article by B.M. Astashkevich, A.S. Bulyuk, All-Union Scientific Research Institute of Railroad Transport and MVIMU; UDC 621.74:669.15-196]

[Abstract] The macro- and microstructure of cylinder bushings made from copper- and boron-alloyed pig iron produced by spin casting at the Kandalaksha Pilot Machine Building Plant as well as their mechanical properties and wear resistance are investigated in order to improve their performance and extend their service life. The positive effect of up to 0.017 percent ferroboron addition on the microstructure is noted and the effect of copper additions on the cast iron strength and hardness is summarized. The dependence of the pig iron wear resistance on the distance from the casting surface for various alloying compositions is plotted; it is shown that the best wear resistance effect is attained by inoculating cast iron with a combination of copper and boron—a carbide forming element. An analysis of the mechanical tests demonstrates that together with boron, copper leads to a certain fracturing of the graphite inclusions, a decrease in the grain size, and an improvement in mechanical properties and wear resistance of castings. An addition of copper and boron oxide composition during spin casting of cylinders improves the structural uniformity, strength, and wear resistance. Figures 1; tables 1.

Failure Diagnostics of Vanyukov Furnace Water Jackets

927D0134A Moscow TSVETNYYE METALLY in Russian No 1, Jan 91 pp 7-9

[Article by V.I. Donets, A.M. Roldugin, A.V. Multanovskiy, I.V. Yelchishcheva, State Institute of Nonferrous Metals; UDC 669.33]

[Abstract] The issue of safe operation of water jackets in nonferrous metallurgy furnaces with a slag and matte melt in the case where a water leak may lead to an explosion is addressed and the need to develop a water jacket diagnostics procedure is stressed. A diagnostic technique is developed on the basis of estimating the thermal condition of the water jackets with the help of a mathematical model of the temperature fields in the water jacket body. The procedure is developed specifically for the operating conditions of water jackets for Vanyukov furnaces at the Norilsk copper smelter. Parabolic heat transfer partial differential equations are used as the initial mathematical model of the thermal processes occurring in the water jackets. Temperature fields in the furnaces are plotted and temperature thresholds in the water jackets are estimated. The adequacy of the model and the validity of the temperature patterns are checked by identifying the real heat flux densities on the fire surface and solving the external inverse heat transfer problems. A sequence of steps for operational checks of the water jacket conditions is suggested. The temperature threshold of the onset of hydrogen embrittlement of copper (400-450°C) corresponds to an outer temperature of the water jacket of 150-200°C depending on the design. The diagnostic procedure makes it possible to identify the anomalies pertaining both to the entire fire surface or its specific locations and predict the water jacket failure probability. Figures 3; references 4.

Metallurgical Gas Utilization Due to Improvement in Oxidative Autoclave Technology at Nadezhdinsky Metallurgical Works

927D0134B Moscow TSVETNYYE METALLY in Russian No 1, Jan 91 pp 10-12

[Article by B.I. Yerokhin, State Institute of Nonferrous Metals; UDC 669.243:66.046.8]

[Abstract] The shortcomings of existing hydrometallurgical flotation of the pyrrhotine concentrate at the Norilsk Mining Works (GMK), especially the poor iron oxide separation from metal sulfides and sulfur, prompted a study to assess the possibility of utilizing metallurgical gases and determining the parameters of selective leaching of iron oxides from the sulfur-sulfide concentrates (SSK) and other products of the autoclave oxidative process (AOT) by these gases. Experiments aimed at determining the gas utilization are described and the effect of the sulfur-sulfide concentrate pulp density and sulfur dioxide concentration on the leaching duration, the effect of the oxygen concentration on the iron recovery during leaching, the iron recovery from the autoclave oxidative process products during leaching, and the effect of the acid addition on the leaching of iron compounds is plotted. An analysis of the data indicates that it is possible, in principle, to utilize the flue gases for selectively dissolving iron compounds in pyrrhotine processing products and thus improve technological indicators of the process and reduce the consumption of imported metallized pellets and sodium sulfate. The use of AOT products as an absorbent also makes environmental and economic sense. A.A. Sedygina and the late F.D. Aptekar participated in this effort which is dedicated to the memory of I.M. Nelen. Figures 4; references 11.

Arsenic Behavior in Pyrometallurgical Process State at Dzhezkazgan Copper Smelter

927D0134C Moscow TSVETNYYE METALLY in Russian No 1, Jan 91 pp 13-14

[Article by I.I. Li, S.D. Ashirbekova, Dzhezkazgantsvetmet Scientific Production Association; UDC 669.33:669.778]

[Abstract] The metal behavior during electric smelting and converting is examined at the Dzhezkazgantsvetmet Scientific Production Association (DMZ) by statistical processing of annual arsenic balances during the 1980-1987 period when the ratio of imported copper- and gold-containing concentrates in the ore smelting furnace (RTP) charge to the local charge reached 44 percent while supply interruptions led to considerable fluctuations in the chemical composition of the charge, matte, and slag. The average annual composition fluctuations of the ore smelting furnace charge and electric smelting and converting process is summarized for Cu, Pb, Zn, SiO_2, CaO, Fe, and S and the arsenic concentration and distribution during various stages of electric smelting and converting in 1980-1987 and 1990 is tabulated. The arsenic distribution in the converting products as a function of the copper and arsenic concentration in the matte and the arsenic concentration behavior in the converter mass and and slag during the blasting are plotted. The findings demonstrate that 76-81 percent of arsenic, i.e., its principal amount, is transferred to the matte, dust, and gas during the electric smelting of the copper charge while As transfer to the dump slag is secondary. The arsenic fraction passing to the matte can be increased and the fraction transferred to the dust, and gas can be decreased by dressing the charge to increase the copper content and decrease the iron content. Atmospheric discharges of arsenic at the plant decreased by more than fourfold from 1980-1987 to 1990 due to a threefold reduction in the As content in the charge and a decrease in the proportion of As transferred to flue gases. Figures 2; tables 2; references 1.

Development of Copper Foil Surface Topography

927D0134D Moscow TSVETNYYE METALLY in Russian No 1, Jan 91 pp 14-17

[Article by A.A. Kucherov, V.N. Samoylenko, Urals Scientific Research and Development Institute of Copper Industry and Urals Polytechnic Institute; UDC 541.138:621.357.7:669.387]

[Abstract] The importance of the foil adhesion to the insulator in foil-plated insulators is stressed and the need to analyze the copper foil topography and determine the

effect of the cathode base material on the precipitated surface topography in order to ensure the necessary adhesion properties of foils used in plated insulators is formulated. The topography development of electrolytic precipitation copper foils is investigated in planar cathodes from mechanically polished (MT) and oxidized (OT) VT1-0 titanium and glass carbon (SU) material. Copper was precipitated onto the cathode immersed in the electrolyte at a strictly constant current density. The surface profile was recorded using a Kalibr-252 surface roughness recorder. The copper precipitate growth front spectrograms are plotted, and the frequency characteristic distribution of the copper precipitate profile on various bases is examined. A harmonic analysis of the profiles reveals a considerable similarity of the copper precipitate topography dynamics on oxidized titanium and glass carbon material while an analysis of spectral responses of the coat on polished titanium shows that an intensive growth of large grains begins at the start of electrodeposition. The results unambiguously point to the advantages of oxidized titanium and glass carbon material cathodes for use as matrices in making thin copper foil with a uniform adhesion surface. Figures 4; references 12.

Arsenic Recovery From Antimony Dust by Alkali Solution in Presence of Oxidants

927D0134E Moscow TSVETNYYE METALLY in Russian No 1, Jan 91 pp 21-22

[Article by M.U. Usubakunov, N.I. Sibichenkova, O. Satyvaldiyev, Ye.V. Muravyeva, R.Zh. Bazakeyev, A.M. Shuklin, INFKh at the Kyrgyz Academy of Sciences; UDC 669.753]

[Abstract] The urgency of processing the constantly increasing amount of production waste is illustrated using the example of the Kadamdzhay Antimony Works which generates such byproducts and waste as antimony dust and other arsenic-containing products forming during the processing of antimony raw materials. Some Sb and As is oxidized to volatile oxides, sublimated, and condensed. The importance of recovering these valuable materials prompted the development of a new technology since complete recovery can be accomplished only by changing the crystalline structure of the Sb- and As-containing materials. Consequently, the task of selecting reagents which change the crystalline structure of the antimony dust components and facilitate the formation of more easily soluble compounds is formulated, and an experiment conducted for this purpose is described. Arsenic and antimony recovery from the antimony dust as a function of the salt and base concentration, As recovery from the Sb dust as a function of nitric acid and hydrogen peroxide concentration, and As recovery from the Sb dust by a mixture of NaOH and hydrogen peroxide solutions are summarized. As a result, a simple method is proposed: adding antimony dust to a prepared NaOH solution while constantly stirring it and ensuring a solid:liquid ratio of 1:6 or 1:7, then, while still stirring the mixture, gradually adding the oxidant. Arsenic is recovered in the form of barium arsenate; 98.5 percent pure arsenic is subsequently recovered. The method was successfully tested at the Kadamdzhay Antimony Works. Tables 4; references 6.

Resistance of Nonmetallic Refractory Compounds to Cryolite-Alumina Melts

927D0134F Moscow TSVETNYYE METALLY in Russian No 1, Jan 91 pp 24-25

[Article by Ye.S. Gorlanov, Yu.V. Borisoglebskiy, M.M. Vetyukov, S.N. Akhmedov, Leningrad State Engineering University and Leningrad Engineering Physics Institute; UDC 669.713.7:666.762.856]

[Abstract] The effect on the cathode lining resistance to melts at high temperatures on the service life of aluminum smelter electrolyzers and the shortcomings of today's side lining made from carbon materials which fail under the effect of the electrolyte and aluminum melt are discussed. The corrosion resistance of AlN, BN, SiC, Si_3N_4 and BNC refractory materials (TM) to cryolite-alumina melts are investigated, and the experimental procedure is described. The sintering rate, density, porosity, and corrosion rate of various refractories in a cryolite-alumina melt (with 8.6 percent Al_2O_3) at a 100°C temperature are summarized, and the aluminum nitride corrosion curve in a cryolite-alumina melt at a 1,000°C temperature in the air, CO, and CO_2 and at 1,200°C in argon is plotted. The discrepancy of corrosion data is attributed to the difference in oxygen's and carbon dioxide's ability to dissolve in the electrolyte. An analysis of the corrosion resistance of refractories to cryolite-alumina melts indicates that silicon carbide and aluminum nitride materials are promising for use as side lining; its service life under normal conditions depends primarily on the alumina concentration, anodic gas composition, and the electrolyte temperature and hydrodynamics which determine the thermodynamic and kinetic conditions of refractory material corrosion. Figures 1; tables 1; references 6: 1 Russian, 5 Western.

Properties and Efficiency of Using Fluorine-Containing Flux for Removing Harmful Impurities From Aluminum by Refining

927D0134G Moscow TSVETNYYE METALLY in Russian No 1, Jan 91 pp 26-28

[Article by V.F. Anosov, Ye.N. Karnaukhov, G.V. Telyakov, V.S. Morozov, IF at All-Union Scientific Research and Design Institute of Aluminum, Magnesium, and Electrode Industry; UDC 669.714]

[Abstract] Various aluminum refining methods used throughout the world are discussed and the shortcomings of aluminum refining with the help of potassium chloride, sodium chloride, and cryolite fluxes are outlined. The possibility of refining aluminum with the help of a compact nonhygroscopic flux, e.g., fused, which does not contain chlorides and has an elevated concentration of aluminum fluoride—the active ingredient—is examined, and the feasibility of producing a flux with the highest possible aluminum fluoride concentration and studying its principal physical and chemical properties as well as checking its practical efficiency is analyzed. To this end, the properties of a two-component flux with a 50-70

percent of aluminum fluoride by mass are examined. The volatility and hygroscopicity of aluminum fluoride flux, the dependence of interface surface tension on temperature, and the dependence of the Al_2O_3 wetting angle on the fluoride concentration in the flux at 960°C are plotted. The initial flux solidification temperature, density at the melting point, surface tension, hygroscopicity, volatility, interface tension, and degree of adsorption by aluminum oxide are summarized, and the aluminum refining efficiency as a function of flux composition is determined. The conclusion is drawn that the use of fused binary flux with a 55-57 percent AlF_3 makes it possible to attain a higher refining degree than chloride and universal chloride-fluoride flux. The use of fused fluoride-containing flux eliminates the slagging conditions in the transfer ladle and lowers the hydrogen concentration from 0.17 to 0.1 $cm^3/100$ g or more and lowers the sodium, magnesium, and aluminum oxide impurity concentration by more than twofold. Figures 4; tables 2; references 8: 7 Russian, 1 Western.

Production Technology of Ferronickel With Elevated Nickel and Cobalt Content

927D0135A Moscow TSVETNYYE METALLY in Russian No 10, Oct 91 pp 20-21

[Article by N.N. Alekseyeva, I.I. Kapran, V.V. Koreneva, S.P. Kormilitsyn, State Nickel Industry Design Institute and Pobugskoye Nickel Works; UDC 669.15'24]

[Abstract] The poor utilization of cobalt contained in commercial ferronickel prompted attempts to increase the economic indicators of ferronickel production by finding new ways of cobalt utilization. A new method of producing FN-5K ferronickel with an elevated nickel and cobalt content is discussed, and the results of balance smeltings performed for the purpose of investigating the quantitative metal distribution among the converting products are summarized. The Si, C, Cr, S, and P impurity concentration in FN-5K ferronickel is analyzed and the Ni, Cu, and Co distribution curves are plotted. The metal balance is summarized on the basis of 14 smeltings; the imbalance does not exceed -7.23 percent, attesting to the correctness of theoretical analyses and the reliability of experimental data. The cobalt extraction into commercial ferronickel is sufficiently high—96.4 and 90.5 percent, respectively. The actual impurity concentration in FN-5K ferronickel is substantially below the permissible level. Production of permanent magnets on the basis of FN-5K ferronickel is underway at the Novocherkassk Magnet Production Association, making it possible to replace pure iron and cobalt with ferronickel. The economic impact at the Pobugskoye Nickel Works (PMZ) amounts to 1,000-1,100 rubles per ton of (Ni+Co) in 1987 and 1988. The service properties of permanent magnets made on the basis of ferronickel instead of pure metals are equal to those made by traditional methods. Figures 1; tables 2.

Anodic Behavior of Antimonite in Chloride Solutions

927D0135B Moscow TSVETNYYE METALLY in Russian No 10, Oct 91 pp 22-23

[Article by Guo Bin-Kun, Dai Ping-Wang, Yang Song-Zeng, Central-Southern Polytechnic University, China; UDC 669.753]

[Abstract] The anodic behavior of antimonite in chloride solutions is investigated by the potentiodynamic method, and constant potential electrolysis whereby the effect of the $[H^+]$ and $[C^-]$ concentration and the temperature and stirring rate on the process indicators is analyzed. The cyclical voltage-current curve of the Sb_2S_3 electrode prepared by compaction and vacuum sintering, anode polarization curves of Sb_2S_3 at various HCl and Cl^- concentrations and at various disc rotation speeds, and the effect of temperature on the anodic dissolution of Sb_2S_3 in HCl and NaCl are plotted. The solution composition behavior after constant potential electrolysis is summarized. The absence of cathode peaks corresponding to anode peaks indicates that Sb_2S_3 anodizing is an irreversible process; consequently, temperature significantly affects the reaction rate. An increase in the $[H^+]$ and $[C^-]$ concentration, temperature, and stirring rate leads to an increase in the polarization current and the Sb_2S_3 dissolution rate. The findings may be used in examining the process of acidic antimonite leaching. Figures 5; tables 1; references 4: 2 Western; 2 Eastern.

Low-Dislocation Single Crystals of Semiconductor GaAs for LSI Circuits

927D0135F Moscow TSVETNYYE METALLY in Russian No 10, Oct 91 pp 33-34

[Article by V.I. Biberman, A.V. Markov, V.B. Osvenskiy, S.S. Shifrin, State Institute of Rare Metals Industry; UDC 621.315.592]

[Abstract] The need for large-scale single crystals of gallium arsenide characterized by high electrical properties and purity as well as sufficiently perfect crystalline structure for making high-speed LSI and VLSI circuits by the ion implantation method and the shortcomings of Czochralski's method with liquid melt pressurization (ZhGCh) prompted the development of the modified Czochralski's method (MMCh) which makes it possible to grow GaAs crystals with a size close to the crucible diameter under a flux layer at temperature gradients reduced to <30°C/cm. The procedure of growing 85-90 mm dia. GaAs single crystals from cylindrical quartz crucibles is outlined, and it is noted that the resulting nondoped crystals have a dislocation density as low as $4 \cdot 10^3$ cm^{-2} with a local dislocation density in the cell walls of close to $5 \cdot 10^4$ cm^{-2}. Typical dislocation density distributions along the <100> and <110> radii in the (100) cross section of GaAs crystals grown by the conventional and modified methods and the EL2 center concentration distribution in polycrystalline GaAs single crystal grown by the modified method are plotted. An analysis of the GaAs single crystals shows that those grown by the modified method differ favorably from those grown by the conventional method with respect to their resistivity and Hall mobility and are characterized by significantly higher micro- and macrohomogeneity, making them an attractive materials for use as the substrate material for ion implantation VLSI chips. Figures 3; references: 4 Western.

Structure and Electric Properties of Rapidly Quenched Bi-As System Foils

927D0150C Moscow IZVESTIYA AKADEMII NAUK SSSR: SERIYA NEORGANICHESKIYE MATERIALY in Russian Vol 28 No 1, Jan 92 pp 16-19

[Article by V.G. Shepelevich, Belarussian State University imeni V.I. Lenin; UDC 548.5:669.76]

[Abstract] An electron and hole energy spectrum reordering in bismuth doped with under 10 percent antimony due to the difference in the atomic radii of Bi and Sb and the resulting strain in the crystals of their alloys prompted an investigation of the effect of arsenic doping on the electric properties and charge carrier parameters in bismuth, in rapidly quenched foils of the Bi-As system. To this end, Bi-As alloys are produced by smelting the components in quartz vials and crystallizing them in the same vials by a cold water jet, then remelting and splashing onto a rapidly spinning copper cylinder surface. X-ray studies of the foils are carried out in DRON diffractometers. The foil texture is studied by the inverse pole figures method, the pole density of diffraction lines is calculated by Harris's method, the foil resistivity, Hall coefficient, magnetoresistance, and differential thermo-emf are measured within a 77-300K temperature range using a R363-2 potentiometer. The concentration dependence of the relative lattice cell constant variation, electric resistivity, magnetoresistance, and Hall coefficient at 293K and the temperature dependence of resistivity, Hall coefficient, and thermo-emf of foils with 4 percent As are plotted, and the pole densities of diffraction lines at various As concentrations are summarized. The temperature behavior of resistivity and magnetoresistance during the isochronous annealing of foils with 8 percent As is examined. An analysis of the findings indicates that a 10T2 texture forms in the rapidly quenched alloy while the nonequilibrium As solubility in Bi reaches 6 percent. The behavior of the electric properties of rapidly quenched foils with concentration and temperature shows that bismuth doping with arsenic does not lead to a change in the electrons' and holes' concentration but decreases their mobility. Figures 3; tables 1; references 13.

Precrystallization Behavior of Pulse-Condensed Amorphous InSb Films

927D0150D Moscow IZVESTIYA AKADEMII NAUK SSSR: SERIYA NEORGANICHESKIYE MATERIALY in Russian Vol 28 No 1, Jan 92 pp 20-24

[Article by V.I. Petrosyan, O.I. Vasin, Saratov Department of the Radio Engineering and Electronics Institute at the USSR Academy of Sciences and Semiconductor Physics Institute at the Siberian Department of the USSR Academy of Sciences; UDC 538.9; 539.2; 548.5]

[Abstract] The effect of rapid pulse condensing in a vacuum at a rate exceeding the phase transition rate (about 1 μm/s) on the precrystallization behavior and crystallization of InSb films and the specific features of the A- and K-phase properties and behavior are studied. In so doing, the temperature dependence of the rapidly condensed A-film conductivity and short-range order structure are investigated. The films are deposited in a vacuum with a nitrogen trap by the pulse method at a 1 μm/s rate onto 50-100 μm thick mica substrates cooled to an 80K temperature. The substrates have metal film contacts made in them beforehand. The Hall signal of the A- and M-phases are beyond the instrument sensitivity range, so only the film resistivity is measured by the four-probe method using a special DC source and an X-Y plotter. The temperature dependence of resistivity of rapidly condensed InSb films, the radial density function, and the free energy of the metastable micronuclei formation are plotted, and the irreversible changes in the short-range order structure under heating within a 128-290K temperature range are summarized. It is shown that the irreversible changes occur with an increase in the maximum temperature while reversible changes occur below the maximum temperature, and the structure is preserved; the closer to the phase transition point, the sharper the resistivity's dependence on temperature in each cycle. Moreover, equilibrium is maintained in the system at all stages. Figures 3; tables 1; references 7: 6 Russian, 1 Western.

Forming $Hg_uCd_{1-u}Te$ Layers by Ion Exchange Method in Salt Solutions

927D0150G Moscow IZVESTIYA AKADEMII NAUK SSSR: SERIYA NEORGANICHESKIYE MATERIALY in Russian Vol 28 No 1, Jan 92 pp 57-60

[Article by V.A. Ganshin, Yu.N. Korkishko, V.A. Fedorov, Moscow Electronic Engineering Institute; UDC 621.315.595.4+541.183.12]

[Abstract] The shortcomings of liquid-phase and molecular beam epitaxy and gaseous phase precipitation from organometallic compounds for producing $Hg_uCd_{1-u}Te$ (KRT) layers on CdTe substrates—one of the most efficient structures for making infrared (IK) band photodetectors—are discussed, and the possibility of using the ion exchange substitution method for forming $Hg_uCd_{1-u}Te$ layers on CdTe substrates is examined. To this end, an experiment is made with (111) oriented CdTe wafers after mechanical and chemical polishing in a bromine solution in methanol. X-ray diffractometry in CuK_1 radiation using a *D*-2 Rigaku Denki, swing curve recording by a two-crystal DRON-0.5 diffractometer in CuK_1 radiation and by a Si (333) monochromator, and high-energy reflection electron diffractometry by a Philips CM-30 instrument are used to examine the crystalline structure while the element distribution in the layer depth is examined by X-ray fluorescent spall microanalysis using a Philips SEM-515. The element distributions in the layer depth and the (333) plane swing curve are plotted the electron diffraction pattern of the sample surface is recorded. The forming KT layer has a single crystal structure and the ion exchange layers have a variband structure. The results confirm the possibility of forming $Hg_uCd_{1-u}Te$ layers on CdTe substrates in a glycerin solution at a 160°C temperature. The mercury and cadmium ion self-diffusion coefficients are calculated: they are $1.2 \cdot 10^{-13}$ and $7.66 \cdot 10^{-13}$ cm^2/s. Figures 4; references 7: 3 Russian, 4 Western.

Phase Composition and Physical and Mechanical Properties of Cr_2O_{3-Al-C} System Products During Self-Propagating High-Temperature Synthesis

927D0150J Moscow IZVESTIYA AKADEMII NAUK SSSR: SERIYA NEORGANICHESKIYE MATERIALY in Russian Vol 28 No 1, Jan 92 pp 87-91

[Article by N.S. Sharipova, T.G. Chernoglazova, L.A. Chernenko, Kazakh Interbranch Scientific Technical Center; UDC 546.75.669,661.87]

[Abstract] Combustion in the Cr_2O_{3-Al-C} ternary system and its use for making composites by the self-propagating high-temperature synthesis (SVS) method are discussed, and the effect of the carbon on the phase composition and mechanical properties of the products of self-propagating high-temperature synthesis of the Cr_2O_{3-Al} system is studied. Sample preparation procedures are outlined; the X-ray phase analysis is carried out in a DRON-3M unit in Co*K* radiation, the material structure and morphology of the fractured grains are examined under an MBT-71 optical microscope, and the individual grain microhardness and crushing load are determined by I.A. Pudovkin's method. The dependence of the solid solution lattice constants *a* and *c* on the carbon content in the charge, the dependence of the oxide phase and metallic Cr microhardness on the carbon content in the charge, and the dependence of the oxide phase grain strength on the carbon content in the charge are plotted; an analysis shows that addition of 1 mass percent C to Cr_2O_3+Al during self-propagating high-temperature synthesis leads to carbon implantation into the lattice of the Cr_2O_3-Al_2O_3 solid solution forming in the reaction while the oxide phase microhardness increases to 30-33 GPa. As the carbon content in the charge increases above 1 percent by mass, it becomes active as the second reducer and chromium carbides form in the synthesized products. At levels above 6 percent, carbon increases the total porosity from 10-20 percent to 60-70 percent, increases the metallic component's microhardness, lowers the oxide component microhardness, and decreases the oxide phase grain strength. Figures 4; references 7.

Investigation of Spin Casting of Ceramics. Principal Process Parameters and Patterns

927D0120A Moscow OGNEUPORY in Russian No 11, Nov 91 pp 2-6

[Article by Yu.Ye. Pivinskiy, T.I. Litovskaya, O.N. Samarina, I.B. Volchek, F.S. Kaplan, All-Union Refractories Institute; UDC 666.76.022.66]

[Abstract] The low molding rate and the need to use rapidly wearing gypsum molds in slip casting stimulated interest in the spin casting method for making quartz ceramic products using the same high-concentration binding suspensions (VKVS) on the basis of quartz glass of fused glass. The general patterns of the spin casting process and the effect of the main technological factors on the end product are studied. To this end, fused quartz suspensions with a 0.70-0.75 concentration for making nonroasted quartz ceramics are used as the source materials and experimental samples are molded in a metallic nonporous spinning mold. The effect of the circumferential molding velocity on the spin casting pressure indicator P_c, the correlation of the number of mold turns and the circumferential velocity for products of various diameters, the behavior of the solid phase's fraction by volume during the spinning, the grain size distribution of the initial fused quartz suspension, the effect of the peripheral velocity on the molded layer thickness, solid phase volume fraction, and product porosity, and the solid phase excess ratio as a function of the solid phase volume fraction are plotted. It is clear from the findings that the volume fraction of the high-concentration binding suspension, circumferential velocity, and solid phase excess ratio are the principal components affecting the process; spin (centrifugal) casting makes it possible to accelerate the molding process by several orders of magnitude compared to slip casting whereby the ready product porosity is within 10-12 percent. Figures 7; references 11: 10 Russian, 1 Western.

Increasing Corundum Concrete's Eroding Surface Resistance

927D0120B Moscow OGNEUPORY in Russian No 11, Nov 91 pp 13-14

[Article by T.G. Galchenko, I.F. Usatikov, A.G. Karaulov, R.J. Abraitis, V.Yu. Romashev, Ukrainian Scientific Research Institute of Refractories and Erosion Problems Institute at the Latvian Academy of Sciences; UDC 666.76.11.017:620.193.1]

[Abstract] The physical and chemical mechanism of adhesion between two substances in a mixture and the surface behavior at various temperatures are discussed; in particular, the interaction of materials with high-temperature combustion products and the patterns of the eroding ceramic surface recovery are considered. The results of experiments aimed at restoring the eroding surface of corundum concrete used as lining in the technical carbon production reactor exposed to a high-temperature high-velocity (300 m/s) gaseous combustion product flow are cited. The method developed at the Ukrainian Scientific Research Institute of Refractories calls for adding a discrete phase to the combustion product flow. The dependence of the corundum concrete mass variation on duration of exposure to the gaseous high-speed flow is plotted and the microstructure of corundum concrete with an erosion plaster formed on its surface after a six hour test is shown. An analysis of the surface formations created by the moving medium—the so-called erosion plasters—have such components and the flow separation point, flow merger zone, recirculation zone, depressions, etc. The study demonstrates that brief introduction of a discrete phase, such as an $AlCl_3$ solution, to the high-temperature high-speed combustion product flow restores the eroding surface virtually fully and is therefore more efficient and ensures longer service life of corundum concrete. Figures 3; references 9.

Phase Composition and Microstructure of Domestically Produced G-00, G-0, and GSK Alumina

927D0120C Moscow OGNEUPORY in Russian No 11, Nov 91 pp 22-24

[Article by L.V. Mezhuyeva, Z.V. Komova, I.P. Zrelova, V.V. Voynovskaya, A.M. Akimov, State Nitrogen Industry Research Institute and Severodonetsk Azot Production Association; UDC 666.862.222.001.4]

[Abstract] The use of G-00, G-0, and GSK alumina—a crystalline powder of various aluminum oxide modifications—for production of different types of ceramics, refractories, electronics materials, and catalysts is discussed, and attention is focused on the use of alumina in the catalyst industry. The properties of G-00, G-0, and GSK alumina are examined for the purpose of developing recommendations on stabilizing the production of nickel-containing hydrocarbon reforming catalysts. The chemical composition of the alumina under study meets the requirements of current standards; the phase composition of alumina is examined by the crystal optical (or immersion) method by a MIN-8 polarization microscope, and six phases are identified. The concentration of high- and low-calcination phases in 10 alumina samples produced by the UAZ, NGZ, BAZ, and PAZ is summarized, and the microstructure of the samples is photographed. The study reveals that G-00, G-0, and GSK alumina is a multiphase system containing different forms of aluminum oxides; the ratio of high- to low-calcinated phases varies from manufacturer to manufacturer. It is shown that alumina produced by BAZ and UAZ with a spherulite structure containing 20 +/- 5 percent α-Al_2O_3 with $N \geq 1.737$ and at least 50 percent of low-calcination phases with $N < 1.705$ (where N is the refractive index range of the phase) meets the standard requirements most fully. In NGZ alumina, the α-phase concentration must be 6-10 percent; this alumina is easy to grind, ensures a high body peptizing degree, and is characterized by high mechanical strength. Figures 1; tables 1; references 4.

Vibrational Unit for Refractory Block Compaction

927D0120D Moscow OGNEUPORY in Russian No 11, Nov 91 pp 28-29

[Article by V.T. Oleynik, I.Ya. Prokhorova, V.V. Vlasov, V.A. Yegunov, S.I. Oblivin, A.A. Tarasov, All-Union Refractories Institute and Krasnoyarsk Metallurgical Works; UDC 666.76.032.65]

[Abstract] Various methods of making refractory blocks and their shortcomings, such as high labor outlays and poor occupational safety, are discussed, and the vibration molding method developed at the All-Union Refractories Institute for making shaped products with a 10-50 kg mass and in particular, elements of hot air oven lining for the Krasnoyarsk Metallurgical Works, is outlined, and the operating principle of the V-21 unit developed for this purpose is described. The specification of the vibration compaction method are listed, and schematic diagrams of the refractory products made by the new method are cited. The vibrational compaction impact force can be regulated in four steps within a 60-150 kN range, and the vibration frame moves at a 50 Hz frequency with a 0.5-2 mm swing. The chemical composition of the body used for making refractories by the vibration compaction method is summarized. The use of the V-21 unit for making shaped refractory blocks used as induction heater lining elements makes it possible to enhance their production and eliminate manual labor operations. Figures 1; tables 2; references 5.

Strength Properties of Basalt Fibers

927D0126B Moscow STEKLO I KERAMIKA in Russian No 10, Nov 91 pp 8-9

[Article by M.A. Sokolinskaya, L.K. Zabava, T.M. Tsybulya, A.A. Medvedev, Institute of Materials Science Problems at the Ukrainian Academy of Sciences; UDC 666.193:539.4]

[Abstract] The expanding use of polymer composite materials reinforced with mineral fibers and the scarcity of special glass fiber filler components, such as boron and soda, necessitated a study aimed at finding substitute fillers and expanding their applications. It is shown that basalt fibers not only have all the positive properties of glass fibers but also have a number of advantages: their production does not call for adding special components while the raw materials are easily available and virtually limitless. The chemical composition of basalt fibers from two different deposits is summarized and compared to that the chemical composition of three types of glass fibers. The dependence of the rupture strength of basalt and glass fibers with a 8-9 μm diameter on temperature and the dependence of the strength of a complex basalt thread with a close to 50 tex linear density treated with various types of oil during the molding on temperature are plotted. Basalt fibers maintain higher strength even under the effect of hot water while complex basalt threads are also stronger than glass threads under the effect of high temperature. The use of oils on the basis of organosilicon block-copolymers greatly increases the thermal stability of basalt fibers. The use of special oils makes it possible to use basalt fibers for making new heat-resistant insulating materials for integrated circuits, radio electronics, and communications engineering. Figures 2; references 5: 4 Russian, 1 Western.

Polycapillary Porous Medium Model for Analyzing Filtering Processes in Ceramic Materials

927D0126C Moscow STEKLO I KERAMIKA in Russian No 10, Nov 91 pp 13-14

[Article by Yu.N. Kryuchkov, Engineering Thermal Physics Institute at the Ukrainian Academy of Sciences; UDC 666.3.022.69:539.23]

[Abstract] The use of the porous structure models for predicting the operating characteristics and performance and for monitoring the production of ceramic material filters and the shortcomings of existing capillary models are discussed. A porous structure model of permeable materials whereby the medium is represented as a system of curving communicating capillaries of various diameters is formulated, and an attempt is made to analyze the filtration processes on its basis. It is assumed that the porous structure is formed by the intersection of chaotically positioned spheres and the medium porosity is equal to the specific volume of the intersecting spheres. In addition to the pore size distribution, the polycapillary model makes it possible to calculate the open porosity parameters necessary for filtration analyses. An analogue of an electric model of the porous material impregnation is considered in order to derive the mathematical model, and the dependence of the water rise in a ceramic material with a bicapillary structure on the impregnation process duration is plotted. It is shown that the flow rate of the fluid in a narrow capillary does not depend on the drag in a wide capillary and that if the total capillary drag over a certain length is high, the fluid level in a narrow capillary may rise due to the drop in its level in the wide one. The proposed polycapillary model may be used for analyzing the filtration processes in permeable ceramic materials and optimizing their manufacturing and operation. Figures 3; references 4: 3 Russian, 1 Western.

Production of Conducting Surface Layer on Lead Titanate Zirconate Piezoelectric Ceramic

927D0126D Moscow STEKLO I KERAMIKA in Russian No 10, Nov 91 pp 19-20

[Article by L.A. Solovyev, L.M. Lobas, T.G. Lupeyko, L.A. Karimova, Rostov State University; UDC 666.655: 537.226.86]

[Abstract] The need to use expensive materials for making piezoelectric ceramics and the difficulty of applying electrodes to piezoelectric ceramics as well as the constantly rising demand for them prompted a search for new, cheaper electrode materials and easier methods of their application. In so doing, an attempt is made to depart from conventional methods of forming electrodes on piezoelectric ceramic items and developing an electric conducting layer by reducing their surface. Lead titanate zirconate (TsTS) ceramics are selected for this purpose due to their electrophysical properties and stability to external actions,

including strong mechanical and electric fields, and the presence of lead. To reduce the ceramic sample surface, the samples are placed in nickel capsules with finely ground graphite and heated without air. During gaseous reduction, carbon monoxide produced from formic acid is used; the samples are placed in a quartz tube and heated while CO is passed through. Both processes are conducted within a 750-870°C temperature range for 24-45 min; the samples are then cooled to room temperature in a reducing medium. The dependence of the voltage drop on the piezoelectric ceramic sample temperature is plotted and the Curie temperature, dielectric loss tangent, capacitance, and dielectric permeability of the samples are measured and summarized. Emission spectral analysis of the reduced surface layer is performed using an ISP-28 infraspectrometer. The study demonstrates that the electrophysical characteristics of samples after six months and one year of storage do not deviate from the initial values but decrease in three-year-old samples due to Pb and Pb_xO_y oxidation. The new method of producing piezoelectric ceramic materials which combine the properties of conductor and insulator is recommended for commercial implementation. Figures 1; tables 1; references: 2 Western.

Improving Light Transmission of Optically Transparent Lithium-Alumosilicate Glass Ceramics

927D0126E Moscow STEKLO I KERAMIKA in Russian No 10, Nov 91 pp 25-27

[Article by R.M. Boyko, T.A. Derbeneva, E.V. Lameko, P.A. Tseytlin, Polyus Scientific Research Institute; UDC 666.11.01:535.343]

[Abstract] The poor light transmission (60-70 percent) in the visible spectrum of the SO-115M and SO-33M optically transparent commercial glass ceramics prompted attempts to improve their light transmission. It is shown that the principal condition of increasing the glass ceramics light transmission is to ensure that the crystal size is smaller than the incident light wavelength and the amorphous and crystalline phase refractive indices are close. An analysis of existing glass ceramics production methods reveal that the main cause of the insufficient light transmission is the poor charge production technology and the lack of high-temperature founding equipment. Experiments aimed at producing lithium-alumosilicate glass ceramics by the hydroxopolymer method (GP) are described: the spectral transmission of glass ceramics measured by an SF-26 spectrophotometer is plotted. The light transmission, birefringence, and temperature coefficient of thermal expansion (TKLR) of the new glass ceramics as well as their chemical composition and concentration of impurities are summarized. The effect of the refractory and heater material on the light transmission of glass ceramics and the effect of the molybdenum concentration on the glass ceramics light transmission are determined. An analysis of the findings demonstrates that it is possible to produce optically transparent glass ceramics with better optical properties than commercial specimens using the hydroxopolymer method. The development of a new commercial technology and new glassmaking furnaces make it possible to mass-produce glass ceramics with superior qualities. Figures 1; tables 5; references 8: 6 Russian, 2 Western.

Materials Based on Chemically Strengthened Silicon Carbide

927D0128A Moscow OGNEUPORY in Russian No 10, Nov 91 pp 8-11

[Article by V. V. Vikulin and T. V. Leshchuk, Okhtin "Tekhnologiya" Scientific Production Association; UDC 666.762.852]

[Abstract] A process for enhancing the high-temperature strength and heat resistance of silicon carbide materials was described. The process involves making a pure silicon carbide matrix and chemically modifying it to induce chemical transformations and the formation of secondary phases that prevent the material from losing strength at temperatures between 1400 and 1600°C. The matrix was made from 64C granular silicon carbide, which is 99.2 percent SiC. The powder, which had a grain size of 20 μm, was ground to an even finer grain size in corundum-lined corundum ball or SiC-lined SiC ball mills. The specimens were cast from a thermoplastic slip containing 10-14 percent paraffin wax binder and, after removal of the binder, packed in a bed of powdered (200 μm) SiC and sintered in graphite crucibles at 1800-2100°C in a nitrogen atmosphere. The sintered porous specimens were then impregnated with silicone compounds and, after the degradation process, heat-treated at 1350-1400°C in a nitrogen atmosphere to form silicon nitride in the surface layer of the ceramic. A layer of silicon dioxide was then formed on the specimen surfaces in order to protect them from oxidation. The chemically modified specimens were 1.6-1.8 times stronger than the untreated specimens (specimens made from powder ground in SiC ball mills were not as strong as specimens made from powder ground in corundum ball mills due to the presence of aluminum oxide in the former). Bending strength in air, for example, was as high as 250-280 N/mm^2 at 1400-1500°C. The new material, designated OTM-910, can be easily worked with a variety of tools to form near-net shape components of all shapes and sizes that can withstand operating temperatures up to 1600°C and extreme vibration (400 g on a base of $2y10^6$) cycles) whether exposed to air or combustion products. Figures 5, tables 3.

Obtaining Silicon Carbide From Processed Rice Husks

927D0128B Moscow OGNEUPORY in Russian No 10, Nov 91 pp 15-17

[Article by A. S. Vlasov, A. I. Zakharov, O. A. Sarkisyan, and N. A. Lukasheva, Moscow Chemical Engineering Institute; UDC 666.792.32:665.584.43]

[Abstract] The feasibility of obtaining silicon carbide from the hydrolyzed lignin of rice hulls was studied. The lignin was first thermally processed at no more than 700°C in nitrogen. The carbide-forming catalysts were then added, and the material roasted in a stream of argon or helium at 1400-1500°C with holding periods of two to five hours.

Unhydrolyzed rice hulls were also processed in this manner for comparison. This process yielded light green, highly crystallized SiC powder or fibers. X-ray phase and petrographic analyses showed that most of it was in the B-modification form. More SiC was obtained from the hydrolyzed lignin than from the raw rice hulls (40 percent vs 30 percent), as the lignin contains more silicon dioxide than the raw rice hulls (25-35 percent vs 15-20 percent), and also because the hydrolysis process pulverizes the hulls while preserving their structure, with further reduction in particle size being accomplished during thermal processing. The carbon impurity in the synthesized SiC can be removed by thermally processing the latter in air at 500-800°C with subsequent flotation and the use of surfactants. The powders, which have a grain size of 1-2 μm, and the fibers, which are 1 μm in diameter and 20-50 μm in length, were separated in a pH-balanced mixture of water and a hydrophobic liquid. Thus, processed rice hulls are a promising source of inexpensive raw material for synthesizing finely dispersed SiC powders and fibers. Figures 1, tables 2; references 9: 7 Russian, 2 Western.

Heat-Resistant Sodium-Silicate Concretes With Aluminous Slurry Additive

927D0128C Moscow OGNEUPORY in Russian No 10, Nov 91 pp 21-22

[Article by A. I. Khlystov, S. F. Korenkova, and T. V. Sheina, Samar Architectural and Building Institute; UDC 666.974.2:666.76]

[Abstract] Aluminous slurry obtained from waste water treatment was proposed as an additive for heat-resistant concretes. An experimental cement was made from pulverized spent fireclay scrap, a composite binder made by simultaneously pulverizing silicate chunks and the fireclay filler in a 1:4 ratio until the specific surface reached 3200 g/cm^2, and slurry from the water-treatment facilities of the Kuybyshev metallurgical plant. The slurry consisted of 50-55 percent $Al(OH)_3$, 10-15 percent $Ca(OH)_2$ and $Fe(OH)_3$, 15-20 percent $CaCO_3$, and 3-5 percent $CaSO_4$ (wt. percent). The proportion of slurry added was 5, 10, or 15 percent of the weight of the composite binder. Optimal slurry content was 5-10 percent—any more, and there was too much shrinkage, any less, and the plasticizing effect was too weak. With the optimal slurry content, consistency improved nearly twofold, while stiffness fell by about 50 percent. The water requirement remained virtually unchanged at 0.32. Due to the presence of the calcium and aluminum hydroxides in the slurry, the formation of highly refractory compounds such as C_2S, CA, CA_2, and mullite occurred as the specimens were subjected to higher and higher temperatures, with the compressive strength of concrete specimens with optimal slurry content increasing as temperature increased (e.g. from 17.1 to 42.1 N/mm^2 within a temperature range of 400 to 1200°C). Thus, the addition of the aluminous slurry enhances the strength and heat resistance of high-temperature concretes and the workability of the cements from which they are made. Tables 1.

The Microhardness and Relaxation Properties of Carbon Glass

927D0130B Moscow FIZIKA I KHIMIYA OBRABOTKI MATERIALOV in Russian No 5, Sep-Oct 91 (manuscript received 11 Dec 90) pp 9-13

[Article by Ye.I. Kurolenkin, Ye.V. Muravyeva, and Yu.S. Virgilyev, Moscow; UDC 541.64:662.749]

[Abstract] The authors of the study reported herein examined the changes occurring in the microhardness and relaxation properties of carbon glass when it is subjected to heat treatment and neutron bombardment. Carbon glass produced from cast (FM-2) and granulated (Bakelite A) thermosetting resin were heat-treated at temperatures ranging from 1,100 to 3,300 K. A portion of the specimens were bombarded with neutrons in a VVR-M reactor (for neutrons with E /G 0.18 MeV) to a fluence of 1.5-3.5 x 10^{20} cm^{-2} at temperatures of 340-360 and 700 K. Abrasives were used to remove the surface layer of the specimens to a depth of 200 μm. The specimen surfaces were polished and held in air at room temperature for different amounts of time. A PMT-3 microhardness gauge was used to measure the microhardness of both the test and control specimens. An indenter load of 200 g and a holding time of 10 s were used. The measurement error (allowing for the variance from specimen to specimen) did not exceed 5 percent. As the treatment temperature was increased to 1,900 K, the microhardness of the starting specimens increased somewhat; at temperatures above 1,900 K, their microhardness began to decrease (at first sharply and then more moderately). The microhardness of the treated specimens after polishing differed markedly from that of the starting specimens. The initial microhardness of the low-temperature carbon glasses (those heat-treated to 2,000 K) was lower than that of the starting specimens, whereas the microhardness of the high-temperature carbon glasses was higher than that of the starting specimens. Over time, the microhardness of the specimens treated with abrasives returned to its starting value. Two time intervals were evident in this return process: Up to 94 percent of the return to initial microhardness occurred during the initial interval fairly rapidly. The carbon glass specimens underwent significant changes in microhardness immediately after heat treatment. In the case of the heat-treated specimens that were not polished, there was a smooth drop in microhardness until a stable microhardness was achieved (this stable microhardness was about half that measured just after heat treatment). The nature of the change in microhardness experienced by the polished specimens after heat treatment was found to be more complicated. Polishing initially caused a decrease in microhardness. During the course of their holding period, the specimens' microhardness increased to the microhardness values characteristic for the unpolished specimens. After these values were reached, another drop in microhardness began, this time following the course of the curve of the change in microhardness plotted for the unpolished specimens. Neutron bombardment reduced the microhardness of carbon glass that had been heat-treated at low temperatures and increased the microhardness of the carbon glass that had been heat-treated at high temperatures. Abrasive

treatment also had different consequences in the neutron-bombarded carbon glasses than in their non-neutron-bombarded counterparts: Microhardness increased significantly (by 20 to 60 percent) following bombardment. This effect decreased as the irradiation temperature was increased; after irradiation at 700 K, the microhardness of the carbon glass specimens that had been treated with abrasives was even lower than that of the unpolished specimens. The changes discovered were attributed to stress changes in the near-surface layers of the specimens and were found to be dependent on the characteristic features of the supermolecular structural organization of the carbon glass. Figures 5, tables 2; references 7: 6 Russian, 1 Western.

Effect of Raw Material Quality on High-Purity Silicon Production

927D0134H Moscow TSVETNYYE METALLY in Russian No 1, Jan 91 pp 29-32

[Article by A.A. Bakhtin, L.V. Cherbnyakhovskiy, L.P. Kishchenko, P.S. Menshikov, IPI and IF at All-Union Scientific Research and Design Institute of Aluminum, Magnesium, and Electrode Industry; UDC 621.315.692:669.782]

[Abstract] The urgency of electric power generation by ecologically pure methods and the effect of the silicon purity on the quality of solar batteries are discussed and the shortcomings of existing methods of carbothermal silicon production used by, *inter alia*, Union Carbide are outlined. Nontraditional silica- and carbon-containing materials suitable for producing high-purity silicon are investigated, their properties are examined, and a new reduction technology is evaluated. Reduction smeltings are conducted for determining the best charge composition and optimum silica reduction conditions. The temperature, exposure duration, end product yield, and principal element concentration attained in a Tamman resistance furnace are summarized, the constitution diagram of the Si-containing products interacting with SiO_2 and H and a Si-O-C-H equilibrium system, the dependence of the silicon and silicon carbide content in the smelting products on the moisture concentration and exposure time, and the dependence of the silicon purity on its recovery at various impurity concentrations in the initial charge are plotted. The smelting indicators of high-purity raw materials in an electric arc furnace are calculated. An analysis of the findings indicates that given an impurity concentration of under $5 \cdot 10^{-3}$ percent in the initial charge and a $\geq$60 percent silicon recovery, the resulting silicon has a purity of at least 99.98 percent which is sufficient for use in solar batteries. For carbothermal reduction at >1,900°C, energy outlays for one kg of Si are 25-28 kWh. The use of cataclastic quartz from eastern Siberia and MG-OSCh and GMZ-OSCh graphite is suggested. Figures 4; tables 2; references 5.

Production of Al-Si Alloying Composition in Electrothermics Shops

927D0135C Moscow TSVETNYYE METALLY in Russian No 10, Oct 91 pp 26-27

[Article by I.M. Sedykh, L.V. Chernyakhovskiy, IF at the All-Union Aluminum and Magnesium Industry Institute; UDC 669.782:621.365]

[Abstract] Ways of increasing the profitability of crystalline silicon smelting at Siberian plants by mastering new types of products which are in high demand due to their improved properties and by making high-silicon alloys and alloying compositions using liquid aluminum and silicon are discussed. The disperse silicon powder production technology for making new products is outlined, and it is noted that powders made by dispersing liquid metal have better characteristics while the electrothermal process itself results in fewer discharges into the atmosphere. Methods of making aluminum-silicon alloying compositions with a 20-30 percent Si concentration are tested. Test data demonstrate that production of alloying compositions in electrothermics shops does not call for new capital outlays, increases profitability, and improves the alloy quality as well as softens the ecological impact, improves the work place environment, and lowers labor outlays for producing silicon ingots and ready products. References 2.

Effect of Dust Byproduct Additions on Physicochemical Transformations in Charge During Technical Silicon Smelting

927D0135D Moscow TSVETNYYE METALLY in Russian No 10, Oct 91 pp 29-31

[Article by N.V. Yevseyev, N.V. Golovnykh, N.F. Radchenko, Irkutsk Branch of the All-Union Aluminum and Magnesium Industry Institute; UDC 536.7:669.054]

[Abstract] The effect of additions of furnace top dust from technical silicon production on the physical and chemical transformations occurring in the charge, especially the effect of large-particle silicon carbide dust on the process of carbothermal silicon reduction from silicon dioxide during the production of technical silicon is investigated. It is shown that the use of dust byproducts is economically efficient only in a single-stage process when it is added to the principal charge. To establish the qualitative correlation of the process, equilibria are studied by physicochemical computer simulation with the help of a "Selector" routine using known mathematical models. The dependence of the equilibrium composition on temperature for various types of charge is plotted and the charge composition is summarized. The dependence of the amount of liquid silicon and free energy of the thermodynamics system on the initial charge composition and process temperature is examined and process indicators of silicon smelting with dust byproducts are summarized. Test smeltings show that the use of large-particle gas scrubbing dust makes it possible to lower the specific consumption of electric power by 14-18 percent and increase the furnace output by 15-20 percent. The best indicators are attained in the case where granulated dust is the principal component; the high properties of this burden are attributed to the high concentration of the SiC reduction product. The findings are used for formulating charge pelletizing process specifications. Figures 3; tables 3; references 7.

Stressed State and Failure of Nonuniformly Heated Graphite Discs

927D0135E Moscow TSVETNYYE METALLY in Russian No 10, Oct 91 pp 31-33

[Article by E.S. Varypayev, N.V. Negutorov, A.O. Chernyavskiy, State Scientific Research Institute of Economic and Planning and Chelyabinsk Polytechnic Institute; UDC 661.666.2]

[Abstract] The inadequacy of model studies which makes it impossible to extend simulation results to real electrodes prompted an analysis of the state of stress and thermal failure of nonuniformly heated discs with various diameters allowing for electrode graphite strain diagrams. The graphite discs are heated by passing a 1,000 A current through their center and the failure moment is recorded by a sharp change in the disc diameter. Thermal stresses in the discs are analyzed in two phases: in the first, the electrode graphite is regarded to be elastic until failure and in the second real strain diagrams are taken into account. The stress distribution in a 100 mm dia. disc at the moment of failure, the stress maxima behavior during the heating, the hoop stress distribution in the discs, the effect of the strain diagram type on the stress distribution, and the acoustic emission pattern during the disc test are plotted. The theoretical estimates of the discs' thermal stability are compared to experimental data which generally confirm the analytical conclusions showing that inelastic straining of electrode graphite decreases the failure probability and may be the reason for the absence of visible failure signs on the disc surface. Although disc sample tests do not provide adequate data on the electrode failure, they may be used for estimating the thermal strength of electrode graphite. Figures 5; references 7.

Structural Ceramics Hardness and Crack Resistance

927D0138B Kiev FIZIKO-KHIMICHESKAYA MEKHANIKA MATERIALOV in Russian, Vol 27 No 3, May-Jun 91 pp 12-18

[Article by G.A. Gogotsi, A.V. Bashta, Strength Problems Institute at the Ukrainian Academy of Sciences, Kiev; UDC 621.178.15]

[Abstract] The importance of the ceramics hardness and crack resistance characteristics for such diverse applications as structural engineering and design on the one hand and medicine and prosthetics on the other is discussed, and the lack of a unified methodology for estimating these characteristics is noted. The mechanical behavior of ceramics being indented by a Vickers pyramid is comprehensively investigated, and the characteristics of the change in the ceramic material's hardness and crack resistance are examined. Two sintered silicon nitride-based materials produced by different methods, hot compacted silicon carbide, and three zirconium dioxide-based materials with various percentage concentrations of the stabilizing yttrium and magnesium oxide additions are tested. The materials' chemical composition and their hardness index, density, dynamic and static moduli of elasticity, bending strength, elongation, and brittleness measured in a 1958U1-10 tester are summarized and the notch sensitivity index is measured by Niihara's method. The dependence of the notch sensitivity index on the radial indentation crack length and the vulnerability characteristics of ceramic material surfaces under indentation are plotted. Characteristic indentations and cracks are shown. It is stressed that in discussing the ceramics harness and crack resistance, one must first define the relevant level of the straining and failure processes, i.e., intragranular or sample-wide. Figures 5; tables 2; references 19: 9 Russian, 10 Western.

Differentiated Approach to Wear Resistance Estimate of Tool Ceramics in Al_2O_3-$ZrO_2(Y_2O_3)$ System

927D0149E Minsk TRENIE I IZNOS in Russian Vol 13 No 2, Mar-Apr 92 pp 328-332

[Article by A.M. Kovalchenko, N.A. Orlovskaya, Materials Science Problem Institute at the Ukrainian Academy of Sciences, Kiev; UDC 620.178.16:539.538:621.922:666.3/3]

[Abstract] The difficulty of direct estimation of the wear resistance of tool ceramics on the basis of nonmetallic refractory compounds, the high metal outlays required for for testing, and the wide spread of experimental data prompted an attempt to develop a new approach to assessing the wear resistance of ceramic cutting tool tips. As a result, a differentiated approach whereby wear resistance is estimated by two mutually complementary techniques and methods is proposed; it calls for determining the mechanical strength of the ceramic tool under abrasive wear and evaluating its wear resistance during the interaction with metal, i.e., the cutting process. The new comprehensive procedure is used to study the wear resistance of aluminum oxide-based ceramics with varying concentrations of zirconium dioxide, both nonstabilized and partially stabilized with yttrium oxide. A comparison of data on the wear resistance of ceramic cutters for continuous turning and friction with steel demonstrates a good correlation for ceramics with stabilized zirconium dioxide. Cutting tips with 30 and 40 percent of partially stabilized zirconium dioxide have the highest wear resistance. The expediency of friction tests for developing new ceramic materials is recognized, but it is stressed that cutting tests cannot be avoided completely. Figures 3; references 13: 9 Russian; 4 Western.

Tribological Characteristics of Sintered Self-Propagating High-Temperature Synthesis Silicon Nitride

927D0149F Minsk TRENIE I IZNOS in Russian Vol 13 No 2, Mar-Apr 92 pp 340-343

[Article by S.Yu. Sharivker, V.D. Zozulya, Structural Macrokinetics Institute at the USSR Academy of Sciences, Chernogolovka, Moscow oblast; UDC 532.526.7:621.891]

[Abstract] The lack of data on the tribological characteristics of silicon nitride—one of the most promising materials for solving the problem of prolonging the life of friction

units—prompted tribological studies of Si_3Ni_4 manufactured by the method of self-propagating high-temperature synthesis (SVS) from a powder produced by the Structural Macrokinetics Institute. The density, bending strength, and wear rate of the samples with and without lubrication are summarized. The dependence of the temperature in the friction zone on the load, the dependence of the friction coefficient on the load under various lubricating conditions and without lubrication, and the dependence of the friction coefficient and wear rate on porosity with wick-fed lubrication are plotted. The possibility of using Si_3Ni_4 impregnated with oil in friction units with steel shafts without regular lubrication or with boundary lubrication is demonstrated. Sintered silicon nitride's tribological characteristics are close to those of bronze and iron graphites. Figures 3; references 8: 7 Russian, 1 Western.

Heat and Mass Transfer During Production of Silicon Layers at Reduced Pressure

927D0150A Moscow IZVESTIYA AKADEMII NAUK SSSR: SERIYA NEORGANICHESKIYE MATERIALY in Russian Vol 28 No 1, Jan 92 pp 5-9

[Article by V.G. Minkina, V.P. Popov, Heat and Mass Transfer Institute imeni A.V. Lykov; UDC 546.281: 536.244]

[Abstract] The heat and mass transfer during the production of epitaxial silicon layers from a gaseous mixture of tetrachlorosilane and hydrogen in a vertical reactor with a truncated pyramid-shaped substrate holder, whereby the holder surface is heated to the precipitation temperature which is much higher than the temperature of the cooled reactor walls, is investigated. The final chemical reactions on the precipitation surface are formulated, and the heat and mass transfer in the reactor in a laminar flow of gas mixture is described by a system of conservation equations in a boundary layer approximation. A schematic diagram of the silicon layer producing reactor is cited as the behavior of the Nusselt number, precipitation rate and diffusion as a function of temperature and pressure. The temperature dependence of the Nusselt number at various diffusion parameter values and the dependence of the Nusselt number on the nondimensional complex λ under various process factors are plotted. The role of thermal diffusion is discussed and it is established that the factors affecting the temperature gradient in the reactor zone plays a significant role in the precipitation rate distribution through the channel length. A decrease in the substrate temperature from 1,600°C to 1,100°C at a fixed wall temperature weakens the role of thermal diffusion due to a decrease in the temperature gradient. Figures 4; references: 1 Western

Effect of Ion-Stimulated Plasma-Chemical Etching on Macrostress Level in GaAs Single Crystal Substrates

927D0150B Moscow IZVESTIYA AKADEMII NAUK SSSR: SERIYA NEORGANICHESKIYE MATERIALY in Russian Vol 28 No 1, Jan 92 pp 10-15

[Article by N.V. Zheltkova, D.G. Krutogin, G.D. Kuznetsov, V.K. Molchanov, E.M. Novikova, Moscow Steel and Alloy Institute; UDC 546.681'193]

[Abstract] The uses of ion-stimulated plasma-chemical etching for removing the damaged subsurface layer of gallium arsenide substrates in order to prepare them for subsequent epitaxy or application of insulating and metallic films and the advantages of the method are discussed. An attempt is made to establish a correlation between the conditions of low-energy material treatment and the macrostresses developing in this material that may greatly alter the electrophysical properties of the substrates and the laminar structures as a whole. Single crystal *n*-type GaAs substrates degreased beforehand are subjected to ion-stimulated plasma-chemical etching (ISPKhT) in a $C_2F_3Cl_3$ freon-113 medium or a mixture of Ar with $C_2F_3Cl_3$ in a 1:4 ratio in a Plazma 600-T unit at a 26 Pa working pressure. The dependence of the ion-stimulated plasma-chemical etching rate on the bias potential on the substrate holder in Ar, freon, and an Ar + freon mixture, the dependence of the macrostress change in substrates subjected to ion-stimulated plasma-chemical etching on the bias potential on the substrate holder in Ar, freon, and an Ar + freon mixture, the dependence of the GaAs substrates resistance after ion-stimulated plasma-chemical etching on the bias potential on the substrate holder in Ar, freon, and an Ar+freon mixture, and the photoluminescence spectra of GaAs wafers after ion-stimulated plasma-chemical etching are plotted. A study of the ISPKhT process at a 0 +/- 600 V bias demonstrates that the microstress distribution in the wafer surface after the treatment depends more on the bias potential and to a lesser extent—on the medium composition; the microstress behavior correlates with resistivity. An analysis of the the transmission and photoluminescence spectra shows that the GaAs absorption edge can be shifted to the shorter wave end of the spectrum, i.e., from 1.33 to 1.26 eV, by ion-stimulated plasma-chemical etching. Figures 4; tables 1; references 10: 7 Russian, 3 Western.

Oscillatory Spectra and Local Structure of GeS_2-$A_2^VS_3$ System Glass

927D0150E Moscow IZVESTIYA AKADEMII NAUK SSSR: SERIYA NEORGANICHESKIYE MATERIALY in Russian Vol 28 No 1, Jan 92 pp 36-41

[Article by D.I. Bletskan, V.S. Gerasimenko, V.N. Kabatskiy, M.Yu. Sichka, Uzhgorod State University; UDC 666.117.2:535.34]

[Abstract] The mechanism of the electron processes occurring in vitreous chalcogenide semiconductors (KhSP) and the inadequacy of the atomic spacing and the number of nearest neighbors derived from the radial atomic distribution function (FRRA) are discussed; vitrification and structural characteristics of GeS_2-Sb_2S_3 and GeS_2-Bi_2S_3 glass systems are examined. The glasses are synthesized by direct fusion of the elemental components in evacuated quartz vials. The Raman scattering (KRS) spectra are recorded by a DFS-24 spectrometer at room temperature using an LG-38 He-Ne laser as an excitation source; long-wave infrared (IK) transmission spectra are studied in finely disperse samples encapsulated in polyethylene with the help of a FIS-3 double-beam spectrophotometer. Infrared transmission spectra and Raman scattering

spectra of the glass systems of various compositions are plotted. A model of the GeS_2 structure is suggested whereby the short-range order is characterized by tetrahedral Ge coordination and the mid-range order has chains of GeS_4 tetrahedrons in the reticle with common apices. An analysis of oscillatory spectra as a function of composition reveals a bimodal reordering character and indicates that ternary glasses of quasibinary cross sections have inhomogeneities only in the form of tetrahedral structural units and pyramidal structures; it shows that a single reticular structure consisting of GeS_4 tetrahedrons and A^VS_3 linked through two-coordinates sulfur atom positions forms in the glass systems. Figures 4; references 16: 8 Russian, 8 Western.

Growing Oriented CdS and CdSe Single Crystals With up to 100 mm Diameter From Vapor Phase

927D0150F Moscow IZVESTIYA AKADEMII NAUK SSSR: SERIYA NEORGANICHESKIYE MATERIALY in Russian Vol 28 No 1, Jan 92 pp 42-48

[Article by A.A. Davydov, V.N. Yermolov, S.V. Neustroyev, L.P. Pavlova, Scientific Research Institute of Materials Science imeni A.Yu. Malinin; UDC 548.522]

[Abstract] The difficulty of growing high-quality single crystals with a large diameter from the vapor phase and the condition preventing the single crystal twinning with the crystallizer are discussed, and a method of growing oriented CdS and CdSe single crystals with a diameter of up to 100 mm from the vapor phase is discussed. A schematic diagram of a crystallizer for growing single crystals is presented, and its operating principle is outlined. To ensure selective cooling relative to the surrounding crystallizer parts, the light guide principle is employed whereby the growing crystal is placed on the face of a solid transparent cylinder with polished surfaces which transmits most of the crystal's thermal radiation. It is shown that sapphire and KI quartz glass are the most suitable materials for the light guide. Crystalline cadmium sulfide and selenide are used as the source materials for growing the crystals. The use of the light guide method ensures the necessary thermal conditions which eliminate the vapor deposition around the growing crystal and its twinning with the walls; thus, CdS and CdSe single crystals with a given crystallographic orientation weighing up to 1.2 and 1.4 kg, respectively, are grown from the vapor phase. Figures 3; references 6.

High-Alumina Ceramics With Low Sintering Temperature

927D0150N Moscow IZVESTIYA AKADEMII NAUK SSSR: SERIYA NEORGANICHESKIYE MATERIALY in Russian Vol 28 No 1, Jan 92 pp 184-185

[Article by N.T. Yerofeyeva, L.G. Sakharov, Mechanical Engineering Institute imeni A.A. Blagonravov and leningrad Department of the USSR Academy of Sciences; UDC 546.284:54-143]

[Abstract] The possibility of activating the sintering of refractory ceramic materials by creating the conditions under which a liquid phase forms between the refractory component grains and the possibility of substantially increasing the refractoriness of ceramic materials while maintaining a low sintering temperature and a short sintering duration are investigated; to this end, an experiment using glass powders whose compositions correspond to those of ternary eutetics of the $CaO-Al_2O_3-SiO_2$ systems is conducted in order to activate the sintering of corundum. The dependence of the spalling resistance and bending strength on the glass powder concentration at a 1,400°C temperature and a one hour exposure for various glass compositions is plotted; the activating effect of glass additions is attributed to that fact while softening. They wet the corundum grains, then crystallize developing strong polycrystalline bonds between the corundum grains. An X-ray phase analysis indicates that the sintered ceramics have an equilibrium composition. The differences in the strength of various samples is explained by the difference in the morphology and phase composition of the growing crystals in the liquid phase. The high electric resistivity and absence of volatile oxides make these ceramics promising as high-temperature insulators operating in a vacuum or at normal pressure, even in oxygen. Figures 1; references 9: 8 Russian, 1 Western.

Effect of Heat Treatment on Properties of Nickel-Doped Silicon

927D0151A Moscow IZVESTIYA ROSSIYSKOY AKADEMII NAUK: SERIYA NEORGANICHESKIYE MATERIALY in Russian Vol 28 No 2, Feb 92 pp 283-287

[Article by F.M. Talipov, M.K. Bakhadyrkhanov, Tashkent State University imeni V.I. Lenin; UDC 546.28-121]

[Abstract] The effect of nickel on the behavior of electrical properties in nickel-doped silicon during heat treatment within a broad temperature range is investigated. Parallel piped-shaped wafers cut from single crystal ingots of *n*- and *p*-type silicon doped with phosphorus and boron grown by Czochralski's method are examined. The total nickel concentration is measured by the tracer method; the electrical properties of the wafers are studied by measuring the Hall effect and conductivity. The dependence of silicon's electric resistivity on the heat treatment duration at 450°C and the dependence of the charge carrier concentration and life in silicon on the heat treatment duration at 800°C and 900°C are plotted and the effect of the diffusion condition on the electric parameters of silicon wafers is summarized. The effect of the nickel diffusion temperature on the electric parameters of KDB-10 silicon wafers is evaluated. An analysis of the findings shows that the high diffusivity and concentration of the electrically inactive interstitial nickel atoms and their intensive interaction with lattice defects (e.g., oxygen), hinder the thermal donor generation and precipitation of SiO_2; as the Ni concentration increases, the stability of silicon's electric properties under heat treatment improves. Consequently, by selecting the original wafers and optimum doping conditions, it is possible to expand the temperature range of this material in semiconductor engineering. Figures 3; tables 2; references 12: 8 Russian, 4 Western.

$ZnAs_2$ Thermal Conductivity, Thermoelectric Coefficient, and Electric Resistivity Anisotropy

927D0151B Moscow IZVESTIYA ROSSIYSKOY AKADEMII NAUK: SERIYA NEORGANICHESKIYE MATERIALY in Russian Vol 28 No 2, Feb 92 pp 293-298

[Article by Yu.G. Nadtochiy, D.I. Pishchikov, Yu.N. Burtsev, S.V. Zakharov, S.F. Marenkin, V.B. Lazarev, General and Inorganic Chemistry Institute imeni N.S. Kurnakov at Russia's Academy of Sciences; UDC 546.47'19]

[Abstract] The crystallographic structure and mechanical, chemical, and thermal and optical properties of $A^{II}B^{V}$ semiconductor compounds are discussed, and the anisotropy of the thermoelectric coefficient, thermal conductivity, and electric resistivity of $ZnAs_2$ within a broad temperature range is investigated and compared to known properties of other $A^{II}B^{V}$ compounds. The temperature dependence of electric resistivity in the [100] and [001] direction, the temperature dependence of thermal conductivity and thermal resistance in the [100], [001], and [010] directions, the thermal dependence of the thermoelectric coefficient in the [100], [001], and [010] direction and the thermoelectric coefficient anisotropy, and the temperature dependence of the thermoelectric coefficient in the [100], [001], and [010] direction and the CdSb thermoelectric coefficient anisotropy are plotted for single crystals grown by the vertical Bridgeman-Stockbarger method. An analysis of the temperature behavior of monoclinic zinc diarsenide crystals within a 77-340K temperature range reveals a strong anisotropy, making $ZnAs_2$ a promising element for use as an anisotropic thermocouple. Figures 5; references 12: 10 Russian, 2 Western.

Properties and Morphology of Carbon-Doped GaAs Layers Grown by Metal Organic Chemical Hydride Method

927D0151C Moscow IZVESTIYA ROSSIYSKOY AKADEMII NAUK: SERIYA NEORGANICHESKIYE MATERIALY in Russian Vol 28 No 2, Feb 92 pp 299-303

[Article by T.S. Babushkina, L.M. Batukova, B.N. Zvonkov, L.N. Znysheva, I.G. Malkina, L.Ye. Nikolayeva, V.N. Portnov, Nizhniy Novgorod State University imeni N.I. Lobachevskiy and Nizhniy Novgorod Engineering Physics Research Institute; UDC 539.216.2: 621.315.592.3]

[Abstract] The advantage of using C as an acceptor dopant in growing GaAs layers by the metal organic chemical vapor deposition and molecular flow (MP) methods is discussed, and the electrophysical and optical properties and structural perfection and morphology of carbon-doped epitaxial GaAs layers (ES) are investigated. The growth process is described. The properties of the layer are determined by the Van der Pau method and by analyzing the photoluminescence spectra (FL) at 77K. The dependence of the hole concentration and defect size in epitaxial GaAs/C on the relative CCl_4 concentration in the flow, the dependence of the hole concentration and defect shape parameter in epitaxial GaAs/C layers on the AsH_3/trimethylgallium (TMG) concentration ratio, and the dependence of the photoluminescence spectra maximum and edge energies on the hole concentration are plotted. An examination of defects and an analysis of the curves demonstrate that carbon's amphoteric properties are manifested more vividly in a trimethylgallium system than in a triethylgallium (TEG) system. When GaAs layers are grown by the MOCVD method in the presence of carbon tetrachloride, the polycrystalline particle and growth hill defects increase in size; an increase in the AsH_3/trimethylgallium ratio enhances the defect growth anisotropy. Better epitaxial layers can be produced in a system with triethylgallium. Figures 4; references 9: 2 Russian, 7 Western.

Single Crystal Growth, Photoelectric Properties, and Absorption Edge of New $CuGa_{2.5}In_{2.5}S_8$ Laminar Compound

927D0151D Moscow IZVESTIYA ROSSIYSKOY AKADEMII NAUK: SERIYA NEORGANICHESKIYE MATERIALY in Russian Vol 28 No 2, Feb 92 pp 304-308

[Article by N.A. Moldovyan, Applied Physics Institute at the Moldovan Republic Academy of Sciences; UDC 546.784'231]

[Abstract] The $CuGa_{2.5}In_{2.5}S_8$ single crystal production conditions, optical absorption band edge, and electric and photoelectric properties are investigated. Single crystals of the new laminar chalcogenide with octahedral and tetrahedral cation coordination (SKhOTKK) are produced by the method of transport chemical reactions in an enclosed volume using iodine as the transport agent. The crystals split easily like mica. X-ray analyses show that the compound crystallizes as a hexagonal lattice whose *c*-axis is perpendicular to the layers. The volt-ampere characteristic of the Pt-crystal-In surface barrier structure (PBS) with opaque Pt and In contacts for various crystal thicknesses, the photoconduction spectrum of the crystals and spectral photoresponse distribution of surface barrier structures at a +4.5 V bias and in a photovoltaic operation at 300K for various crystal thicknesses, and the optical absorption band edge of the crystals at 300 and 70K are plotted. The *n*-type crystals are found to be good photoconductors; their dark conductivity can be improved by heat treatment in a vacuum. The surface barrier structures made on the basis of these crystals have high coefficient of detection and photosensitivity. The new compound has a very close-packed hexagonal anion structure in which the cations are located in layers in octahedral and tetrahedral voids. The crystal has photosensitive centers at a 1.9 eV level and its absorption band edge has an extended exponential section with the characteristic parameter of 43 meV. Figures 3; references 6.

Effect of CdTe on Thermoelectric and Mechanical Properties of Single Crystal $Bi_2Te_{2.85}Se_{0.15}$

927D0151E Moscow IZVESTIYA ROSSIYSKOY AKADEMII NAUK: SERIYA NEORGANICHESKIYE MATERIALY in Russian Vol 28 No 2, Feb 92 pp 316-320

[Article by T.Ye. Svechnikova, C.N. Chizhevskaya, N.V. Polikarpova, P.P. Konstantinov, G.T. Alekseyeva, L.Ye.

Inozemtseva, Metallurgy Institute imeni A.A. Baykov at Russia's Academy of Sciences; UDC 546.87'231'241]

[Abstract] The absence of data on the effect of group IIv, IIIv, and IVv elements on the properties of bismuth telluride-based solid solutions is noted and the effect of cadmium—a group IIv element—on the thermoelectric and mechanical properties of the $Bi_2Te_{2.85}Se_{0.15}$ solid solution is investigated; in addition, an attempt is made to determine the effective cadmium distribution coefficient which is indicative of the dopant distribution along the single crystal length. The cadmium concentration in the original charge is determined by the atomic absorption method using a Perkin Elmer 403 spectrophotometer. The temperature dependence of the thermoelectric efficiency of single crystals at a 1, 2, and 3 percent CdTe concentration in the charge and the dependence of the bending strength on the cadmium concentration in the sample are plotted and the electrophysical properties of $Bi_2Te_{2.85}Se_{0.15}$-CdTe single crystals are summarized. Bending tests are performed in an Instron tester. The effective Cd distribution coefficient is equal to 0.2. The study shows that doping with CdTe in an amount of under 2 molar percent in the burden (or 0.16 percent by mass in the sample) leads to a slight increase in thermoelectric efficiency of Czochralski-grown single crystals within a 100-350K temperature range and an increase in mechanical strength at room temperature. Figures 3; tables 4; references 11: 10 Russian, 1 Western.

Microhardness of PbTe and $Pb_{1-x}Mn_xTe$ Crystals

927D0151F Moscow IZVESTIYA ROSSIYSKOY AKADEMII NAUK: SERIYA NEORGANICHESKIYE MATERIALY in Russian Vol 28 No 2, Feb 92 pp 340-343

[Article by V.G. Guk, Ye.V. Osipova, T.I. Papushina, Urals Polytechnic Institute imeni S.M. Kirov; UDC 621.315.592.3:546.815.711.24]

[Abstract] The relationship between the microhardness and the character of chemical bonds in the substance is discussed and the microhardness of PbTe and $Pb_{1-x}Mn_xTe$ crystals grown by Czochralski's method under a layer of liquid B_2O_3 flux in the [100] direction is studied. The samples are cut in a low-speed lathe perpendicular to the growth direction; as a result, microhardness is measured on the (100) plane; the 70 μm damaged layer is removed by grinding and polishing. The samples' microhardness is measured in a PMT-3 tester; the cubic lattice constant of intrinsic and Mn-doped crystals is measured by a standard DRON-3 diffractometer in Cu*K* radiation accurate within 0.001 angstrom. The effect of the charge carrier concentration and lattice constant on the microhardness of crystal samples grown from various types of charge and the effect of manganese concentration in the charge and crystal on the microhardness and lattice constant are summarized. An analysis of the findings reveals that the microhardness of PbTe single crystals does indeed depend on the original charge composition, charge carrier concentration, and crystal growth conditions. The manganese concentration affects the microhardness of *p*-type single crystals ($10^{-5}<x<0.1$) while the short-range solid solution stratification affects their mechanical properties. Figures 1; tables 2; references 9.

Zirconium or Hafnium Interaction With Vanadium and Phosphorus

927D0151G Moscow IZVESTIYA ROSSIYSKOY AKADEMII NAUK: SERIYA NEORGANICHESKIYE MATERIALY in Russian Vol 28 No 2, Feb 92 pp 373-377

[Article by Ya.F. Lomnitskaya, M.S. Brilyak, Yu.B. Kuzma, Lvov State University imeni I. Franko; UDC 546.831.832.881.181.1]

[Abstract] The interaction of Zr or Hf with V and P is investigated in samples synthesized from powder by fusing the charge components in an electric arc furnace. To equilibrate the system, the samples are exposed to diffusion annealing at a 1,070K temperature for 800 hours. The interaction in the system is studied by X-ray phase and structural analyses using a DRON-3.0 diffractometer in Cu*K* radiation. The lattice constants are refined by the least squares method and the reflex intensity is computed by the POWLSQ routine on an SM-4 computer. Phase equilibria in the Zr-V-P system at 1,070K and the behavior of the lattice cell constant and volume in the domain of $Zr_xV_{2-x}P$ and $Zr_xV_{2-x}P$ phase homogeneity are plotted; $Zr_xV_{2-x}P$ diffraction patterns ($x = 1$), atomic coordinates and temperature coefficients in the $Zr_xV_{2-x}P$ structure, and interatomic spacing and coordination numbers (KCh) of atoms in the $Zr_xV_{2-x}P$ structure are summarized. A $V_{2.8}Zr_{0.2}P$ solid solution forms on the basis of the V_3P phosphide. A compound with a $Zr_{0.6-1.0}V_{1.4-1.0}P$ homogeneity range is discovered in the Zr-V-P system for the first time. An isostructural compound also forms in the Hf-V-P system. The ZrVp phase has a TiNiSi structure. In addition, interaction in Zr-M-P system where M is a period IV transition metal is also considered. Figures 2; tables 3; references 10: 7 Russian, 3 Western.

Doping Characteristics of Ceramic TiO_2

927D0151H Moscow IZVESTIYA ROSSIYSKOY AKADEMII NAUK: SERIYA NEORGANICHESKIYE MATERIALY in Russian Vol 28 No 2, Feb 92 pp 385-389

[Article by G.A. Tarabanov, Saint Petersburg Department of the All-Union Electric-Grade Ceramics Scientific Research Institute; UDC 549.514.6]

[Abstract] The origin of the TiO_2 activity in semiconductor ceramics and the effect of the original titanium dioxide characteristics on their doping kinetics, i.e., the formation of solid solutions, are discussed, and the development kinetics and electric properties of doped TiO_2<Nb> ceramics on the basis of various commercial TiO_2 preparations are investigated. The samples are prepared by standard technology, and the properties are examined using a DRON-2.0 diffractometer with a copper anode, a model 5000D sedimentometer, and a MREM-200 scanning electron microscope. The granulometric composition of the original TiO_2, the TiO_2 shrinkage curves, and the dependence of the TiO_2+0.05 percent Nb_2O_5 ceramic resistivity on the hardening temperature for various TiO_2

brands are plotted and the TiO_2 production methods, conditions, and classification are summarized. The physical and chemical properties of TiO_2 and ceramics on its basis are examined. The findings do not confirm the assumption that the original TiO_2 surface hydration has a great effect on its reactivity. The findings show that the formation kinetics of conducting $Ti_{1-x}Nb_xO_2$ solid solutions during the TiO_2 alloying with a donor dopant are mostly determined by the granulometric composition of the original titanium dioxide and do not depend on its structural modification or hydration degree. Figures 3; tables 2; references 7: 6 Russian, 1 Western.

Formation Kinetics of $YBa_2Cu_3O_x$, $YBa_2Cu_3O_y$, Y_2BaCuO_5, $BaCuO_2$ and $Y_2Ba_2O_5$

927D0151I Moscow IZVESTIYA ROSSIYSKOY AKADEMII NAUK: SERIYA NEORGANICHESKIYE MATERIALY in Russian Vol 28 No 2, Feb 92 pp 394-399

[Article by Ye.N. Solovyeva, V.B. Glushkova, V.A. Krzhizhanovskaya, Ye.S. Gryaznova, Silicate Chemistry Institute imeni I.V. Grebenshchikov at Russia's Academy of Sciences; UDC 541.124:546.641'56'431]

[Abstract] The inconsistency of available data on the precipitation of various intermediate reaction products during the production of Y-Ba-Cu-O compounds by heat treatment of the constituent components, probably due to the difference in experimental conditions, is discussed, and the reaction kinetics of barium carbonate with yttrium and copper oxides and the sequence of phase formation during the synthesis of binary and ternary compounds are examined. To this end, powder mixtures are roasted in the air in a Naberterm furnace at 850, 900, and 950°C (accurate within 1°C) with isothermal exposures for 0.5-24 h. The samples hardened in the air are examined by X-ray phase analysis (RFA) in a DRON-3 in Cu*K* radiation and complex thermal analysis of the original mixtures is performed in a Setaram unit. The barium concentration is determined by conductometric titration (accurate within 1 percent). The phase formation during the $YBa_2Cu_3O_x$ and $YBa_2Cu_3O_y$ synthesis, complex thermograms of various barium carbonate and copper oxide mixtures, and the interaction kinetics of barium carbonate and yttrium and copper oxides during the synthesis are plotted and the kinetic parameters of the $BaCO_3$ reaction with copper and yttrium oxides during the synthesis are summarized. The jump in the reaction rate constant within a 900-950°C range during the synthesis of $YBa_2Cu_3O_x$ is attributed to a change in the reaction mechanism. The enhancing role of the liquid phase during the $YBa_2Cu_3O_x$ production is established. Figures 3; tables 1; references 12: 4 Russian, 8 Western.

Single Crystal Growth and Photoelectric and Optical Properties of New Layered $MgGaInS_4$ Compound

927D0151J Moscow IZVESTIYA ROSSIYSKOY AKADEMII NAUK: SERIYA NEORGANICHESKIYE MATERIALY in Russian Vol 28 No 2, Feb 92 pp 432-434

[Article by N.A. Moldovyan, Applied Physics Institute at Russia's Academy of Sciences; UDC546.784.231]

[Abstract] Layered multicomponent chalcogenides with an octahedral and tetrahedral cation coordination which are promising materials for developing new solid state devices are discussed, and the growth conditions of single crystal $MgGaInS_4$—a quaternary sulfide with a layered crystalline structure—and their photoelectric properties and optical absorption band edge are investigated. The single crystals are grown by the chemical transport reactions with iodine in quartz vials. The electric and photoelectric characteristics are examined in samples with coplanar In electrodes and in Pt-crystal-In surface barrier structures (PBS) where the opaque platinum film forms a contact with rectifying properties while indium serves as an ohmic contact. The crystal photoconduction spectra and photoresponse of the surface barrier structures in a photovoltaic operation, under a direct +4.5 V bias, and under the photocapacitance effect and the absorption band edge of the single crystal at 300 and 80K are plotted. The crystal's dark conductivity is 10^{-8}-10^{-9} and 10^{-7}-10^{-8} S/cm in the directions parallel and perpendicular to the *c*-axis, respectively. The 0.3 eV red shift of the photoconduction (FP) spectrum indicates the existence of photosensitive acceptor centers with a small electron capture cross section. The single crystals have a 2.81 eV forbidden gap and an *n*-type conduction. The photocapacitance effect is manifested within a 2.5-3 eV range and the photoelectromotive force—within a 3-5 eV range. Figures 2; references 8: 3 Russian, 5 Western.

Two New CW Laser Diode-Pumped Lasers Based on Disordered $Ca_3(Nb, Ga)_2Ga_3O_{12}$ and $KLa(MoO_4)_2$ Crystals With Nd_{3+}

927D0151K Moscow IZVESTIYA ROSSIYSKOY AKADEMII NAUK: SERIYA NEORGANICHESKIYE MATERIALY in Russian Vol 28 No 2, Feb 92 pp 438-440

[Article by A.A. Kaminskiy, H.R. Verdun, B.V. Mill, A.A. Pavlyuk, A.V. Butashin, Crystallography Institute imeni A.V. Shubnikov at Russia's Academy of Sciences, Fibertek Inc., (USA), and Moscow State University imeni M.V. Lomonosov; UDC 546.654:548.55+535.371]

[Abstract] Single-mode continuous-wave stimulated emission (SI) excited for the first time at room temperature by a laser diode in Nd^{3+} ion ($^4F_{3/2}$—$^4I_{11/1\ 2}$ channel) in two disordered $Ca_3(Nb, Ga)_2Ga_3O_{12}$ and $KLa(MoO_4)_2$ crystals is reported. To study the emission properties, active elements are cut from single crystals in the form of plane parallel wafers of various thickness without an antireflection coat. Absorption spectra fragments of Nd^{3+} ions at 300K in the two disordered crystals are plotted and compared to the spectra of $Y_3Al_5O_{12}$ with an ordered structure. The principal parameters of single-mode CW emission and luminescent characteristics of Nd^{3+} ions in the disordered crystals are summarized. The authors are grateful to V. Koeschner and Ti-Chuang for support and help. Figures 1; tables 1; references 14: 7 Russian, 7 Western.

Lowering Manganese Losses During High-Manganese Melt Making

927D0139H Moscow IZVESTIYA VYSSHIKH UCHEBNYKH ZAVEDENIY: CHERNAYA METALLURGIYA in Russian No 11, Nov 91 pp 96-97

[Article by A.N. Pshenichnyy, A.Ye. Semin, L.N. Kats, Moscow Steel and Alloy Institute; UDC 669.187.2.046.5: 621.365.22]

[Abstract] High losses of manganese due to its transition to the slag phase and vaporization during the smelting of the Kh14AG15 high-manganese alloy at the Dneprospetsstal plant prompted an investigation of the effect of such smelting parameters as the manganese and carbon concentration, the presence of slag, temperature, and the atmosphere over the melt on manganese losses. As a result, a mathematical model is derived, making it possible to describe the behavior of the principal melt constituents during the nitrogen and oxygen blasting. The dependence of the manganese concentration in the melt on the blasting duration during the refining is plotted and compared to the model curve. An analysis of the laboratory experiment shows that it is possible to lower manganese losses during the metal tapping from the furnace by creating a protective reducing atmosphere. Figures 1; references 1.

Effect of Copper on High-Strength Pig Iron Structure and Properties

927D0140D Moscow LITEYNOYE PROIZVODSTVO in Russian No 1, Jan 92 pp 10-11

[Article by V.I. Ovchinnikov, D.V. Tyutin, A.S. Zvolinskiy, Rostov Institute of Agricultural Machinery and Rostselmash Plant; UDC 621.74:669.131.7]

[Abstract] Alloying as an efficient means of controlling the structure and properties of pig iron with globular graphite (ChShG) is discussed, and it is shown that copper additions make it possible to produce a uniform pearlite structure in pig iron with globular graphite. Moreover, at high temperatures copper helps to increase the dissolved carbon activity coefficient but at a $\leq$900°C temperature, this coefficient decreases to <0, attesting to the fact that Cu serves as a graphitizing agent during the eutectic transformation in cast iron and as a pearlitizing agent during the eutectoid cast iron transformation. The results of dilatometry studies of the supercooled austenite are discussed, and the chemical composition of the samples used in the studies is summarized. Critical polymorphous $\alpha \rightarrow \gamma$ transformation points are recorded. An analysis of the findings and an examination of the microstructure of cast samples shows that an addition of 0.06 percent Cu to the alloy decreases the polymorphous $\alpha \rightarrow \gamma$ transformation temperature while the critical points are lowered by 7-10°C. As a result, the pearlite forming during the austenite decay has a more disperse structure. Given an identical ratio of the structurally free ferrite and pearlite (90 percent П and 10 percent Фе), samples of cast iron alloyed with copper have a higher strength without a noticeable decrease in ductility. Figures 1; tables 1.

Technology and Equipment for Making High-Strength Pig Iron. Principal Research Trends

927D0141A Moscow LITEYNOYE PROIZVODSTVO in Russian No 9, Sep 91 pp 5-8

[Article by Yu.I. Senkevich, Ye.B. Shitsman, Scientific Production Association of the Scientific Research Institute of Special Casting Methods; UDC 621.74:669.131]

[Abstract] The most important efforts toward developing the technology and equipment for making high-strength cast iron are summarized. The methods of making high-quality castings with a specified mix of physical, mechanical, and operating characteristics and microstructure in the cast state which have been investigated, developed, and commerically implemented are reported. New efficient processes of making castings without nonmetallic inclusions (the so-called black spots) and with a lowered lost head are described, and the parameters necessary for producing large quantities of pig iron with globular graphite (ChShG) for large castings, primarily for metallurgical ingot molds, are formulated. The comparative effect of graphitizing inoculants on the microstructure and properties of pig iron with globular graphite produced by inoculation with magnesium in an autoclave is examined. The specifications of a magnetohydrodynamic (MGD) unit for continuous inoculation are cited. A technique for selecting the chamber inoculation process parameters and analyzing the reaction chamber dimensions is formulated; the method makes it possible to make castings with isotropic characteristics pursuant to GOST 7293-85. An Inmold analytical routine is developed for IBM PC/XT or Iskra 1030 microcomputers. The software has been used for designing a casting method and is recommended for commercial use. Tables 1; references 4.

Bismuth- and Rare Earth Metal-Containing High-Strength Pig Iron Inoculant

927D0141B Moscow LITEYNOYE PROIZVODSTVO in Russian No 9, Sep 91 pp 8-9

[Article by Ya.B. Bulayevskiy, L.Ya. Kozlov, E.B. Ten, Scientific Production Association of the Scientific Research Institute of Special Casting Methods and Moscow Steel and Alloy Institute; UDC 621.74:669.13]

[Abstract] The inconsistency of published data on the graphitizing inoculation of pig iron with globular graphite (ChShG) by additions of bismuth and rare earth metals (RZM) prompted an effort to determine the optimum inoculant composition. To this end, a quantitative correlation between the graphitization parameter, i.e., the number of graphitization centers (ChTsG), and the inoculant composition is established by the experimental design method and a "composition-property" constitution diagram is plotted. The procedure of pig iron inoculation in a model 99111M autoclave is outlined and the graphitizing treatment efficiency is assessed by chemical and microstructural analyses. The dependence of the amount of structurally free carbides (SSK) in the microstructure of pig iron with globular graphite and the number of graphitization centers on the inoculant rate for specimens of

various thickness is plotted; the curves indicate that the castings have a stable range of high ductility and strength characteristics. An analysis of the joint and several effect of various inoculants shows that Bi, Sb, and As do not form compounds with a dimensional correspondence to graphite's crystal lattice and cannot be present in the solid form if added separately to pig iron while biatomic intermetallic compounds of Bi with rare earth metals meet the dimensional correspondence criteria. These facts explain the experimental phenomenon of graphitizing inoculation "longevity" of a mixture of bismuth, ferrosilicon, and rare earth metals. The new combined inoculant makes it possible to produce pig iron with globular graphite with high ductility and strength properties in the cast state and is recommended for commercial use. Figures 1; references 4: 3 Russian, 1 Western.

On Effect of External Surplus Pressure on Porosity Development in Aluminum Castings

927D0141C Moscow LITEYNOYE PROIZVODSTVO in Russian No 9, Sep 91 pp 9-11

[Article by A.A. Khomitskiy, Scientific Production Association of the Scientific Research Institute of Special Casting Methods; UDC 621.74:669.715]

[Abstract] The effect of the gas liberation process conditions in the solidifying casting metal on the volume and type of porosity and especially the effect of surplus external pressure applied to the metal which feeds the casting is discussed and the mechanism of the external surplus pressure effect on the development of endogenic porosity in the metal during autoclave casting, low-pressure die casting, and backpressure die casting is considered. The effect of a decrease in the dissolved hydrogen diffusion rate and an increase in the solidification rate due to external surplus pressure is outlined. The behavior of the casting solidification duration of aluminum and binary Al-Si system alloys on the surplus pressure at various silicon concentrations, the behavior of the hydrogen concentration in the liquid phase during the flat casting solidification in a metal mold, and the behavior of surplus pressure during the solidification process for various casting processes are plotted. An analysis shows that the effect of an increasing surplus pressure on the gas shrinkage porosity formation in the solidifying casting is more beneficial than that of constant pressure; the proposed method—referred to as medium pressure die casting with solidification—is recommended for use in existing low-pressure die casting machines. Figures 3.

Characteristics of Electroslag Remelting of Tool Steel Chip Scrap

927D0141D Moscow LITEYNOYE PROIZVODSTVO in Russian No 9, Sep 91 pp 11-12

[Article by Ye.V. Odegov, Scientific Production Association of the Scientific Research Institute of Special Casting Methods; UDC 621.74.01:669.187.56]

[Abstract] Electroslag remelting—making consumable electrodes and then remelting them (EShP)—of tool chip scrap under a layer of refining flux and its shortcomings are discussed; for example, electroslag remelting in a mold at a constant current load is inefficient and expensive. Consequently, the design of consumable electrodes form compacted chips; the methods of their remelting are analyzed; the mechanism of electroslag remelting of small size metal scrap in a mold and a crucible (EShTP) with a discrete scrap feed to the melting zone is examined; and an attempt is made to establish a correlation between the characteristics of the chips and the parameters of electroslag remelting in a mold or a crucible. The advantages of the method of feeding the scrap to the melting zone through a hollow refractory element, such as a magnesite part in lab furnaces, are considered, and it is shown that the dependence of the electric parameters of the process on the mass, volume, and density of the remelted material is linear. A mathematical model of the process is developed, and the conclusion is drawn that the use of this method makes it possible to use the metal for auxiliary needs repeatedly, to lower irretrievable losses of scarce alloying materials (W, V, Cr, etc) by sixfold to tenfold, as well as to increase the metal utilization by 15-25 percent and to reduce the cost of products by 1.5-2 times.

Pretreatment of Alloying Compositions for Aluminum Alloy

927D0141E Moscow LITEYNOYE PROIZVODSTVO in Russian No 9, Sep 91 pp 12-13

[Article by A.V. Guretskiy, I.I. Karbovskiy, N.F. Mikotina, Scientific Production Association of the Scientific Research Institute of Special Casting Methods; UDC 621.74.011:669.171.55]

[Abstract] The effect of Al-Cr, Al-Ni, and Al-Mo alloying composition pretreatment on the structure and mechanical properties of the resulting aluminum alloy is examined using AK5M2 alloy pigs, and the mechanical properties of the alloy are summarized. The effect of casting and solidification in mold rolls under reduction and high cooling rate conditions on the alloying composition grain and intermetallic compound structure is discussed. A microstructural analysis of the AK5M2 metal alloyed with these compositions and cast into strips shows that the α-solid solution grain becomes refined to a 10-15 μm size with a corresponding improvement in mechanical properties; the ductility of the metal alloyed with compositions and cast into mold rolls with rapid quenching increased by twofold, its rupture strength rose by 10-12 percent, and its hardness increased by 15-17 percent.

Production of Copper Alloy Billets

927D0141F Moscow LITEYNOYE PROIZVODSTVO in Russian No 9, Sep 91 p 13

[Article by M.V. Mikhaylyk, B.V. Odarchenko, Scientific Production Association of the Scientific Research Institute of Special Casting Methods; UDC 621.74.047:669.35]

[Abstract] Production of copper alloy blanks for various machine elements by permanent mold casting, sand and loam casting, and spin casting and the resulting high percentage of waste (5-10 percent for ingots and 30-50 percent for billets) are discussed, and a new continuous

casting method is described. Blanks produced by continuous casting are characterized by a low consumption of scarce materials, an absence of cavities, porosity, and scaling, and a decrease in the amount of chips and scrap. Moreover, the metal utilization factor (KIM) increases to 88-92 percent. Experience shows that given production of continuously cast blanks with varying standardization levels and a broad range of specifications ensures a 600-850 kg saving of such scarce metals as tin, zinc, lead, and copper for each ton of blanks.

Continuous Horizontal Casting in Machine Building

927D0141G Moscow LITEYNOYE PROIZVODSTVO in Russian No 9, Sep 91 pp 21-22

[Article by G.G. Tsarev, Scientific Production Association of the Scientific Research Institute of Special Casting Methods; UDC 621.74.047]

[Abstract] The horizontal continuous casting process (NGL) is used extensively throughout the world, yet out of the 345 horizontal continuous casting machines shipped by the manufacturing companies, only 20 are in the USSR. The capabilities of the horizontal continuous casting process are far from being fully utilized; consequently, the possibility of producing blanks from pig iron with globular graphite (ChShG) without subsequent annealing is investigated at the Scientific Research Institute of Special Casting Methods (NIISL), and the results are reported. The methods of adding magnesium to pig iron in the autoclave chamber or to the ladle and the graphitizing alloying compositions are described. The microstructure of the resulting pig iron, i.e. the pearlite, ferrite, and cementite concentration as a function of the alloying composition, is summarized, and it is shown that under certain conditions, it is possible to attain the necessary casting structure of pig iron with globular graphite. The characteristic features of making castings from poorly machinable alloys, such as corrosion-resistant electrodes, are discussed, and the possibility of using graphite molds for casting high-alloy pig iron and steel is demonstrated. It is noted that multilayer and clad metal castings can be produced by the horizontal continuous casting method. Figures 1; tables 1; references 1.

Investigation of Strontium's Effect on AK11M2 Alloy Properties in Liquid and Solid State

927D0142A Sverdlovsk RASPLAVY in Russian No 6, Nov-Dec 91 pp 3-8

[Article by A.A. Ofengenden, V.Z. Kisunko, L.D. Kuleshova, All-Union Scientific Research Institute of Secondary Nonferrous Metals; UDC (669.046.516.4: 669.715.48).519.2]

[Abstract] The use of strontium for inoculating casting aluminum alloys and the shortcomings of existing methods of determining the optimum strontium concentration prompted a study of the correlation of the properties of the AK11M2 alloy in the liquid and solid state and the use of methods of applied statistics in order to develop sound recommendations for selecting the optimum Sr concentration. The effect of Sr within a 0.0-0.265 percent concentration range by mass on the structure-sensitivity characteristics, kinematic viscosity, density, surface tension at 750°C, flowability in the liquid state at 750°C, ultimate strength, elongation, and HB hardness of the AK11M2 in the liquid and cast states is investigated. The alloy's chemical composition is analyzed by standard procedures accurate within 0.005 percent by mass, and the closeness of the correlation between the properties is determined. A matrix of paired correlations is derived, and statistical estimates of experimental data are made at a 95 percent confidence level. The dependence of fluidity, elongation, and kinematic viscosity on the Sr concentration, the dependence of the alloy density and surface tension on the kinematic viscosity, and the dependence of the ultimate strength and hardness on the fluidity are plotted. The study demonstrates the expediency of using the mathematical statistics methods for examining the heredity phenomenon in metals and alloys and establishes the correlation between the alloy properties in the liquid and solid states as well as confirms the possibility of using the correlation and regression analysis methods for examining the functional dependence of the physical-chemical, process, and mechanical properties of alloys and optimizing the inoculant concentration in casting aluminum alloys. Figures 3; tables 5; references 13.

Atomic Ordering in Surface Liquid Metal Layers: Copper, Gold, and Germanium

927D0142B Sverdlovsk RASPLAVY in Russian No 6, Nov-Dec 91 pp 16-21

[Article by A.V. Lavrov, S.I. Popel, M.A. Spiridonov, Urals Polytechnic Institute imeni S.M. Kirov, Sverdlovsk; UDC 548.74:669.36:621.386]

[Abstract] The poor accuracy of existing methods of studying the atomic ordering in the surface layer of melts by small-angle electron scattering and the advantages of increasing the electron beam energy to 50-100 keV prompted the development of a new cell and a device which make it possible to melt a specimen in a commercial microscope and record the diffraction pattern created by the electron beam reflected by the surface layer of the resulting drop. The structure of the surface layers of three metals—Cu, Au, and Ge—whose surface conditions greatly determine the performance of many semiconductor and electronics products is investigated. Electron diffraction patterns are recorded slightly above the melting point in a vacuum and photometric measurements are taken in a direction perpendicular to the axes of diffuse rods. The structural factors of liquid metals and difference functions of the cylindrical atomic distribution in the metal surface are plotted and the structural parameters of copper, gold, and germanium are summarized. The total structural factor's components are determined. The new cell makes it possible to obtain information about the short-range order structure parameters in melts with different fractions of covalent interaction. Sequences of different interatomic distances relative to the central atom are discovered in metals with dense and loose fusion structure; the extent of

ordering areas determined by the structural maxima attenuation in the surface layer is measured making it possible to speculate that there are microordering areas with a 5-6 atomic diameter size in Cu and Au layers and a nine atomic diameter size in Ge. Figures 2; tables 1; references 8: 5 Russian, 3 Western.

On Volatilization of Microcomponents From Inhomogeneous Melts

927D0142C Sverdlovsk RASPLAVY in Russian No 6, Nov-Dec 91 pp 36-41

[Article by S.V. Stefanovskiy, I.A. Knyazev, S.A. Dmitriyev, Radon Scientific Production Association, Moscow; UDC 666.1.031:621.039.73]

[Abstract] One of the most important tasks in nuclear power engineering which can be solved with the help of vitrification technology—containment of radioactive waste (RAO)—is addressed, and two methods of vitrifying radwaste products are considered. The low volatilization of ^{137}Cs nuclides during the high-temperature treatment of solid radwaste in a shaft furnace is discussed, and an attempt is made to check the hypothesis that this is due to the radionuclide localization in the minerals which formed as a result of the solid phase reaction in the shaft's mid-section and do not dissociate fully in the lower section at a 1,300-1,500°C temperature. The experiment staged to check the theory is described. The characteristics of the model products after heat treatment at various temperatures and the phase composition of the resulting slag products are summarized, and the diffraction patterns of the slags and glass produced at 1,400°C are plotted. The exposure dose variation of the simulated radioactive waste slag, the real solid radwaste slag, pilot plant slag, and glass with liquid radwaste oxides are measured by scanning gamma-recording and compared to a standard. The methods of emission, spectral, radiometric, and X-ray phase analysis and scanning gamma-recording are compared. The results show that the inhomogeneous slag melt in the lower part of the shaft furnace and on its bottom makes it possible considerably to lower the volatilization of volatile microcomponents due to their localization in the crystal lattice sites of the minerals forming in the slag; radioactive nuclides of iron and cobalt are concentrated in the metallic component of the slag while those of cesium and strontium are concentrated in the silicate component. Figures 2; tables 2; references 19: 14 Russian, 5 Western.

Effect of Conditions of Grinding Wheel Dressing by Diamond-Studded Rolls on Workpiece Surface Roughness After Plunge-Feed Grinding

927D0145D Kiev SVERKHTVERDYYE MATERIALY in Russian No 1 (76), Jan-Feb 92 pp 34-39

[Article by M.N. Sheyko, Ye.S. Lavrinova, I.Kh. Cherepovetskiy, Superhard Materials Institute at the Ukrainian Academy of Sciences, Kiev; UDC 621.923:621.922:621.921.34]

[Abstract] Various published studies of the effect of the grinding wheel dressing conditions on the roughness of the surface machined by these grinding wheels are discussed, and the theoretical and experimental dependence of the workpiece surface roughness on the conditions of grinding wheel dressing by diamond-studded rolls are compared. In so doing, a mathematical model of the surface roughness development during dressing and grinding which also explains the effect of dressing conditions is used. The theoretical and experimental dependence of the maximum profile height R_{max} on the infeed grinding and dressing parameters are plotted; here the plunge-feed grinding and infeed dressing parameters are understood as the wheel and roll velocity and their ratio, the roll feed per wheel turn, and the number of truing turns without the infeed. The values of the maximum profile height after grinding with a wheel dressed at various truing conditions and the values of the maximum profile height as a function of the grinding wheel to roll speed ratio are summarized and the theoretical dependence of the maximum profile roughness on the truing duration and the grinding wheel to roll speed ratio is plotted. The findings as well as simulation experience indicate that the microprofile development mechanism can in a first approximation be represented on a purely mechanical level. It is speculated that the grinding model can be used for controlling certain initial characteristics of the diamond-studded roll's working layer during its manufacturing and finishing, selecting the dressing conditions, and assessing the dressing efficiency. Figures 3; tables 2; references 8: 6 Russian, 2 Western.

High-Speed Steel Surface Quality Under High-Efficiency Grinding With CNB Wheels

927D0145E Kiev SVERKHTVERDYYE MATERIALY in Russian No 1 (76), Jan-Feb 92 pp 40-45

[Article by Yu.Ya. Savchenko, V.G. Delevi, F.G. Smaglenko, I.V. Leshchuk, N.G. Bagno, L.I. Peschanskaya (deceased), Superhard Materials Institute at the Ukrainian Academy of Sciences, Kiev; UDC 621.923:661.65:661.55]

[Abstract] A high-efficiency nonburning grinding and sharpening process developed at the Superhard Materials Institute at the Ukrainian Academy of Sciences for high-speed steel cutting tools is reported; grinding is performed at high rates of up to $\geq$600 mm^3/min without cooling using synthetic corundum and kubonit borazon and elbor borazon CNB grinding wheels (KNB) with the K17 ceramic and PK-03 mineral polymer binder. The effect of various process factors, primarily the graininess and speed, on the finished surface quality is investigated. To this end, samples from high-speed steel R6M5 are ground without cooling with 12A2-45° wheels at a 2.4 mm/min feed. The dependence of the arithmetic mean deviation of the profile in the kubonit CNB graininess with and without truing and the dependence of the arithmetic mean deviation of the profile on the wheel velocity with and without truing are plotted. The results of metallographic and X-ray structural analysis of the machined surface of steel R6M5 and and steel R12F3K10M3 (for comparison) are summarized, and the dependence of the residual stress in steel on the grinding wheel characteristics is plotted. To assess the effect of the tool surface layer condition and surface microgeometry after grinding by the new method on the tool resistance, comparative tests are carried out. An

analysis of the findings indicates that the new process makes it possible to attain an arithmetic mean deviation of the profile of R_a=0.2-0.6 μm by using truing passes without cross-feed and produce a surface layer with an insignificant change in structure and with residual compressive stresses of up to 1,600 MPa, thus substantially increasing the cutting tool endurance (by 1.3-2.3 times). Figures 5; tables 2; references 4.

Diamond Sticks for Centerless Superfinishing of Small-Diameter Shafts and Axles

927D0145F Kiev SVERKHTVERDYYE MATERIALY in Russian No 1 (76), Jan-Feb 92 pp 63-64, 69

[Article by A.A. Orap, A.V. Galkov, V.S. Barkov, Superhard Materials Institute at the Ukrainian Academy of Sciences, Kiev; UDC 621.922.03]

[Abstract] Methods of decreasing the surface roughness of small-diameter shafts and axles by superfinishing in model 3D878 multiposition centerless automatic grinding machines are outlined, and the inadequacy of the synthetic corundum sticks with a cast ceramic binder is emphasized. Consequently, the possibility of developing superfinishing sticks for centerless machining of cylindrical parts with a 2.5-5.0 mm diameter and 25-100 mm length from alloy steels under automated production conditions is investigated. The study reveals that diamond sticks on a metal base meet these requirements. The tool selected for this purpose is tested during the superfinishing of tape recorder shafts with a three mm diameter from steel KhVG using a cooling lubricant (SOTS) consisting of a mixture of kerosene and industrial oil. The tests demonstrate that two mm wide ASM diamond sticks with a 14/10, 10/7, and 7/5 graininess ensure a surface roughness (arithmetic mean deviation of the profile) of less than 0.08 μm, given an initial roughness of 0.16 μm and wear out twenty times slower than regular abrasive sticks. The linear wear of one diamond stick used to grind 1,000 shafts does not exceed one mm while the grinding efficiency is 20-25 shafts per minute. Implementation of the new technology makes it possible to master mass production of class 2 tape recorders; the economic impact at one plant amounts to 50,000 rubles per annum. References 2.

Effect of Strained State on Powder Metal Compaction During Hot Die Forging

927D0146A Kiev POROSHKOVAYA METALLURGIYA in Russian No 2 (350), Feb 92 pp 8-12

[Article by V.A. Pavlov, M.I. Nosenko, Zaporozhye Mechanical Engineering Institute; UDC 621.762.4]

[Abstract] The shearing strain intensity, shearing strain, and relative density distribution in a sample volume of powder metal during the hot die forging process as well as the intense and impeded straining zones, optimal designs, and hot die forging parameters of samples of various density produced from the PTES-1, PTEK-1, and TG-TV titanium powders, PMS-1 copper powder, and the PA-2 aluminum powder by cold two-sided compaction are investigated. The samples are heated in argon prior to compaction; the sample density after cold compaction and hot die forging are measured by hydrostatic weighing pursuant to GOST 25281—82. The strained state and compaction degree are determined by analyzing the local strain distribution by coordinate grid distortions. The results indicate that an increase in the straining degree during the first phase of die forging in a closed die and an increase in the outflow factor during die forging by dies with outflow elements lead to an increase in the shearing strain intensity and density distribution uniformity within the metal. Figures 5; references 1.

Dimensional Changes in Al—4.4 Percent Cu and in Al—4.4 percent Cu and 0.5 Percent Mg Compacts Under Sintering

927D0146B Kiev POROSHKOVAYA METALLURGIYA in Russian No 2 (350), Feb 92 pp 13-17

[Article by V.A. Brodov, A.V. Zhiltsov, Yu.V. Levinskiy, G.N. Romanov, All-Union Scientific Research Institute of Electromechanics; UDC UDC 621.762]

[Abstract] Dimensional changes in compacts during sintering—especially their growth—with a liquid phase and the diverging views on the contribution of diffusion saturation are discussed, and several patterns of the growth mechanism of Al-Cu alloy compacts and the effect of Mg additions on this process are investigated. Cylindrical Al—4.4 percent Cu, Al—4.4 percent Cu and 0.5 percent Mg, Al—50 percent Cu, and Al—0.5 percent Mg samples made from standard powders are tested; the relative sample density is measured by the differential thermal analysis (DTA) and dilatometry methods. An analysis of the sample behavior during sintering within a 530-620°C temperature range shows that the formation of intermetallic compounds during the heating is accompanied by an exothermal reaction as a result of which the eutectic melting point occurs sooner than in the ambient volume and intensive growth of the Al—4.4 percent Cu and the Al—4.4 percent Cu and 0.5 percent Mg compacts is accompanied by the appearance of a molten phase at 543 and 530°C, respectively. A correlation between the liquid phase and dimensional changes is established: A disappearance of the liquid phase during the exposure corresponds to growth, and liquid phase retention corresponds to shrinkage. The results also demonstrate that copper and magnesium diffusion is not the sole cause of growth; melt propagation along the aluminum grain boundaries and surface is a contributing factor (by about a third). Ternary alloy compacts grow more than binary alloys not due to the Mg diffusion into Al but due to an increase in the liquid phase amount. Figures 3; tables 2; references 14: 10 Russian, 4 Western.

Effect of Initial Powder Properties on Structural Characteristics of Porous Materials

927D0146H Kiev POROSHKOVAYA METALLURGIYA in Russian No 2 (350), Feb 92 pp 47-52

[Article by V.K. Sheleg, V.M. Kaptsevich, V.V. Savich, A.N. Sorokina, Belarussian Republican Scientific Production Association of Powder Metallurgy; UDC 621.762]

[Abstract] The relationship between the properties of porous powder materials (PPM) and the properties of the initial powders is discussed, and the results of an investigation of the effect of the powder properties on such structural characteristics of porous powder materials and porosity and pore size are summarized. The porosity, pore dimensions, bulk density, and settled packed density are measured using standard techniques; the particle form factor is determined by Saltykov's method on a MOP-AMO3 optical analyzer made by Reichert (Austria) while pycnometric density is measured in a model 1200 helium-filled automatic pycnometer made by Micrometrics (USA). The results demonstrate that the maximum porous powder material pore dimension depends more on the initial powder's form factor than the mean dimensions due to an increase in the structural irregularity. Composite characteristics of the initial powder properties may be thus used for predicting the properties of the porous powder materials made from them and for developing and designing PPM products. Figures 5; tables 1; references 17.

Electrospark Coat Utilization Trends in Electrical Engineering

927D0148A Kishinev ELEKTRONNAYA OBRABOTKA MATERIALOV in Russian No 5 (161), Sep-Oct 91 pp 7-9

[Article by Ye.A. Zaytsev, Institute of Materials Science Problems at the Ukrainian Academy of Sciences, Kiev]

[Abstract] The shortcomings of existing methods of applying precious metal coats in electrical engineering, particularly the negative environmental impact and poor coat adhesion with the base, are discussed, and the factors which determine the quality of electrospark coats are considered. The main problems facing electrospark coat application are identified as these: developing the necessary dedicated equipment, electrode materials, and application methods. The coats applied to electric contacts are divided into two groups: those on the fastening (technological) surfaces and those on the working surfaces. The principal factors affecting the selection of working surface coats are their thickness, contact resistance, surface purity, and base material. Electrode materials for electrospark alloying (EIL) are recommended for various base metals. It is suggested that multilayer coats be used in order to increase the layer thickness and extend its service life, and the application duration and maximum thickness of two-layer coats are summarized. Two-layer coats are tested at various current levels, and the number of their switchings to failure as a function of current strength is established. The outlook for using palladium and gold-based electrode materials is evaluated, and it is noted that the resource-saving electrospark alloying method can facilitate the coat application automation and mechanization. Tables 3.

Erosion of Silicon Alloys With Group IV Transition Metals in Steady Electric Arc

927D0148B Kishinev ELEKTRONNAYA OBRABOTKA MATERIALOV in Russian No 5 (161), Sep-Oct 91 pp 14-17

[Article by Zh.A. Mrochek, B.A. Eyzner, I.A. Ivanov, Engineering Physics Institute at the Belarussian Academy of Sciences, Minsk]

[Abstract] The possibility of expanding the capabilities of vacuum electric arc deposition of protective coats by using new alloys in eroding electrodes and the lack of data on the process of multicomponent system erosion in the vacuum arc are discussed, and erosion of a silicon alloy with group IV transition metals under the effect of a steadily burning vacuum arc on their surface is investigated. To this end, a Hall's end plasma evaporator whose vacuum chamber walls serve as the anode is examined. Alloys of silicon with group IV transition metals are used as the cathode; the Si concentration in the alloys is varied within 66-95 percent (at.) and the alloy phase composition is examined by a DRON-3.0 unit in Cu*K* radiation. The element distribution in the surface layers is examined by a CAMECA MS-46 microprobe analyzer, and the erosion rate is measured by the weighing method. The titanium and Si+80 percent Ti alloy distribution in the modified surface layer and the dependence of the energy generation value and mass transfer coefficient on the electrode composition are plotted. An analysis demonstrates that an increase in the silicon concentration to 86-88 percent leads to the appearance of thermal cathode spots. It is speculated that the spots are due to a deterioration of the cathode surface emissivity; this transition is accompanied by an increase in the erosion rate and a decrease in the energy value for generating a unit of cathode volume. Moreover, the alloy erosion occurs without predominant evaporation of its constituents. Figures 3; references 9.

Outlook for Using High-Power CO_2 Lasers for Treating Quartz Glass Products

927D0126A Moscow STEKLO I KERAMIKA in Russian No 10, Nov 91 pp 7-8

[Article by S.G. Vologdina, V.M. Ganyuchenko, N.A. Kalinin, Yu.G. Kolmogorov, V.A. Lipakov, Gyuys Design Office, Leningrad Electrical Engineering Institute imeni V.I. Lenin, and Elvaks Plant; UDC 666.192:621.039]

[Abstract] The importance of the diffusion oxidation and epitaxial unit reactors and fixtures made from quartz glass for making integrated circuits and the need to weld, cut, grind, and drill the quartz glass surfaces are stressed, and it is shown that many of these operations can be performed by means of laser treatment using a single technological complex; the use of lasers in products intended for VLSI circuits (SBIS) is also characterized by a total lack of contamination and the possibility of extensively automating the production process. An important drawback of the laser method—the need to eliminate or reduce residual thermal stresses in the ready products—is discussed, and it is demonstrated on the basis of experimental studies that by using CO_2 lasers with a beam power of 1 kW, it is possible to treat parts up to 12 mm thick, attain a cutting accuracy of 0.1 mm which is almost ten times better than mechanical cutting, make 0.1-0.2 mm wide cuts, produce a 0.4-0.8 mm wide weld, make holes with a 0.06-0.40 taper, and produce no defective layers on the treated surfaces. Thus, CO_2 lasers are promising for use in making electronics industry attachments, ensure a high surface treatment quality, and make it possible to automate the process. References 2.

Effect of Zirconium on Nitrogen and Carbon Solubility in Chromium

927D0127B Kiev METALLOFIZIKA in Russian Vol 13 No 12, Dec 91 pp 41-47

[Article by V.G. Ivanchenko, Institute of Physics of Metals at the Ukrainian Academy of Sciences; UDC 669.26]

[Abstract] The effect of the solubility of the phase with a high surface area to volume ratio in the matrix on the thermal stability of heterophase structures with a well-developed interface surface used as hardening phases or barrier layers is discussed, and a new thermodynamic analysis of the zirconium carbide and nitride solubility in chromium is performed, making it possible to take into account the most recent data on phase equilibria and thermodynamics of alloys that limit binary systems. The thermodynamic properties of the alloy constituents are described in terms of their activities in order to avoid using model concepts. A thermodynamic analysis of the mutual solubility of Zr and C and Zr and N in Cr makes it possible to compare the solubility of ZrN and $ZrC_{0.72}$ to the N and C solubility in binary systems at various temperatures and determine the effect of Zr on the N and C solubility in chromium. It is shown that the zirconium nitride and carbide solubility in chromium is very low, indicating that Zr is a highly efficient refining addition to Cr, i.e., chromium hardened with highly disperse particles of these phases should have an elevated ductility at room temperature. The rate of hardening particle coalescence within a 1,100-1,300°C temperature range is not high. The same is true for the stability of barrier layers. The temperature dependence of the limit of ZrN and ZrC solubility in chromium is established. The results are found to be consistent with earlier findings and data obtained by transmission electron microscopy. Tables 1; references 17: 3 Russian, 14 Western.

The Physicochemical State of the Surface Layers and the Performance Properties of the Alloy VT18U Subjected to the Effect of a High-Power Ion Beam

927D0130C Moscow FIZIKA I KHIMIYA OBRABOTKI MATERIALOV in Russian No 5, Sep-Oct 91 (manuscript received 13 Jun 90) pp 14-23

[Article by A.N. Didenko, V.A. Shulov, G.Ye. Remnev, A.E. Strygin, A.D. Podgrebnyak, N.A. Nochovnaya, and Yu.D. Yagodkin, Moscow; UDC 539.213.621.17.533]

[Abstract] VT18U is an alloy consisting of titanium and the following (percent by mass): C, 0.1; Al, 6.5; Mo, 3; Nb, 1.5; Zr, 4.5; Fe, 0.2; Sn, 3; O, 14; N, 0.04; and H, 0.015. Plates measuring 150 x 15 x 5 mm^3 were cut from heat-treated bars of VT18U (hardened from 950°C and annealed at 600°C for 15 minutes in a vacuum of at least 1.33×10^{-4} Pa). The specimens were bombarded with a high-power ion beam with a current density of 20 to 150 A/cm^2 (five pulses each lasting 80 to 100 ns). After the ion beam bombardment the specimens were annealed at 550°C for two hours in a ULVAK vacuum furnace and were cut into several sections measuring 15 x 7 x 5 mm^3. Auger electron spectroscopy (on a 09IOS10-005 unit) was used to determine the chemical composition of the specimens' surface layers. The sputtering rate was estimated experimentally from plotted profilograms. The structural state of the specimens' surface layers was studied by X-ray structural analysis on a DRON-UM1 diffractometer. Exoelectron emission studies were performed, and the specimens' microhardness and roughness were measured. The studies performed confirmed that ion bombardment at a current density of 140 to 150 A/cm^2 followed by diffusion annealing at 550° for two hours results in the formation of a surface layer of finely dispersed titanium carbides about 0.2 μm thick on the surface of VT18U. The said treatment regimen also gave the test specimens a uniform structural state, "healed" the macrodefects along their edges, increased their microhardness, and reduced their surface roughness. Ion beam treatment at the current densities studied increased the endurance limit of the specimens by 10 percent, increased their cyclic durability by a factor of 20 when $\sigma = 370$ MPa, increased their refractoriness by a factor of 2.3 (when the specimens were held in air at 550°C for 200 hours), and increased their resistance to dust erosion by a factor of 1.8. A catastrophic drop in fatigue strength was observed upon irradiation with a current density of 160 A/cm^2 that was attributed to the formation of high-temperature α-TiO_2 oxide on the alloy's surface. Figures 5, tables 2; references 14: Russian, Western.

Structural Changes in Carbon Steel Irradiated With High-Energy Electrons

927D0130E Moscow FIZIKA I KHIMIYA OBRABOTKI MATERIALOV in Russian No 5, Sep-Oct 91 (manuscript received 4 Jul 90) pp 29-34

[Article by V.Yu. Fomichev, A.S. Filippov, Yu.F. Tomashchuk, and V.I. Gorodetskiy, Moscow; UDC 669.1.11: 519.677]

[Abstract] Specimens of St3 and U10 steel in the form of cylinders 30 mm in diameter and 10 and 12 mm high were bombarded with electrons in a Fakel linear electron accelerator at the Atomic Energy Institute imeni I.V. Kurchatov. An average beam current during irradiation of 250 to 350 μA was used along with an electron energy of E = 30 MeV. The duration of the irradiation did not exceed 10 s. Microsections of the irradiated specimens were etched with a 3 percent alcohol solution of HNO_3 to make the metal's microstructure more apparent, and an NU-2 microscope was used to study the specimens' microstructure. The evolution of the temperature field, local volumetric melting, and motion of the boundaries of the melt bath were studied at different experiment parameters. Specifically, the effect of electron fluxes with E = 25 and 30 MeV at average currents of 150, 170, 200, 250, 300, and 350 μA onto steel cylinders measuring 30 and 90 mm in diameter and 10, 12, and 15 mm high were studied. The radial distribution of the current density in the beam was kept constant with a radius r_0 of 0.5 cm (equal to the radius of the opening in the collimator). Metallographic studies performed on polished cross sections of the irradiated St3 specimens confirmed that the radiation regimens tested do cause structural changes in the metal. Specifically, irradiation was found to result in the formation of a number of axisymmetric zones that each had its own specific microstructure. A melt bath was detected metallographically in the cross sections of all the specimens in which paraxial cavities appeared upon irradiation. The said melt bath was found to expand at a rate of less than or about 10 mm/s in an axial direction and less than or about 1.3 mm/s in a radial direction. Concentric zones of structural changes were found to occur around the bath. The metal in these segments was found to include stretched crystallites oriented perpendicular to the boundary of the melt bath. The following zones of structural change were found (moving outward from the boundary of the melt bath in a radial direction): a superheating zone, a recrystallization zone, a perlite transformation zone, and a zone of starting metal that appeared to have remained untouched by the bombardment. When the melt front reached the surface of an irradiated specimen, the melt was ejected. This in turn resulted in the formation of paraxial cavities and micropores in the metal. This phenomenon in turn may create complications in attempts to make purposive localized changes in the structure and properties of metal by irradiation in a regimen involving melting. Figures 5; references 11: Russian.

Calculating the Melting and Solidification of Metal Subjected to Pulses of Concentrated Energy Fluxes

927D0130F Moscow FIZIKA I KHIMIYA OBRABOTKI MATERIALOV in Russian No 5, Sep-Oct 91 (manuscript received 15 Jan 91) pp 36-40

[Article by A.A. Uglov and O.G. Sagdedinov, Moscow; UDC 536.421.539.211]

[Abstract] Numerous other researchers have examined the problem of calculating the melting and solidification of metal subjected to pulsed concentrated energy fluxes. Each of the calculation methods that has been proposed to date has one type of complication or other. The authors of the study reported herein worked to develop a simple yet precise method of describing the aforesaid melting-solidification process. Specifically, the authors focus their attention on the processes of the melting and solidification of a semicontinuous metal target subjected to a surface-absorbed constant heat flux. The thermophysical characteristics of the metal and its melt were assumed to be identical, and the convection-related heat loss from the target surface relative to the absorbed energy flux density was assumed to be negligible. An approximate analytical method was developed to solve the problem. It was demonstrated to have an error on the order of only a few percentage points. Time dependences of the temperature fields and position of the melting temperature-metal crystallization isothermic line were derived. Sample calculations performed for the example of titanium confirmed that the proposed method is both simple and accurate. Figures 2; references 9: 8 Russian, 1 Western.

Experiments on Directed Crystallization of Indium Antimonide in Ampules on the Kosmos 1744 and Foton Artificial Earth Satellites

927D0130G Moscow FIZIKA I KHIMIYA OBRABOTKI MATERIALOV in Russian No 5, Sep-Oct 91 (manuscript received 20 Feb 91) pp 46-52

[Article by V.S. Zemskov, M.R. Raukhman, Ye.A. Kozitsyna, and I.M. Arsentyev, Moscow; UDC 621.315.592.3+548.523]

[Abstract] A series of experiments on the directed crystallization of tellurium-doped indium antimonide in ampules was conducted on board the Kosmos 1744 and Foton artificial earth satellites. The crystals were grown in ampules about 140 mm in length with an outer diameter of about 16 mm and a wall thickness of about 1.5 mm. The inner surface of the ampules was coated with graphite, and the ampules were evacuated to about 10^{-3} mm Hg (0.13 Pa) before being sealed. An entire InSb monocrystal with a p-n junction grown by the Czochralski method in the direction B(111) was used as a starting ingot. The starting crystal had a diameter on the order of 13 mm and an overall length of about 105 mm. The concentration of holes in the p region was about 1×10^{15} cm^{-3}, and the concentration of electrons in the n region was about 3-4 x 10^{18} cm^{-3}. An ingot was secured in each ampule by a graphite pin from the side of the p region. The directed crystallization process was implemented with each ampule in a stationary position in

the gradient field of the furnace ($\Delta T \approx 15°C/cm$) by controlling the temperature decrease at a rate of 11.3°C/h. The morphology and macro- and microstructures of the crystals were studied. The primary objective of the studies performed was to increase the length of the region of noncontact crystallization. This was achieved after a slight modification of the ampules' original design so as to increase the length of that space in the hot portion of the ampule that was free from the melt. Each of the crystals grown on the Kosmos 1744 and Foton artificial earth satellites was found to have a region of contactless growth with specific features differing from those of the analogous region on crystals grown on the Salut 6 and Soyuz manned spacecraft. The researchers hypothesized that these differences may be due to the different magnitudes and directions of the effect of residual microaccelerations of the respective spacecraft. In addition, the studies performed revealed that tellurium-doped indium antimonide crystals grown under zero-gravity conditions are virtually free of lamellar impurity microheterogeneity. This finding, while secondary from the standpoint of the original purpose of the experiments, is additional confirmation of previously published studies establishing the possibility of growing layerless indium antimonide crystals under zero-gravity conditions. Figures 6; references 8: 6 Russian, 2 Western.

Modeling the Effect of Cosmic Radiation on Semiconductor Microcircuits

927D0130H Moscow FIZIKA I KHIMIYA OBRABOTKI MATERIALOV in Russian No 5, Sep-Oct 91 (manuscript received 7 Dec 89) pp 53-54

[Article by A.I. Akishin, L.M. Savelyeva, and Yu.I. Tyutrin, Moscow; UDC 538.95-405;539.125.4]

[Abstract] The authors of the study reported herein examined the radiation resistance of LSI circuits subjected to the effect of protons with an energy of 100 MeV. A previously reported method of monitoring the working parameters of the LSI circuits in a computer memory was used to examine the effect of different fluences on semiconductor microcircuits. A computer program was developed to monitor the following parameters of a memory circuit located in the path of ionizing radiation: correctness of the information written into each memory cell, voltage in each memory cell, and correctness of the address of the memory cell with which an exchange is made. The tests performed revealed that at fluences of 100 MeV, protons with a fluence of 10^9 to 1.5×10^{10} cm^{-2} induce reversible failures in semiconductor microcircuits. Fluences of more than 10^{11} resulted in fatal (irreversible) failures. References 2 (Russian).

Laser Borating of High-Strength Cast Iron

927D0130L Moscow FIZIKA I KHIMIYA OBRABOTKI MATERIALOV in Russian No 5, Sep-Oct 91 (manuscript received 9 Aug 90) pp 89-95

[Article by I.A. Tananko, A.A. Levchenko, R.T. Guyva, V.A. Guyva, and Ye.Yu. Sittsevaya, Kharkov; UDC 669.14:621.785]

[Abstract] The authors of the study reported herein examined the process of laser borating of high-strength cast iron. As a starting material they used high-strength cast iron containing the following (percent): C, 3.47; Si, 2.150; and Mn, 1.36 with a perlite-ferrite structure (85 to 90 percent perlite) after preliminary treatment. A LATUS-type continuous-wave CO_2 laser with a power up to one kW was used for the laser treatment. The rate at which specimens were moved through the beam was varied from two to four mm/s, the thickness of the boron-containing putty was varied from 0.15 to 0.3 mm, and the defocusing was varied so that the irradiation spot ranged from two to four mm. A mixture of amorphous boron with acetone and nitrocellulose lacquer was used as a putty. The structure and phase composition of the borated layers were studied by optical microscopy with conventional and stain etching. The studies performed demonstrated that laser borating of high-strength cast iron is more effective (results in a harder surface) than does conventional laser heat treatment. The studies also confirmed that laser borating results in practically usable coatings that are deeper than those produced by diffusion borating. X-ray structural analysis confirmed that the borated layer on the treated cast iron specimens consisted of four phases: FeB, Fe_2B, α phase, and borocementite $Fe_3(B, C)$ (a solid solution with a variable concentration of boron and carbon in the cementite phase). Metallographic studies revealed two morphological types of eutectics in the surface layers resulting from the laser borating: a eutectic in the form of independent regions in a layer and a eutectic combined with the excess phase. The first had a clearly pronounced cellular substructure with a characteristic coarsening of the structure along the cell boundaries, whereas the second clearly had visible base wafers of borocementite leading to the formation of eutectic colonies. The eutectics in the different layers and within the confines of a single layer had different dispersivities and different phase ratios. Two additional eutectics appeared when high cooling speeds were used. The boride segments were the hardest. The top hardness values of the said borides were higher than those usually found for the system Fe-B and medium carbon steels. Extensive variations in microhardness were found for the eutectic structures, and the hardness of the hypo- and hypereutectic structures depended largely on their quantitative ratio of excess phases to eutectic. In general, the composition of the borated layer was nonuniform. A rather clear relationship between a decrease in boron content deeper into the layer and an increase in the carbon content toward the surface was observed, however. The highest boron content was found along the edges of the irradiation paths with a decrease in the boron content toward the center part of the layer. When all other conditions were equal, thicker putty layers resulted in thicker borated layers, and faster irradiation rates resulted in reduced layer depths. Figures 3, table 1; references 9: Russian.

Laser Methods of Hardening a Titanium-Zirconium Alloy

927D0130N Moscow FIZIKA I KHIMIYA OBRABOTKI MATERIALOV in Russian No 5, Sep-Oct 91 (manuscript received 29 Jan 91) pp 148-150

[Article by T.V. Bukhtina, O.V. Dolzhonkov, P.Yu. Kikin, A.I. Pchelintsev, and P.V. Chernyshev, Nizhniy Novgorod; UDC 621.373.826:669.295]

[Abstract] The authors of the concise report reported herein examined methods of using lasers to modify the surface of titanium-zirconium alloys. Alloys consisting of 80 percent Ti and 20 percent Zr were studied. Specimens of the study alloys were subjected to pulses of quasi-stationary radiation from a YAG laser operating at a wavelength of 1.06 μm with a pulse duration of 4 ms and an energy of 15 J. The intensity of the irradiation was varied by changing the diameter of the spot treated. First, the researchers studied the possibility of hardening the study alloy by using a range of beam intensities that would not result in surface melting. Rapid phase transformation were found to occur. In the metallographic studies performed on the test specimens, these changes appeared in the form of reduced etchability and a moderate increase in the near surface layer's microhardness. Despite the fact that only moderate increases in microhardness were achieved, the method of laser treatment with beam intensities insufficient to induce surface melting appeared to be extremely promising in that it did not worsen the specimen's surface roughness and may thus be used during finishing. No differences in microhardness distribution of specimens treated in argon and helium were noted. Next, the intensity of irradiation was increased to values of $I > 4.5 \times 10^4$ W/cm^2. As a result a metal bath formed in the laser-affected zone, and high-speed thermocapillary flows developed. The resultant intensification of heat and mass transfer processes resulted in dissolution of the nitrogen medium and synthesis of titanium and zirconium nitrides throughout the entire depth of the melt bath. The surface hardness of the specimens treated nearly tripled, reaching values of 550 to 570 kg/mm^2; however, the crystallization defects and surface roughness accompanying this increase in microhardness make it impossible to recommend the method of laser surface modification by melting. The possibilities of using laser treatment to increase the corrosion resistance of Ti-Zr alloys were also studied. Nickel foil was applied to the specimens' surfaces and the specimen subjected to laser radiation with an intensity of 2.0×10^5 W/cm^2 in a helium medium. A harder and deeper surface layer resulted, but the final structure was noticeably nonuniform. Repeated remelting of the treated surface resulted in a better-quality layer, with the number of pores and cracks decreasing sharply. Figures 3; references 9: 7 Russian, 2 Western.

Structural Transformations in High-Nickel γ-FeNiCr Alloys During Annealing

927D0131I Sverdlovsk FIZIKA METALLOV I METALLOVEDENIYE in Russian No 9, Sep 91 pp 162-168

[Article by A.Ye. Teplykh, A.Z. Menshikov, Institute of Physics of Metals at the Urals Department of the USSR Academy of Sciences; UDC 669.15-194.56:669.017.167.2]

[Abstract] The structural transformations occurring during the annealing of high-nickel alloys is examined with the help of thermal neutron diffraction using elements with substantially differing scattering amplitudes in order to record diffuse scattering determined by the short-range order. To this end, three model alloys are studied: 52Ni41Fe7Cr, 50Ni37Fe13Cr, and 48Ni34Fe18Cr; their compositions are close to those of industrial steels in which an increase in resistivity was detected after annealing at a temperature of 500-550°C. Neutron diffraction patterns of the three face-centered cubic lattice alloys (GTsK) are plotted. An analysis of the findings confirms that a short-range order does indeed form within a 400-600°C range. The numerical values of the short-range order parameters for three coordination spheres with a "zero matrix" are calculated for various heat treatment conditions; they are negative on the first sphere, attesting to a short-range atomic ordering. It is speculated that an increase in resistivity during the annealing of alloys is due to the formation of short-range order areas which serve as additional electron scattering centers. The authors are grateful to I.P. Kursevich and V.A. Nikolayev for stimulating the effort and discussing the findings. Figures 4; tables 1; references 11: 8 Russian, 3 Western.

Effect of Superplastic Deformation Conditions on Steel 03Kh26N6T Structure

927D0139B Moscow IZVESTIYA VYSSHIKH UCHEBNYKH ZAVEDENIY: CHERNAYA METALLURGIYA in Russian No 11, Nov 91 pp 64-68

[Article by M.F.A. Fouad, M.A. Tsepin, A.A. Lobach, Moscow Steel and Alloy Institute; UDC 620.162.2: 539.214:620.183]

[Abstract] The dependence of structural superplasticity manifestations on the size and shape of the material's structural components and changes in structure during the straining process are discussed, and it is noted that the superplasticity phenomenon is manifested especially well in an ultrafine grain structure (UMZ) with a mean grain size of no more than 10-15 μm. Thermal stability plays an important role in attaining superplasticity. The production chart for making sheets of steel 03Kh26N6T with an ultrafine grain structure for the tests is shown. The effect of superplastic forming (SPF) conditions on the structure of steel 03Kh26N6T is investigated using samples cut from the central section of axisymmetric shells formed at a constant straining rate at the dome center during the entire forming cycle. The dependence of the mean austenite grain size on the superplastic metal forming duration at a constant temperature and varying straining rates and the effect of the superplastic forming duration at a constant straining rate and varying temperatures are plotted; likewise, the effect of the superplastic forming duration on the austenite grain form factor at a constant temperature and varying straining rates and a constant straining rate and varying temperatures is examined. The austenite grains' growth rate as a function of their mean size, temperature, and straining rate is plotted. An analysis of the structural characteristics of steel 03Kh26N6T with a nonequilibrium initial structure and a study of the structural change behavior during annealing and plastic deformation reveal that the initial metallographic texture of ultrafine grain sheets and its subsequent development are nonuniform in relation to the rolling direction whereby the austenite particle growth rate depends more on deformation than on annealing; this factor can be used for preliminary heat

treatment and straining of superplastic sheets in order to refine their metallographic texture. Figures 8; references 10: 5 Russian,, 5 Western.

Strain Hardening of Structural Steels After Pulse Treatment

927D0139C Moscow IZVESTIYA VYSSHIKH UCHEBNYKH ZAVEDENIY: CHERNAYA METALLURGIYA in Russian No 11, Nov 91 pp 72-75

[Article by G.A. Vorobyeva, A.M. Sizov, Leningrad Mechanics Institute; UDC 669.01:620.178]

[Abstract] The effect of pulse treatment—blasting molten steel with inert gases in the ladle and simultaneously applying ultrasonic vibrations—on the mechanical and magnetic properties of steel is discussed and strain hardening of structural steels subjected to such pulse treatment both at the refining stage and during the hardening is investigated. The chemical composition of structural steels St5ps and 40Kh used in the tests and the mechanical properties and contamination with nonmetallic inclusions of test samples as a function of the treatment conditions are summarized. The effect of steel St5ps blasting with argon in the ladle on the amount and size of nonmetallic inclusions and the $S=f(e^{1/2})$ diagrams of steel St5ps and 40Kh samples are plotted. The microstructure of steel 40Kh after conventional hardening and tempering and after hardening and tempering with pulse treatment is examined. The refinement of martensite crystals and blocks as a result of pulse treatment ensures a favorable change in properties both at room temperature and below the freezing point. An analysis shows that pulse treatment of steel both in the molten state and during hardening using pulsing gas jets at a close to 30 kHz frequency or 200-1,500 Hz frequency noticeably improves the mechanical properties and lowers the cold shortness threshold due to the changes occurring in the steel's micro- and substructure. Figures 3; tables 3; references 12.

Improving Service Properties of Martensitic-Austenitic Steel N17MT2 by Nitriding

927D0139D Moscow IZVESTIYA VYSSHIKH UCHEBNYKH ZAVEDENIY: CHERNAYA METALLURGIYA in Russian No 11, Nov 91 pp 75-77

[Article by A.V. Bilchenko, V.G. Gorbach, A.A. Kozlovets, I.V. Sidoruk, Kiev Polytechnic Institute; UDC 669.018.25:621.785.53]

[Abstract] The use of nitriding for additional hardening of cobaltless martensitic-austenitic steels is discussed, and an attempt to optimize the conditions of principal heat treatment and subsequent nitriding of the new N17MT2 martensitic-austenitic steel in order to improve its service properties is reported. This steel combines high strength and ductility due to the complex martensite-austenite structure forming during the direct $\gamma \rightarrow \alpha$ and reverse $\alpha \rightarrow \gamma$ transformations. The microstructure of steel N17MT2 after hardening, hardening + aging, and hardening + aging + nitriding is examined under a microscope and the effect of the nitriding temperature and duration on the thickness and surface microhardness of diffusion layers of steel N17MT2 and the effect of heating on the nitrided layer microhardness of steel N17MT2 are plotted. Nitriding substantially improves the endurance strength, wear resistance, and cavitation erosion resistance as well as other service properties of steel N17MT2 which may be thus recommended as an efficient materials for tool attachments. Figures 3; references 3.

Cyclical Durability of Welded Joints From Steel 12Kh18N10T After Plastic Working by Various Methods

927D0139E Moscow IZVESTIYA VYSSHIKH UCHEBNYKH ZAVEDENIY: CHERNAYA METALLURGIYA in Russian No 11, Nov 91 pp 77-79

[Article by G.V. Pachurin, G.P. Guslyakova, Gorkiy Polytechnic Institute; UDC 620.178.3]

[Abstract] The subcritical nature of welding defects which cannot be detected by nondestructive testing yet may lead to catastrophic failure under the effect of cyclical loads and overloads makes the problem of cyclical strength especially important; consequently, the methods of optimizing the plastic weld hardening in order to increase the cyclical strength of steel 12Kh18N10T are investigated. To this end, planar samples from cold-rolled steel 12Kh18N10T with a 2x20 mm cross section are electric-arc butt-welded and treated by various plastic working methods and the welds are tested. Fatigue curves of welded steel steel 12Kh18N10T after various pretreatment conditions are plotted at a 20°C testing temperature and their fatigue equations are derived. In addition, the cyclical strength distribution curves of welded samples from steel 12Kh18N10T after various types of treatment are plotted. The tests demonstrate that the cyclical durability of welded joints from steel 12Kh18N10T largely depends on the conditions of preliminary heat treatment and plastic working. As a result, a new treatment process is suggested: heat treatment with heating to 975°C and a 5 min exposure, then gradual cooling in the air; and a 5 percent-reduction hardening by shot blasting on both sides at 0.4 MPa with 0.6-1.0 mm shot for one min. Data obtained in samples are borne out by full-scale tests of ready products, confirming that the service life of products made by the new technology increases by more than twofold. Figures 3; references 2.

Using Bismuth, Tellurium, and Their Compounds for 'Counter'-Inoculation of Pig Iron

927D0140C Moscow LITEYNOYE PROIZVODSTVO in Russian No 1, Jan 92 pp 9-10

[Article by A.V. Afonaskin, O.D. Opalikhina, A.A. Zhukov, I.O. Pakhnyushchiy, Kurganselmash Production Association and Vinnitsa Polytechnic Institute; UDC 621.746:669.13]

[Abstract] The use of pig iron counterinoculation at the Kurganselmash Production Association is described; commercial smeltings are conducted in 10 induction furnaces for making "housing" and "rotor" castings for centrifugal pumps from pig iron (containing 3.63 percent C, 2.48 percent Si, 0.60 percent Mn, 0.098 percent P, and 0.045

percent S) inoculated in 100 kg ladles. The inoculation conditions are outlined; the inoculant is placed on the bottom of the ladle while Bi and Bi_2Te_3 batches are added in paper bags and Te is added in the form of Te+Cu tablets (Cu is added to increase the weight). The resulting alloys are tested for machinability. Test data indicate that the pig iron inoculated by a ternary complex inoculant which causes the counterinoculation phenomenon has the best combination of properties; Bi will be replaced for the more efficient Bi_2Te_3 alloying composition when its production technology is mastered. Tables 1.

Experience of Using Electrospark Alloying Electrodes Produced by Self-Propagating High-Temperature Synthesis Extrusion

927D0148F Kishinev ELEKTRONNAYA OBRABOTKA MATERIALOV in Russian No 5 (161), Sep-Oct 91 pp 66-68

[Article by V.V. Podlesov, A.M. Stolin, Structural Macrokinetics Institute at the USSR Academy of Sciences, Chernogolovka]

[Abstract] A new approach to producing electrospark alloying electrodes by the method of self-propagating high-temperature synthesis (SVS) extrusion which makes it possible to simplify the electrode manufacturing and shorten the synthesis and compaction processes from several hours to several seconds in a single technological cycle is presented. The essence of the new method is using self-propagating high-temperature synthesis of the tungstenless hard alloy with subsequent extrusion of the resulting synthesized material into rods with a two to five mm diameter and 300 mm length, then cutting them into ready electrodes. The properties of the electrodes and electrospark alloyed items hardened with their help are summarized and compared to those of tools alloyed by commercial hard alloys. The results attest to the advantages of SHS electrodes from STIM alloys. Depending on the alloying system used, the 10-60 μm thick electrospark layer produced by SHS STIM electrodes has a microhardness of 11-19 GPa. The authors are grateful to M.V. Inadze and N.N. Zhilyayev. Figures 2; tables 4; references 2.

Foreign Broadcast Information Service (FBIS) and Joint Publications Research Service (JPRS) publications contain political, military, economic, environmental, and sociological news, commentary, and other information, as well as scientific and technical data and reports. All information has been obtained from foreign radio and television broadcasts, news agency transmissions, newspapers, books, and periodicals. Items generally are processed from the first or best available sources. It should not be inferred that they have been disseminated only in the medium, in the language, or to the area indicated. Items from foreign language sources are translated; those from English-language sources are transcribed. Except for excluding certain diacritics, FBIS renders personal names and place-names in accordance with the romanization systems approved for U.S. Government publications by the U.S. Board of Geographic Names.

Headlines, editorial reports, and material enclosed in brackets [ ] are supplied by FBIS/JPRS. Processing indicators such as [Text] or [Excerpts] in the first line of each item indicate how the information was processed from the original. Unfamiliar names rendered phonetically are enclosed in parentheses. Words or names preceded by a question mark and enclosed in parentheses were not clear from the original source but have been supplied as appropriate to the context. Other unattributed parenthetical notes within the body of an item originate with the source. Times within items are as given by the source. Passages in boldface or italics are as published.

SUBSCRIPTION/PROCUREMENT INFORMATION

The FBIS DAILY REPORT contains current news and information and is published Monday through Friday in eight volumes: China, East Europe, Central Eurasia, East Asia, Near East & South Asia, Sub-Saharan Africa, Latin America, and West Europe. Supplements to the DAILY REPORTs may also be available periodically and will be distributed to regular DAILY REPORT subscribers. JPRS publications, which include approximately 50 regional, worldwide, and topical reports, generally contain less time-sensitive information and are published periodically.

Current DAILY REPORTs and JPRS publications are listed in *Government Reports Announcements* issued semimonthly by the National Technical Information Service (NTIS), 5285 Port Royal Road, Springfield, Virginia 22161 and the *Monthly Catalog of U.S. Government Publications* issued by the Superintendent of Documents, U.S. Government Printing Office, Washington, D.C. 20402.

The public may subscribe to either hardcover or microfiche versions of the DAILY REPORTs and JPRS publications through NTIS at the above address or by calling (703) 487-4630. Subscription rates will be provided by NTIS upon request. Subscriptions are available outside the United States from NTIS or appointed foreign dealers. New subscribers should expect a 30-day delay in receipt of the first issue.

U.S. Government offices may obtain subscriptions to the DAILY REPORTs or JPRS publications (hardcover or microfiche) at no charge through their sponsoring organizations. For additional information or assistance, call FBIS, (202) 338-6735,or write to P.O. Box 2604, Washington, D.C. 20013. Department of Defense consumers are required to submit requests through appropriate command validation channels to DIA, RTS-2C, Washington, D.C. 20301. (Telephone: (202) 373-3771, Autovon: 243-3771.)

Back issues or single copies of the DAILY REPORTs and JPRS publications are not available. Both the DAILY REPORTs and the JPRS publications are on file for public reference at the Library of Congress and at many Federal Depository Libraries. Reference copies may also be seen at many public and university libraries throughout the United States.